A STUDY
OF THE RATE OF SELF-DIFFUSION OF NICKEL
AND
OF THE RATE OF DIFFUSION OF NICKEL INTO IRON, COBALT AND TWO IRON-NICKEL ALLOYS

by

John Ross MacEwan

A thesis presented to the Faculty
of Graduate Studies and Research
of McGill University in partial
fulfilment of the requirements for
the degree of Doctor of Philosophy

McGill University,
Montreal, Quebec

May, 1956

ACKNOWLEDGEMENTS

I wish to express my appreciation to Professor J.U. MacEwan and to Dr. Leo Yaffe, who directed this research, and also to the staffs of the Departments of Metallurgical Engineering and of Chemistry, who gave generously of their time. The co-operative spirit that was shown made the work a pleasure.

This work was financed by the Defence Research Board, Department of National Defence, and this assistance is gratefully acknowledged as it made the research possible.

TABLE OF CONTENTS

TABLE OF CONTENTS (continued)

TABLE OF CONTENTS (continued)

LIST OF TABLES

LIST OF FIGURES

LIST OF FIGURES (continued)

LIST OF FIGURES (continued)

INTRODUCTION

Fick's laws

It was shown experimentally by Parrot (1815) that when a partition between two gases is removed, the two gases would intermingle even in the absence of mechanical agitation and convection currents. The process which causes this tendency towards homogeniety is called diffusion. One of the earliest direct observations that metals would interdiffuse was the qualitative investigation of Spring[1] in 1894. However, before this, certain familiar metallurgical phenomena had indicated that diffusion occurred in metals, such as occurs during the cold welding of metals, the carburization of iron to form steel, and the preparation of alloys[2] by heating compacted metal powders below their melting points. The velocity of this metallic interpenetration was not realized until the quantitative experiments of Roberts-Austen[3]. He showed that at 300°C the rate of penetration of gold into lead was faster than that of sodium chloride into water at 18°C.

The phenomenological equations covering the diffusion process were proposed theoretically by Fick[4] before any quantitative experiments had been performed. By analogy to Fourier, who had just studied thermal conductivity, he defined a diffusion coefficient, D, for diffusion occurring along the x direction in terms of the equation

$$J = -A D \frac{\partial c}{\partial x} \qquad (1)$$

where

J = Amount of material crossing a plane of area A normal to x -grams/cm.^{2}/sec.

A = Area of the diffusion interface - cm.^{2}

D = Diffusion coefficient - cm.^{2}/sec.

$\frac{\partial c}{\partial x}$ = Concentration gradient - grams/c.c/cm.

The general diffusion equation can be deduced from the previous equation by equating the rate of change of concentration in a small cube to the amount of material diffusing out of the cube faces normal to the x axis.

The resulting equation is

$$\frac{\partial c}{\partial t} = \frac{\partial}{\partial x}\left(D(c)\ \frac{\partial c}{\partial x}\right) \qquad (2)$$

where

$\frac{\partial c}{\partial t}$ = Rate of change of concentration at any point where the concentration gradient is $\frac{\partial c}{\partial x}$ -grams/c.c./sec.

$D(c)$ = Diffusion coefficient which may or may not be concentration dependent.

When the diffusion coefficient is independent of concentration, Equation (2) reduces to the simpler form

$$\frac{dc}{dt} = D \frac{d^2c}{dx^2} \qquad (3)$$

Concentration dependence of D

In 1932 Grube and Jedele[5] studied diffusion in the copper-nickel system. Their results indicated that D was dependent on concentration. The following year Matano[6] correctly interpreted their results and showed that D had a tenfold variation with composition.

With the accumulation of diffusion data, measured over wide concentration ranges, it became interesting to try to correlate the variation of D_c with some function of the composition. Uller[7] pointed out that if the equation

Mass flow = Constant D x Gradient of concentration

was not applicable to a particular diffusion system because D varied with composition, then there were two alternatives: either

$$\text{Mass flow} = -AD(c)\frac{\partial c}{\partial x}, \text{ giving } \frac{\partial c}{\partial t} = \frac{\partial}{\partial x}\left(D(c)\frac{\partial c}{\partial x}\right) \qquad (4)$$

or

$$\text{Mass flow} = -AD^{1}\frac{\partial f(c)}{\partial x}, \text{giving } \frac{\partial c}{\partial t} = D^{1}\frac{\partial^{2} f(c)}{\partial x^{2}} \qquad (5)$$

In the first expression it can be assumed that D(c) varies with composition, and a complete phenomenological description of the system is given when the variation of D(c) with composition is found. In the latter expression, a suitable function of concentration f(c) is to be found, so that D^1 becomes a constant throughout the composition range.

Darken[8] suggested that the thermodynamic activity might be the correct function of concentration to be substituted into Equation (5). Birchenall and Mehl[9], using this approach, were moderately successful in treating the simple case of interstitial diffusion. Equation (5) becomes

$$J_i = -D' \frac{\partial a_i}{\partial x} \tag{6}$$

where $\frac{\partial a_i}{\partial x}$ is the activity gradient of the interstitial component i. The relationship between the experimentally observed diffusion coefficient, D_c, and D^1 was shown to be

$$D(c) = \frac{D'}{\left(f_i + \frac{\partial f_i}{\partial \ln N_i} \right)} \tag{7}$$

where

N_i = Atomic fraction of the diffusing solute

f_i = Activity coefficient of the solute at N_i

The application of Equation (7) to the measured values of D(c) for the diffusion of carbon into gamma iron gave a constant value of D^1, within the errors of the experimental values. The variation of D(c) was twofold over the investigated composition range. Extension of this approach to the case of diffusion in substitutional solid solutions, in particular to the copper-zinc system, was not particularly successful. In this system the variation of D(c) with composition in the alpha brass region was twentyfold.

Darken[10] has pointed out that Fick's law should be written in the form

$$J_i = -\frac{1}{N}\frac{\partial \overline{G}_i}{\partial x} B_i C_i \qquad (8)$$

where

J_i = Flux of atoms of the ith species across a unit plane normal to the x axis

N = Total number of atoms present in a unit cube

$\frac{\partial \overline{G}_i}{\partial x}$ = Partial molal free energy gradient

B_i = Mobility of the ith species under unit potential force

$\frac{C_i}{N}$ = Atomic fraction of i atoms

Use of equations of this type had previously been proposed by Onsager and Foss[11] for dilute electrolytes and by Dehlinger[12] for alloys. Le Claire[13], in discussing Birchenall and Mehl's approach, has pointed out that Equation (6) makes the implicit assumption that the mobility is independent of concentration. The failure of their approach indicates that in a substitutional solid solution, the mobility will depend on concentration, and the use of an activity gradient in place of a concentration gradient is not sufficient to make the mobility constant.

Since the mobility varies with composition this approach still leads to a phenomenological description of diffusion in alloys.

Temperature variation of D

The temperature variation of the diffusion coefficient always appears to obey the equation

$$D = D_{o}e^{-Q/RT} \qquad (9)$$

where

D = Diffusion coefficient at any temperature T - cm.^{2}/sec.

Q = Activation energy - cal./mole

R = Gas constant - cal./$^\circ$K./mole

D_o = Frequency factor - cm.^{2}/sec.

The exponential variation of the diffusion coefficient with temperature seems to have been first employed by Tamman and Schonert[14], and by Weiss and Henry[15], to express the temperature variation of their results.

Actually equations of this type were proposed much earlier by van't Hoff[16] and Arrhenius[17] to express the temperature variation of the rate constant for a chemical reaction. By analogy to the rate expression for a unimolecular chemical reaction Dushman and Langmuir[18] (1922) proposed a semi-emperical equation for the diffusion coefficient.

$$D = (Q/Nh)\, d^2\, e^{-Q/RT} \qquad (10)$$

where

N = Avogadro's number - atoms/mole.

h = Plank's constant - cal. sec.

d = Lattice parameter - cm.

Since this time the constant Q has been identified as the activation energy necessary for a diffusion jump.

Diffusion mechanisms

The early investigators realized that there were at least two possible modes of diffusion. In the interstitial alloys it was proposed that diffusion of the solute took place interstitially through the rigid lattice of the solvent. There has never been any reason to modify this concept. In alloys, where the two components form a substitutional solid solution, it was tacitly assumed that diffusion took place by direct interchange. The most obvious result of this mechanism is that the solute and solvent must diffuse with equal but opposite rates.

Frenkel[19], and Wagner and Schottky[20] proposed that diffusion in metals or crystalline materials could be described by any one or a combination of three basic mechanisms. These possibilities are illustrated in the following figures.

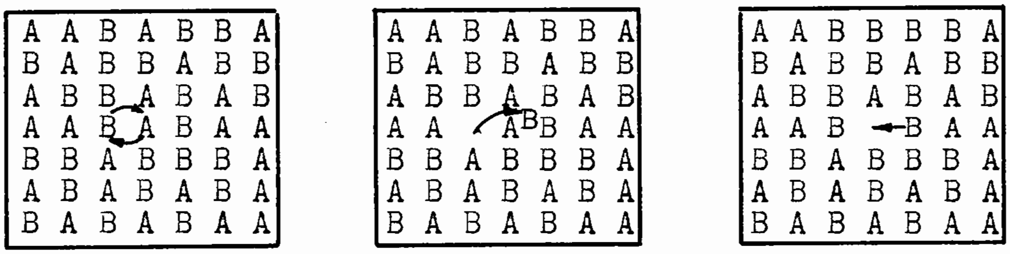

(a) Diffusion by direct interchange

(b) Interstitial diffusion

(c) Vacancy diffusion

FIGURE 1. THE THREE BASIC MECHANISMS OF DIFFUSION

Mechanism (a) illustrates the simple case of direct interchange. The atoms A and B move relative to each other by the direct interchange of neighbouring A and B atoms. Since atoms behave as if they are rigid spheres, it is clear that the neighbouring atoms will have to yield slightly to allow the interchange to take place. The fact that the surrounding lattice is strongly distorted during this type of interchange indicates that large saddle point energies are involved. If this is the only mechanism operating, then a single diffusion constant, D, can describe the motion of the A and B atoms.

Mechanism (b) illustrates a type of interstitial diffusion. Here the atom B leaves its normal lattice position and moves interstitially through the lattice. The migrating B atom could eventually fall into a vacant lattice site such as it created when it moved into an interstitial position. A particular case of this type of mechanism occurs in the interstitial alloys, when the atomic radius of the B atoms is small enough so that the normal positions for these atoms is an interstitial position. In both types of interstitial diffusion the A atoms are assumed to remain stationary, and the migrating B atoms move relative to one another and to the A atoms. If this is the only mechanism operating a single diffusion coefficient will suffice to describe diffusion in a binary alloy.

On an energy basis this mechanism would appear to have an advantage over the direct exchange mechanism, in that a smaller amount of lattice distortion will take place. However there are two considerations which do not place this mechanism at an advantage. Once the B atom has jumped into the interstitial position, its next jump would most likely be back to the vacant site it left behind, rather than to a neighbouring interstitial position. Therefore the chance of a net displacement by diffusion is reduced. Also, if at any time a large number of B atoms are in interstitial positions, seeking vacant sites, the total lattice strain energy will be increased, reducing the chance that any one atom will receive sufficient energy by thermal fluctuations to make a diffusion jump.

Seitz[21] has proposed a type of interstitial mechanism which avoids these objections. After the B atom has moved into the interstitial position, it then forces a neighbouring atom into an interstitial position and takes its place. The displaced atom can repeat this process so that the interstitial distortion moves through the lattice in the manner of a phase pattern. Seitz terms this "interstitialcy" migration.

Mechanism (c) assumes the existence of vacant lattice sites called vacancies. Diffusion occurs in these alloys by a neighbouring atom exchanging places with a vacancy. This particular mechanism is an extremely powerful concept because it can explain the two possible extreme cases which might occur in substitutional alloys. One extreme is that A and B diffuse with equal but opposite rates. To explain this situation it is only necessary to specify that A and B have equal probabilities of exchanging places with the vacancy. The other extreme is that the B atoms diffuse and the A atoms remain stationary. Two assumptions are necessary to explain this circumstance. The probability of a B atom exchanging places with a vacancy is assumed to be so much greater than the probability of an A atom making the same exchange, that the latter circumstance hardly ever occurs. Also, the vacancies must be maintained in thermal equilibrium with the lattice so that we need not assume a net flux of vacancies to balance the flux of B atoms. By modifying the assumptions about the relative probability of exchange of A and B atoms with vacancies, any case intermediate to these two extremes can be explained. Because, in general, the rates of diffusion of A and B atoms are different, it is necessary to use two diffusion coefficients to completely describe the motion.

Evidence in favour of a vacancy mechanism

Theoretically, the vacancy mechanism received considerable support from the calculations, by Huntington and Seitz[22], for the activation energy necessary for self-diffusion in copper. They found that the activation energy, in kcal./mole, is 400 for direct interchange, 230 for an interstitialcy mechanism and, with a more refined calculation[23], 81 for the vacancy case. A further calculation[24] has reduced the energy for direct interchange to 240. Seitz[25], in a recent review article, has quoted the value for the vacancy mechanism as 64, though no reference is given to the origin of this value. Even with the approximations involved, the vacancy mechanism is the only one of the proposals where the calculated activation energy is close to the experimental one of about 47 k cal./mole[26-29]

More recently an alternative mechanism was suggested by Zener[30]. He suggested that diffusion might occur by a simaltaneous movement of a group of n atoms arranged in a ring. Each atom in the ring is the nearest neighbour of the atoms

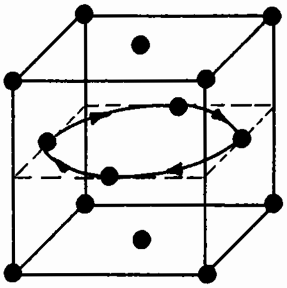

Figure 2. Four-Membered Ring Diffusion Mechanism

immediately before and after it. The above illustration shows a four-membered ring in a face-centered cubic metal. The simple case of direct interchange corresponds to n = 2. Zener has found that the lowest activation energy, 90 k cal./mole, occurs in a four-membered ring. While this energy is higher than the value found for the vacancy mechanism, the difference is not great enough to completely eliminate the ring mechanism from consideration. There is however, a basic difference in the two mechanisms. The vacancy mechanism permits unequal diffusion rates in an alloy, while this is forbidden by the ring mechanism. A choice can be made in favour of the vacancy mechanism in any particular case, where a net flux of atoms relative to the lattice is found.

Until 1947 it was not generally accepted that the two components in a binary alloy could diffuse at unequal rates, although prior to this time several investigators had presented data showing that a simple cyclic interchange of atoms did not agree with their experimental results. Seith and Kiel[31] (1933) showed that the rates of diffusion of gold and silver into lead were not consistent with the measured rate of self-diffusion of lead in the same alloy. The much higher rates of diffusion obtained for gold and silver led them to propose that these atoms were diffusing interstitially into lead. (The concept of vacancies was practically unknown at this time). Johnson[32] (1942) measured the self-diffusion coefficients of silver and gold along with the chemical diffusion coefficient in a 50 per cent gold-silver alloy. The values at 965°C were

$D^*_{Ag} = 5.51 \times 10^{-9}$ cm.^{2}/sec. (self-diffusion coefficient of silver)

$D^*_{Au} = 2.20 \times 10^{-9}$ cm.^{2}/sec. (self-diffusion coefficient of gold)

$D_c = 6.56 \times 10^{-9}$ cm.^{2}/sec. (chemical diffusion coefficient)

Lacking an analysis to connect self-diffusion measurements with standard diffusion coefficients, his results could not be satisfactorily interpreted. However because the self-diffusion coefficients for gold and silver differ, it is evident that they diffuse at different rates.

The relationships necessary to analyse Johnson's results were first presented by Darken[10] (1947). By assuming that a radioactive isotope and a stable isotope of the same metal have equal mobilities under unit potential force, Darken derived from Equation (8) the following relationship

$$D_a = D_a^* \left(1 + \frac{\partial \log f_a}{\partial \log N_a}\right) \qquad (11)$$

where

D_a = Intrinsic diffusion coefficient of an "a" atom where the concentration gradient is $\frac{\partial C_a}{\partial x}$, and the concentration is C_a.

D_a^* = Self-diffusion coefficient of an "a" atom in a homogeneous alloy of concentration C_a.

f_a = Activity coefficient of component "a".

N_a = Atomic fraction of "a" atoms.

The chemical diffusion coefficient in the same binary alloy is given by

$$D_c = N_b D_a + N_a D_b \qquad (12)$$

where

D_c = Standard diffusion coefficient determined by Boltzmann-Matano method[6].

D_a, D_b = Intrinsic diffusion coefficients of a and b atoms.

N_a, N_b = Atomic fractions of a and b atoms.

In 1942 Kirkendall[33] supplemented some earlier work[34] on the rate of diffusion of zinc in alpha brass. He detected a definite shift of the original diffusion interface towards the zinc rich alloy in the diffusion couple. To explain this shift Kirkendall proposed that the zinc diffuses more rapidly than the copper in alpha brass. The result of the zinc diffusing out faster than the copper can diffuse in, necessitates a reforming of the lattice in the zinc rich region. The resultant contraction of the zinc rich region would cause the observed shift in the original interface.

The results of all these researches seem to have been completely ignored by most investigators. However in 1947 Smigelskas and Kirkendall[35] performed an experiment which definitely demonstrated that a net movement of atoms takes place relative to the lattice. The diffusion couple used in their experiment is illustrated below.

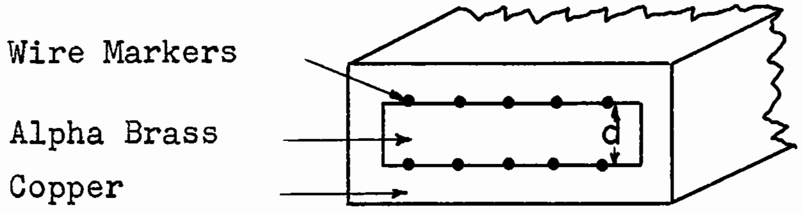

Figure 3. Kirkendall's Sandwich Diffusion Couple.

As shown, a series of inert molybdenum wires are present at the original interface of a copper-alpha brass couple. If there is a net flux of atoms moving relative to the diffusion interface during diffusion, the section of the lattice which is losing atoms contracts. This contraction shifts the position of the diffusion interface relative to a fixed point outside the diffusion zone. As the wires are embedded in the diffusion interface, they move with it, and can be used to determine the extent of contraction.

At regular periods during the diffusion anneal, the interval d between the diffusion interfaces was measured with the aid of the wire markers. The interfaces were found to migrate towards the zinc rich core. The total distance moved by the markers varied as the square root of the annealing time. This was added confirmation that the contraction was a diffusion phenomenon, as the parabolic relationship is characteristic of diffusion processes. The marker shift confirmed Kirkendall's earlier supposition that zinc diffuses faster than copper in alpha brasses. This marker movement in metals is known as the Kirkendall shift.

Kirkendall's measurements were confirmed by Correa Da Silva and Mehl[36], Bückle and Blin[37], and Barnes[38]. The effect has also been found to occur in the face-centered cubic metal systems Cu/Ni[36,38,39,40], Au/Cu[36], Ag/Au[36,39,40], Ag/Pb[39,40], Ni/Co[39,40], Ni/Au[39,40] and Fe/Ni[40], and in the alpha regions of the Sn/Cu[36] and Al/Cu[36,37] alloys.

Kirkendall's marker movement experiment was interpreted by Darken[10] on the assumption of separate intrinsic diffusion coefficients for both components of the alloy. The resultant equations are

$$D_c = N_b D_a + N_a D_b \tag{12}$$

$$v = (D_a - D_b) \frac{\partial N_a}{\partial x} \tag{13}$$

where

v = Velocity of the marker relative to some point well removed from the diffusion zone.

D_a, D_b = Intrinsic diffusion coefficients of a and b atoms.

$\frac{\partial N_a}{\partial x}$ = Mole fraction gradient at the marker.

Theoretically this phenomenon can only be explained by a vacancy or interstitial mechanism. As Huntington's calculations indicate, an interstitial mechanism is energetically unlikely in copper, a face-centered cubic metal, it would appear that diffusion proceeds in such metals due to the presence of vacant lattice sites. Quite recently Le Claire[41], and Buffington and Cohen[42], have proposed theories which permit self-diffusion data to be correlated with other physical data for the associated metals. Their theories were only successful when a vacancy model for self-diffusion was assumed for the face-centered cubic metals. Zener's ring mechanism is not successful in correlating the available data and is thus rejected as a possible mechanism.

There is other evidence to support the premise that vacancies exist in metals. It has been shown[43] that atomic imperfections are characterized by the fact that they can exist in thermodynamic equilibrium in a lattice at finite temperatures. One imperfection which was considered was the Schottky defect or vacant lattice site. The concentration of vacancies[43] at any temperature was shown to be

$$N_v/N = e^{-\Delta G_1/RT} \qquad (14)$$

where

N_v/N = Fraction of sites vacant at temperature T.

ΔG_1 = Isothermal work to remove an atom from the interior, apart from that contributed by changes in the entropy of mixing.

Therefore the equilibrium number of vacancies in the lattice is much larger at high temperatures than at low temperatures.

As vacancies are supposedly instrumental in permitting the migration of atoms, an alloy which is quenched from a high temperature to retain an excess of vacancies, should give larger D values than a well-annealed specimen containing the equilibrium concentration. Turnbull and Hoffman[44] were unable to find any difference in the rate of self-diffusion of silver in quenched and well-annealed specimens. This is not unexpected on the basis of Seitz's[45] suggestion that the concentration of dislocations in a metal is high enough to reduce the concentration of vacancies to its equilibrium value, in a period which is very short compared to the time taken to perform a conventional diffusion experiment.

Recent developments have shown it is possible to measure diffusion coefficients by anelastic techniques[46-50] in substitutional alloys. While the theoretical analysis connecting the observed experimental relaxation time with the mean time of stay between diffusion jumps is not yet completely developed, the technique has tremendous possibilities. Diffusion measurements can be made in a fraction of the time and at much lower temperatures than by standard techniques. Nowick[51] quenched a Ag/Zn (30% Zn) alloy from 400°C to room temperature to trap an excess number of vacancies. At 50°C this quenched alloy, containing an excess of vacancies, initially showed a relaxation time 10^5 times as large as that of an alloy containing an equilibrium number of vacancies. (The relaxation time is proportional to the mean time of stay between diffusion jumps). As time elapsed the relaxation time decayed towards the equilibrium value for a well-annealed, slow-cooled alloy. This experiment suggests that an excess number of vacancies causes higher rates of diffusion. From his measurements Nowick estimated the activation energy necessary to form a vacancy to be equal to or greater than 12.5 kcal./mole. This is about 0.4 times the total activation energy of 32.9 kcal./mole for diffusion in this alloy.

Anomalies in the resistivity of metals at high temperatures have been attributed to the presence of vacancies. Meechan and Eggleston[52] measured the resistivity of copper and gold over a wide temperature range. In the range from room temperature to about 500°C the resistivity was accurately represented by a quadratic equation

$$R = A + BT + CT^2 \tag{15}$$

At higher temperatures there was an additional increment in the resistivity ΔR, the difference between the measured value and the value extrapolated from the quadratic equation, which fitted an expression

$$\Delta R = Ae^{-Q_v/RT} \tag{16}$$

On the assumption that the additional increment in resistivity was due to the existence of vacant lattice sites, the activation energies for the formation of a vacancy in copper and gold were respectively 20.6 and 15.3 kcal./mole. Abeles[53] calculated the increase in resistivity caused by the formation of a vacant lattice site. Using this value the calculated density[52] of vacancies near the melting point was 0.2 and 0.4 atomic per cent respectively for copper and gold.

Thus while the presence of vacancies in the lattice depends on supposition, the increasing number of experimental phenomena which can be easily explained on the basis of vacancy theory gives reason to accept this premise. In the absence of any contradictory evidence, it is assumed that diffusion occurs in face-centered cubic metals by a vacancy mechanism.

Short-Circuiting Paths in Diffusion

Diffusion may take place along three different routes in a polycrystalline specimen; on the surface, through the lattice or along the grain boundaries. Because of the lower binding forces acting on the surface atoms, it is apparent that the activation energy for surface migration is appreciably lower than for lattice diffusion. Similarly in the region of misfit between two adjoining grains, i.e. the grain boundary, the atoms are less tightly bound and here again a migrating atom requires less activation energy than in the interior of the lattice. Particularly at low temperatures these smaller activation energies result in atoms migrating much faster on the surface and along the grain boundaries than through the lattice.

Experimentally, when measuring volume diffusion coefficients, errors introduced by surface diffusion are easily eliminated in the following manner. After the diffusion anneal, the surface layers lying parallel to the diffusion direction are machined off the sample. The layer of material taken off is thicker than the maximum penetration which could occur by lattice diffusion from the surface.

Unfortunately the errors introduced by high rates of diffusion along the grain boundary cannot be eliminated experimentally except by using single crystals. Measurements[54] of the self-diffusion coefficient for silver in single crystals and polycrystalline material indicate that at high temperatures identical volume diffusion coefficients are obtained in both media. At low temperatures however, the coefficient obtained using polycrystalline material is much greater than that obtained using a single crystal. Therefore to obtain values of Q and D_o in polycrystalline material representative of volume diffusion, it is important to have some criterion for rejecting results which are erroneously high due to the contribution of grain boundary diffusion.

The standard technique for measuring diffusion coefficients using radioactive tracers is to electroplate a thin layer of tracer onto one face of a specimen. The solution to Fick's Law corresponding to the case of diffusion of an infinitely thin layer of material into a semi-infinite medium, D assumed constant, is[55]

$$C(x,t) = \frac{Co}{\sqrt{\pi Dt}} e^{-x^2/4Dt} \qquad (17)$$

where

$C(x,t)$ = Concentration of tracer after time t at a distance x below the surface - arbitrary units.

Co = Total quantity of tracer contained in an infinitely thin layer at time t = o - arbitrary units.

D = Lattice diffusion coefficient - $cm.^2/sec.$

t = Diffusion time - sec.

x = Diffusion distance - cm.

Taking the logarithm of Equation (17) gives

$$\ln C(x,t) = \ln Co/\sqrt{\pi Dt} - x^2/4Dt \qquad (18)$$

Therefore the diffusion coefficient can be obtained from the slope of the linear plot of ln C vs x^2.

Fisher[56] has considered diffusion into an infinite bicrystal where the grain boundary is normal to the original diffusion surface. When the concentration at the surface is maintained constant throughout the diffusion anneal, and when the grain boundary diffusion coefficient D_b is much larger than the lattice diffusion coefficient D_l, the following figure shows the type of concentration contour obtained.

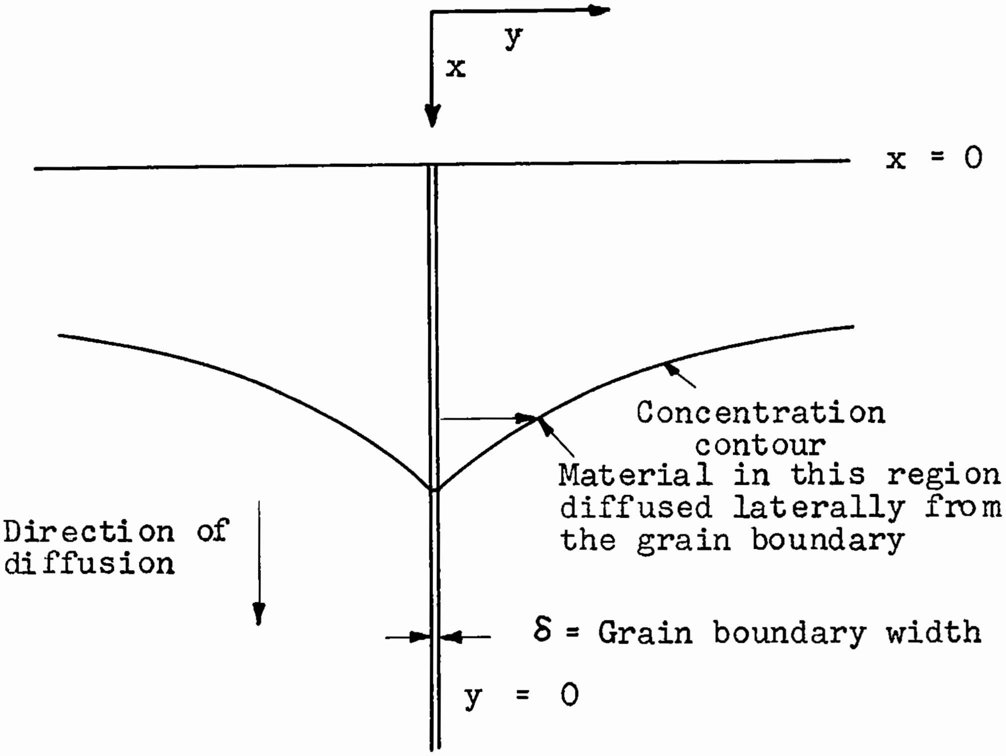

Figure 4. Diffusion in the Neighbourhood of a Grain Boundary.

The amount of material in the grain boundary itself is quite small and would have little effect on the lattice diffusion coefficient. The errors in lattice diffusion coefficients are caused by the material which diffuses laterally away from the grain boundary into the lattice. At a distance x below the surface, which is greater than the maximum penetration by lattice diffusion alone, the average concentration of tracer in a slice is

$$\ln C_b = -\left[2^{\frac{1}{2}}(D_l/D_b\ \delta)^{\frac{1}{2}} \Big/ (\pi D_l)^{\frac{1}{4}}\right] x + \text{Const.} \qquad (19)$$

where

C_b = Concentration of tracer in a slice at distance x below the surface - arbitrary units.

D_l = Lattice diffusion coefficient - cm.^{2}/sec.

D_b = Grain boundary diffusion coefficients - cm.^{2}/sec.

δ = Grain boundary width - assumed = 5×10^{-8} cm.

t = Diffusion time - sec.

x = Diffusion penetration - cm.

and the value of the constant depends only on t not on x.

Equations (18) and (19) indicate for atoms migrating solely by volume diffusion, ln C varies as x^2, and for atoms migrating along the grain boundaries ln C varies as x. This gives a criterion for discriminating against lattice diffusion measurements in which enough grain boundary diffusion takes place to invalidate the results.

Wajda[57] has made a complete investigation of lattice and grain boundary self-diffusion in polycrystalline zinc. At high temperatures where ln C varies as x^2 for all penetration distances, his results are in agreement with previous work[58] using single crystals. At low temperatures where ln C varies as x for all penetration distances, the concentration-penetration curves can be used to evaluate grain boundary diffusion coefficients. In the intermediate range of temperatures both types of diffusion contributed to the migration of the tracer atoms. The types of penetration curve obtained in this range of temperatures are shown in Figure 5.

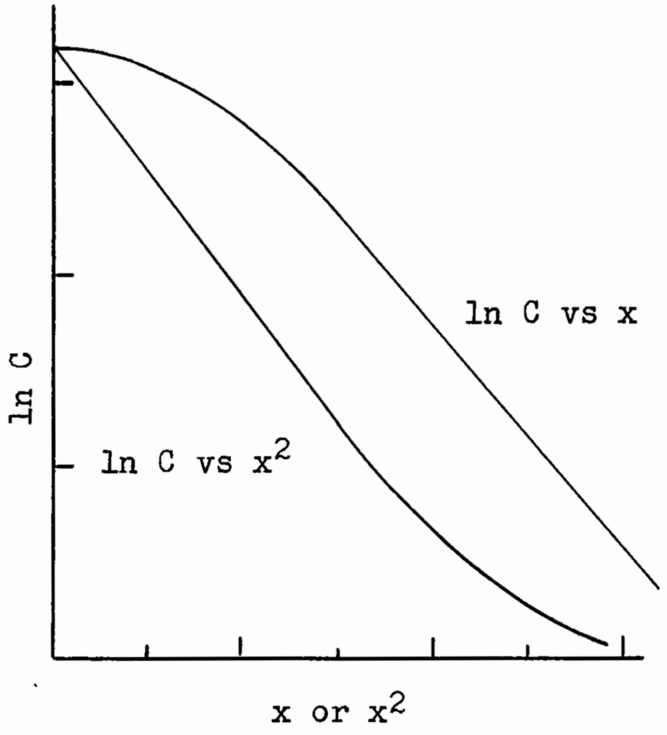

Figure 5. Type of Penetration Curves Obtained When Mixed Diffusion Occurs.

The penetration curve obtained for lattice diffusion is convex to the coordinates at large values of x^2. In this region ln C varies as x showing that most of the tracer atoms in this region migrated with the assistance of the grain boundaries. The lattice diffusion coefficients calculated from the linear portion of the penetration curve (ln C vs x^2) were found to be considerably higher than the values obtained for single crystals. This indicates that even in the linear portion of the plot (ln C vs x^2) the penetrations are too high due to the contributing influence of grain boundary diffusion. Therefore a criterion for accepting experimental results as being truly representative of lattice diffusion is that ln C must vary as x^2 over the whole penetration range.

To give a relative idea of the activation energies associated with the various modes of diffusion the following results are given for self-diffusion in silver.

Lattice Diffusion[44]	$D_l = 0.895\ e^{-45,950/RT}$ cm.^{2}/sec.
Grain Boundary Diffusion[44]	$D_b = 0.03\ e^{-20,200/RT}$ cm.^{2}/sec.
Surface Diffusion[59]	$D_s = 0.16\ e^{-10,300/RT}$ cm.^{2}/sec.

An orientation[60,61] effect has been found for the rate of diffusion along the grain boundaries. The greater the angle between the principle axes of adjoining grains, the higher the rate of diffusion along the boundary. For low angles of misfit (less than 20°) the grain boundary is supposedly composed of a set of parallel individual edge dislocations[62,63]. At these angles the rate of grain boundary diffusion is comparable to that of lattice diffusion. This is in contradiction to the work of Hendrickson and Macklin[64] who found the rate of diffusion along individual edge disclocations was twice as fast as normal grain boundary diffusion. Until this question is resolved the role of individual edge dislocations in short-circuiting diffusion will not be known. Possibly the rate of diffusion along dislocations is easily hindered by foreign atoms making it difficult to compare the results of different investigators.

Empirical correlations for Q

The basic step in the migration of an atom, irrespective of mechanism, involves leaving its equilibrium position in the lattice. As the local disorder occurring during this process may be akin to that occurring in melting or in sublimation, it has been attempted to correlate the activation energy with the melting point, T_m[25, 55], and with the latent heat of sublimation, L_s[25, 55]. More recently Nachtreib[65] has proposed the following empirical expression for the activation energy

$$Q = 16.5\ L_f \qquad (20)$$

where

L_f = The latent heat of fusion - kcal./mole.

The appropriate ratios necessary to check the degree of linear correlation given by these proposals, have been calculated from the experimental results for self-diffusion in some face-centered cubic metals, and are listed in Table 1.

The most obvious feature of Table 1 is the large discrepancies in the reported results for any one metal. The results marked * have been selected as the most reliable[41,42].

TABLE 1

Proportionality of the Activation Energy for Self-Diffusion to the Melting Point, the Latent Heat of Sublimation, and the Latent Heat of Fusion.

Metal	Q $\frac{\text{kcal.}}{\text{mole}}$	Q/T_m $\frac{\text{kcal.}}{\text{deg. mole}}$	Q/L_s	$Q/16.5L_f$	Ref.
Pb	27.4 *	46	0.59	1.36	66
	24.2 *	40	0.53	1.20	67
	25.7 *	43	0.55	1.28	68
Ag	45.9 *	37	0.68	1.03	44, 55
	45.5 *	37	0.67	1.02	69
Au	51.0	38	0.57	1.02	70
	53.0	40	0.60	1.06	71
	45.6 *	34	0.52	0.911	72
Cu	57.2	42	0.72	1.11	26
	61.4	45	0.77	1.19	27
(p. cryst.)	45.1 *	33	0.57	0.876	28
(s. cryst.)	49.0 *	36	0.62	0.952	28
	46.8 *	35	0.59	0.910	29
Co	61.9	35	0.73	1.02	73
	67.0 *	38	0.79	1.10	74
	67.7 *	38	0.80	1.11	75
Fe	74.2	42	0.82	1.26	76
	67.9	38	0.75	1.14	77
Average		38	0.66	1.08	

Values of T_m, L_s, and L_f taken from Reference 78.

While some proportionality exists, none of the ratios is constant enough to indicate an exact linear relationship. In particular, all three ratios for lead differ appreciably from the mean values. As the activation energy for self-diffusion in lead has recently been carefully checked[67], it would appear that this discrepancy is real and the proposed correlations are good only to an order of magnitude.

Theoretical expressions for D

An interpretation of diffusion as a random walk phenomenon[79] gives an expression for the diffusion coefficient

$$D = \tfrac{1}{2} \sum_i \Gamma_i \Delta x_i^2 \qquad (21)$$

where Γ_i is the rate at which an atom makes a particular jump associated with a change Δx_i in the x co-ordinate. Referring to Figure 6 it is evident that each atom in a face-centered cubic structure can make twelve equivalent diffusion jumps, eight of which result in a change of a/2 in the x co-ordinate. The probability of a forward jump is 1/3, of a backward jump is 1/3, and of a jump which leaves x unchanged is 1/3. Assuming a vacancy model, diffusion can only occur when the site towards which the migrating atom is moving is unoccupied. If p is the probability that a particular lattice site is vacant, Equation (21) becomes

$$D = \tfrac{1}{2} \cdot 12 \cdot 2/3 \quad (a/2)^2 \; p$$

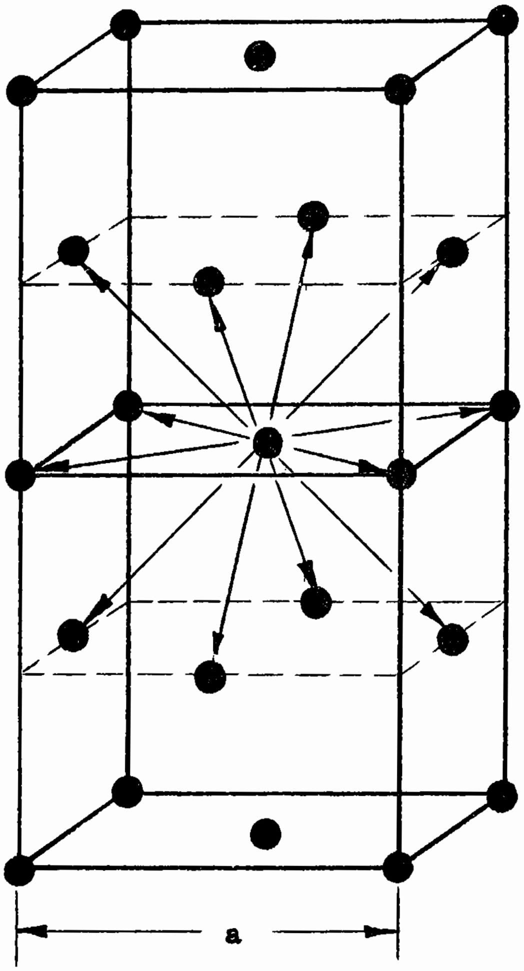

Figure 6. Twelve Equivalent Diffusion Jumps in a Face-Centered Cubic Lattice

thus

$$D = p\,a^2/\tau , \quad (\Gamma = 1/\tau) \qquad (22)$$

where

τ = Mean time of stay between diffusion jumps - sec.

a = Lattice parameter - cm.

Using the same assumptions as Eyring[80,81] but paying closer attention to the particular case of solid state diffusion, Wert and Zener[82] deduced the following expression for τ

$$1/\tau = \nu e^{-\Delta G_2/RT} \qquad (23)$$

where

ΔG_2 = The isothermal work required to move an atom from its equilibrium position to the top of the energy barrier separating adjacent sites.

ν = Frequency of vibration of atoms about their normal lattice sites, generally taken to be the Debye frequency - sec^{-1}.

Combining Equations (14), (22) and (23)

$$D = a^2 \nu \, e^{-(\Delta G_1 + \Delta G_2)/RT} \qquad (24)$$

where

ΔG_1 = The change in free energy necessary to form a vacancy at constant temperature, apart from that contributed by changes in missing entropy.

With each change in free energy, ΔG, there is associated a corresponding change in entropy, ΔS, and heat content, ΔH. Thus Equation (24) becomes

$$D = a^2 \nu\, e^{(\Delta S_1 + \Delta S_2)/R}\, e^{-(\Delta H_1 + \Delta H_2)/RT} \qquad (25)$$

By differentiating the above expression with respect to temperature the heat of activation, $\Delta H_1 + \Delta H_2$, can be identified with the experimentally determined activation energy, Q. Therefore

$$D_o = a^2 \nu\, e^{(\Delta S_1 + \Delta S_2)/R} \qquad (26)$$

and

$$Q = \Delta H_1 + \Delta H_2 \qquad (27)$$

The calculation of any of the quantities ΔS_1, ΔS_2, ΔH_1 and ΔH_2 has not been satisfactorily performed as yet, even for a single metal. As an alternative it should be possible to relate these functions to other physical properties of the lattice. Then the correlation coefficients for each face-centered cubic metal, for which the self-diffusion coefficient has been measured, can be calculated. Identical values for these constants will indicate that the experimental results are consistent, within the assumptions made, with the model chosen to derive expressions for D_o and Q.

This procedure has been followed by Le Claire[41], and Buffington and Cohen[42], who have applied Zener's[83,84] lattice strain theory more carefully to the case of self-diffusion in cubic metals. Le Claire[41] in particular has shown that the experimental results for face-centered cubic metals are consistent only with a vacancy model.

Le Claire's equations for D_o and Q

In the derivation of Equation (23) the term ΔG_2 is associated with the isothermal work done in moving an atom from its equilibrium position to the top of the potential barrier separating adjacent lattice sites. Assuming that all the isothermal work[85] is expended in straining the lattice the value of ΔG_2 can be related to the elastic properties of the lattice. If ϵ represents the strain produced by the diffusing atom and μ is the appropriate shear modulus, then the strain energy per unit volume is $\frac{1}{2}\mu\epsilon^2$. If the further assumption is made that the strains are geometrically similar in similar lattices, and are localized in volumes proportional to the atomic volume of the lattice, then

$$\Delta G_2 = K(\tfrac{1}{2}\mu\epsilon^2)(M/\rho)$$

giving

$$\Delta G_2 = k_2\ \mu\ M/\rho \qquad (28)$$

The choice of modulus μ depends on the type of strain the diffusing atom produces. In Figure 7 the basic act of diffusion can be represented by a jump of the front face-centered atom $(1, \frac{1}{2}, \frac{1}{2})$ to the vacant site $(\frac{1}{2}, 1, \frac{1}{2})$ in the center of the right hand face. As shown in Figure 8 the intervening "barrier" atoms in the $(1\bar{1}0)$ plane are displaced in $\langle 112 \rangle$ directions when the migrating atom is in the saddle position. The resulting $\langle 112 \rangle$ strain can be resolved into a $\langle 001 \rangle$ and a $\langle 110 \rangle$ strain in the $(1\bar{1}0)$ plane. The atom movements in the $\langle 001 \rangle$ directions are similar to those occurring in a $(1\bar{1}0)$ $\langle 001 \rangle$ shear for which the appropriate modulus is c_{44}. Similarly, movement in the $\langle 110 \rangle$ direction is related to a $(1\bar{1}0)$ $\langle 110 \rangle$ shear for which the modulus is $\frac{1}{2}(c_{11} - c_{12})$. Le Claire assumed the appropriate modulus to be the sum of these moduli. Therefore

$$\mu = \frac{1}{2}(c_{11} - c_{12}) + c_{44} \tag{29}$$

where c_{11}, c_{12} and c_{44} are the moduli of elasticity for the cubic system.

Making use of the thermodynamic relation $\Delta S = -\partial \Delta G / \partial T$, an expression for ΔS_2 can be deduced from Equation (28),

$$\Delta S_2 = -k_2 M \frac{\partial(\mu/\rho)}{\partial T} \tag{30}$$

The temperature variation of the shear moduli of polycrystalline metals is approximately linear below the temperatures where viscous slip occurs on the grain boundaries[86]. If it is also assumed that the density varies linearly with temperature,

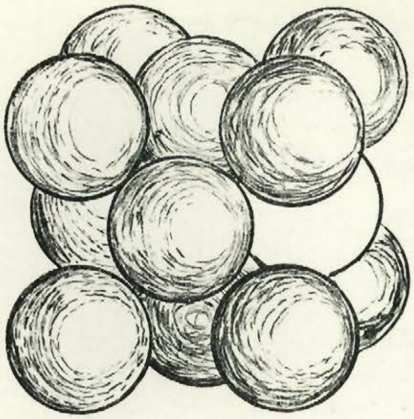

Figure 7. The Face-Centered Cubic Structure Regarded as Being Derived by the Close Packing of Spheres. Consider the Elementary Act of Diffusion as the Movement of the Front Face-Centered Atom to the Vacant Site in the Center of the Right Hand Face.

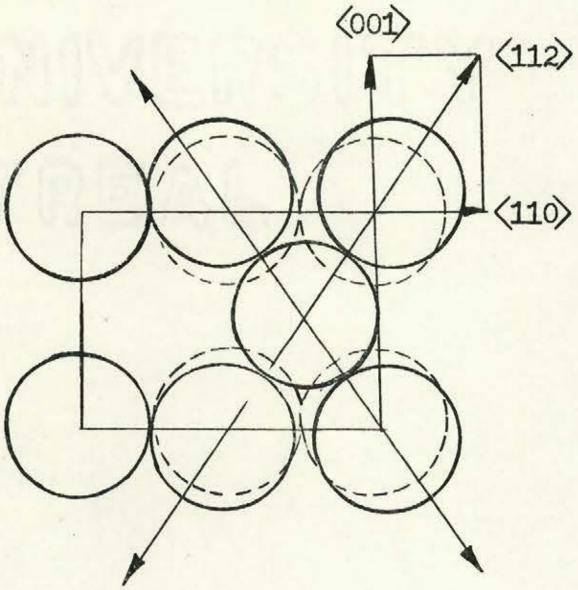

Figure 8. Direction of Displacement of Barrier Atoms when Diffusing Atom is in Saddle Position. The Barrier Atoms are Located in a (110) Plane.

Equation (30) becomes

$$\Delta S_2 = - k_2 M \frac{\mu_o}{\theta_o}\left[\frac{\mu'}{\mu_o} - \frac{\theta'}{\theta_o}\right] \qquad (31)$$

where μ' and θ' are μ and θ respectively differentiated with respect to temperature, and μ_o and θ_o are the values of μ and θ extrapolated to 0°K. The temperature coefficient of the elastic moduli is always negative, and because $\mu'/\mu_o > \theta'/\theta_o$ the strain entropy will always be positive. It also follows that

$$\Delta H_2 = k_2 M \mu_o/\theta_o \qquad (32)$$

It has been suggested[87] that the change in energy, ΔH_1, on forming a vacancy is proportional to the latent heat of sublimation, L_s, of the lattice. Thus

$$\Delta H_1 = k_1 L_s \qquad (33)$$

Combining Equations (27), (32) and (33) gives

$$Q = k_1 L_s + k_2 M \mu_o/\theta_o \qquad (34)$$

The change in entropy, ΔS_1, arises solely from the greater freedom of motion permitted the atoms surrounding the vacancy, resulting in these atoms having reduced frequencies of vibration. Thus the value of ΔS_1 is also positive. Le Claire neglects this contribution to the total entropy change as being small compared to ΔS_2. An order of magnitude calculation performed in Appendix 1 shows that the use of the bulk values of the elastic moduli in calculating ΔS_2, rather than the local values, partially compensates for this omission. The expression for the frequency factor D_o from Equation (26) and (31) is

$$D_o = a^2 \nu \exp \left[S_1(=0) - k_2 M \frac{\mu_o}{\rho_o} \left(\frac{\mu'}{\mu_o} - \frac{\rho'}{\rho_o} \right) \right] / R \qquad (35a)$$

or substituting for k_2 from Equation (34)

$$D_o = a^2 \nu \exp \left[S_1(=0) - (Q - k_1 L_s) \left(\frac{\mu'}{\mu_o} - \frac{\rho'}{\rho_o} \right) \right] / R \qquad (35b)$$

Le Claire, using selected data for the self-diffusion of Au, Ag, Cu and Pb, obtained average values of $k_1 = 0.215$ and $k_2 = 0.215$ using Equations (34) and (35b).

Buffington and Cohen's equations for D_o and Q

Using the same basic approach as Le Claire, Buffington and Cohen deduced a similar pair of equations for correlating the measured values of D_o and Q in face-centered cubic metals. Referring to Figure 8, it may be seen that the barrier atoms are displaced in $\langle 211 \rangle$ directions when the migrating atom is in the saddle position. To calculate the strain energy involved in this event, they have selected as the shear modulus Young's Modulus, E_{211}, for the $\langle 211 \rangle$ direction in a cubic crystal. This difference in choice of modulus does not noticeably affect the degree of correlation, as the ratio of E_{211}/μ is relatively constant for the face-centered cubic metals. The value of this ratio for some metals of interest is recorded in Table 2.

Table 2

Comparison of E_{211} and μ

Metal	E_{211} kcal./cm.^{3}	μ kcal./cm.^{3}	E/μ
Pb	7.28	5.41	1.34
Ag	21.6	15.5	1.40
Au	21.2	14.4	1.47
Cu	35.2	25.4	1.39
Ni	57.0	42.4	1.34

Values of E_{211} and μ calculated from data in Reference 88 and extrapolated to 0°K with data from References 89 and 90.

Le Claire's proposal for evaluating ΔH_1, the change in enthalpy necessary to form a vacancy, is

$$\Delta H_1 = k_1 L_s \qquad (33)$$

Buffington and Cohen used a different approach and assumed that a constant fraction of the activation energy, λ , is associated with straining the lattice. Therefore

$$\lambda = \frac{\Delta H_2}{\Delta H_1 + \Delta H_2} = \frac{\Delta H_2}{Q} \qquad (36)$$

The final expressions for D_o and Q are

$$D_o = a_o^2 \nu \exp \lambda K E_{211} a_o^3 (\phi - 3\alpha) / R \qquad (37)$$

and

$$Q = K E_{211} a_o^3 N \qquad (38)$$

where

E_{211} = Young's Modulus along the <211> direction in a cubic crystal evaluated at 0°K (see Appendix 1) - kcal./cm.^{3}

a_o = Lattice parameter at 0°K - cm.

N = Avogadro's number

$\phi = -\frac{1}{E_o}\frac{dE}{dT}$ - deg.$^{-1}$

$\alpha = -\frac{1}{a_o}\frac{da}{dT}$ - deg.$^{-1}$

and K and λ are the correlation coefficients. Using the accurate self-diffusion data for silver the values of λ and K are respectively 0.64 and 0.0514.

As Buffington and Cohen pointed out it is difficult to choose whether Equation (34) or Equation (38) is the better expression for the activation energy. This arises because of the proportionality existing between $k_1 L_s$ and $E_{211} a_o^3 N$, as illustrated in Table 3.

Table 3

Proportionality Between k_1 L_s and E_{211} a_o^3 N

Metal	E_{211} a_o^3 N kcal./mole	L_s kcal./mole	E_{211} a_o^3 N/Ls
Pb	531	46.5	11.4
Ag	885	69.0	12.8
Au	870	82.3	10.6
Cu	995	81.2	12.3
Ni	1475	101.1	14.6

A calculation of Q from macroscopic considerations

Brooks[91] recently proposed a method for calculating the activation energy required to form a vacancy. He assumed that the formation of a vacancy is equivalent to creating new surface area in the lattice corresponding to one atomic volume. To preserve the total volume, the atom removed to form the vacancy must be placed on the exterior of the lattice. For a low concentration of vacancies the resultant increase in external lattice surface area is negligible. The formation energy of a vacancy, f_v, becomes

$$f_v = 4 \pi r_s^2 \gamma N \qquad (39)$$

where

r_s = Radius of sphere corresponding to one atomic volume - cm.

γ = Specific surface free energy (see Appendix 2) - kcal./cm.^{2}

However the forces of surface tension acting on the surface of this spherical cavity will tend to reduce its size by elastically distorting the lattice. Correcting Equation (39) for this distortional strain energy, and also for the accompanying decrease in surface area resulting from this contraction, the final expression for the formation energy is

$$f_v = 4\pi r_s^2 \gamma N \left[\frac{1}{1 + \frac{1}{2} \gamma / G' r_s} \right] \qquad (40)$$

where

G' = Rigidity modulus of the surrounding crystal (see Appendix 2) - kcal./cm.^{3}

An estimate of the activation energy required for an atom to diffuse can be calculated in a manner similar to that used previously. Referring to Figure 8, consider a sphere of radius r_o which is just small enough to slip in between the barrier atoms. Once this sphere is in the saddle position, it is expanded against the elastic forces until its radius is equal to the radius, r_s, of the other atoms in the lattice.

The total force acting across a spherical surface of radius r is

$$F_r = 16\pi G'' r^2 \ln(r/r_o) \qquad (41)$$

where

r_o = Initial radius of the sphere when the crystal is in equilibrium - cm.

G'' = Shear modulus appropriate to this circumstance (see Appendix 2) - kcal./cm.^{3}

The work done in expanding the sphere from r_o to r_s is

$$f_s = \int_{r_o}^{r_s} F_r\, dr = 8\pi G'' r_s^3 \left[2/3 \ln(r_s/r_o) - 2/9(1 - r_o^3/r_s^3) \right] \qquad (42)$$

The values calculated by Brooks[91] from equations (40) and (42) are entered in Table 4. A comparison with the experimental values make it apparent that little credence can be given to the magnitude of the calculated activation energies. However as the percentage overestimation is quite constant some reliance may be given to the predicted relative magnitudes of the different contributions to the energy. If this is true, it appears that 50 to 60% of the activation energy is required for vacancy formation. This is considerably higher than previous estimates varying from 35 to 45%[41-2,51-2].

These calculations may also be useful for correlating additional diffusion data. In particular it can be seen that the activation energy for lead self-diffusion is consistant with this treatment, which was not true for the emperical correlations considered previously (see Table 1).

Table 4

Calculation of Activation Energy for Self-Diffusion Using Macroscopic Concepts

Element	Saddle Point Energy fs $\frac{\text{kcal.}}{\text{mole}}$	Vacancy Formation Energy fv $\frac{\text{kcal.}}{\text{mole}}$	Total Activation Energy fs + fv $\frac{\text{kcal.}}{\text{mole}}$	Experimental Activation Energy Q $\frac{\text{kcal.}}{\text{mole}}$	Theory Exp. $\frac{fs + fv}{Q}$
Cu	46.1	41.9	88.0	46.1	1.85
Ag	39.9	43.8	83.7	45.7	1.82
Au	37.6	54.6	92.2	51.0	1.81
Al	27.6	33.5	61.0	32.8	1.89
Pb	22.5	26.8	49.3	26.8	1.83

Diffusion of solutes at low concentrations

Rhines and Mehl[92] measured the rate of diffusion of a number of metals in binary copper alloys having compositions in the alpha solution range. The values of D obtained for the various alloys tended to be approximately the same at low solute concentrations. This suggested that the values were characteristic of the solvent rather than the solute, and represented the self-diffusion coefficient of copper. This hypothesis was not confirmed by subsequent measurements of D for copper self-diffusion[26-9]. In general, particularly at low temperatures, the solute atoms diffused at much higher rates, and compared to the self-diffusion values the associated activation energies were as much as 50% lower, and the values of the frequency factor were often 10^{-5} times as small. Similar results have been reported for many other metals.

The following argument led Johnson[93] to conclude that these anomalous results were irreconcilable with a simple vacancy concept of diffusion. For diffusion to occur a solute atom must be adjacent to a vacant site. Then because the successive jumps of a vacancy and solute atom are assumed to be uncorrelated, the rate of diffusion of a solute atom will depend on the rate at which vacancies migrate to it through the solvent. Therefore at low solute concentrations the rate of migration of solute atoms should be comparable to the rate of self-diffusion of the solvent.

As an alternative, Johnson[93] proposed a mechanism based on the assumption that the solute atoms are less tightly bound to the lattice than solvent atoms. Once a vacancy migrates into one of these regions of lower binding forces it tends to be trapped there, forming a "solute-hole molecule". Then before the vacancy escapes, it is available for a multitude of exchanges with the solute atom and those solvent atoms which are nearest neighbours to both members of the complex. Diffusion of the solute atom through the lattice proceeds by a cyclic motion of the vacancy around the solute atom, as illustrated in Figure 9. With a low concentration of vacancies, the time taken for the vacancy to circumvent the solute atom should be short compared to the time taken for the random motion of a vacant site into the correct position for forward migration. Therefore solute diffusion should proceed more rapidly than solvent self-diffusion.

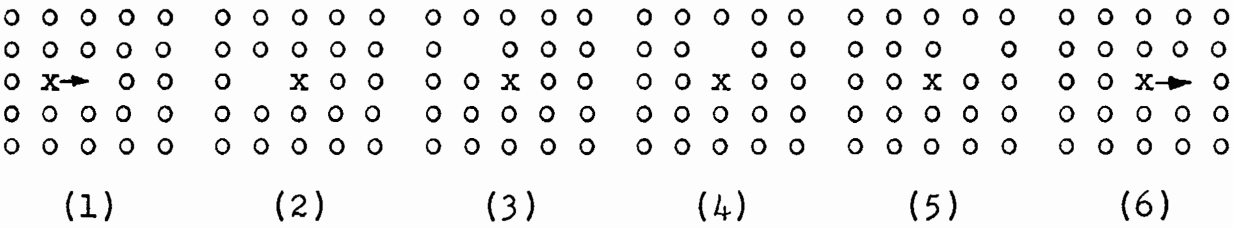

Figure 9. Cyclic Motion of Vacant Site in Johnson's Solute-Hole Molecule Theory.

The formation of a stable solute-hole molecule requires the assumption that the forces binding a solute atom to the lattice are smaller than those acting on solvent atoms. Therefore in this region of lower binding forces the activation energy required for a diffusion jump would be smaller than in the pure solvent. Also it was suggested that the observed D_0 values for solute migration would decrease exponentially (in comparison to the value for solvent self-diffusion) with the number of jumps taken for the vacant site to circumvent the solute atom. In this manner a qualitative explanation was given for the observed numerical values of D_0 and Q for solute diffusion.

Zener[83,84], in reviewing Johnson's solute-hole molecule theory, pointed out that the motion of a solute atom can be represented by the rate of migration of the solute-hole molecule's center of gravity. A statistical analysis of the motion of the center of gravity led to an expression for D_0 identical in form to that for self-diffusion of the solvent. Therefore, Zener concluded, it is valid to use Equation (26) to calculate the entropy change associated with solute diffusion. All the experimental data on which Johnson's mechanism was based gave negative entropies of activation. As this is physically impossible on the basis of Zener's lattice strain theory, the experimental data is now suspect. As emphasised by Zener[83,84], Nowick[94] and Le Claire[41], the diffusion coefficients measured at high temperatures seem to be reasonable, but the low temperature values appear to be erroneously high due to rapid diffusion along short-circuiting paths. Thus the low values obtained for D_0 and Q would appear to be due to errors in experimental technique.

The use of large chemical concentration gradients seems to enhance the tendency for grain boundary diffusion to occur. Barnes[95] demonstrated that diffusion in the presence of large concentration gradients causes polygonization inside individual grains situated in the diffusion zone. These small areas inside the grains differ in orientation by as much as two degrees. If diffusion along edge dislocations is as rapid as has been suggested[64], the presence of this multitude of short-circuiting paths could account for the erroneously low values for D_o and Q obtained by techniques involving a large concentration gradient.

The use of high specific activity radioactive tracers permits the use of much smaller chemical concentration gradients in solute diffusion studies, minimizing these short-circuiting tendencies. The results of recent investigations confirm Zener's critism of the older data, and suggests the following interpretation of diffusion at low solute concentrations. When the solute and solvent atoms have a similar number of valence electrons, and similar atomic radii, the values of D_o and Q obtained for solute diffusion correspond quite closely to those obtained for self-diffusion of the solvent. This is illustrated by a comparison of the data for gold diffusing into copper and for copper self-diffusion.

$$D_{Au}^{Cu} = 0.1\ e^{-44,900/RT} \qquad \text{(Reference 96)}$$

$$D_{Cu}^{Cu} = 0.32\ e^{-46,800/RT} \qquad \text{(Reference 29)}$$

However when the solute atoms have an excess or deficit of valence electrons compared to the solvent atoms, there appear to be marked differences in the D_o and Q values obtained for solute diffusion into the solvent compared to solvent self-diffusion. For example compare the following results for the diffusion of antimony into silver single crystals, and for silver self-diffusion. (Antimony has four extra valence electrons)

$$D^{Ag}_{Sb} = 0.167\ e^{-38,200/RT} \qquad \text{(Reference 97)}$$

$$D^{Ag}_{Ag} = 0.72\ e^{-45,500/RT} \qquad \text{(Reference 69)}$$

The above results have been theoretically interpreted by Lazarus[98]. Starting with the values of D_o and Q for the solvent, he calculated expressions for D_o and Q for solute diffusion, taking into account the screened coulomb potential surrounding the impurity atom. These expressions indicate that electronegative impurities should diffuse more rapidly than solvent self-diffusion, and electropositive elements should diffuse more slowly.

Object of research

Le Claire[41], Buffington and Cohen[42], and Brooks[91] have deduced equations for correlating the rate of self-diffusion in a metal to its elastic properties. However the data for only four face-centered cubic metals are suitable for testing the validity of these expressions. To provide a further test it seemed of interest to study the rate of nickel self-diffusion. This is a particularly interesting metal, as it is the only one of the three transition elements, cobalt, iron and nickel, whose elastic properties are known sufficient to permit this correlation. (Iron and cobalt assume a face-centered cubic structure only above temperatures of 910°C and 600°C respectively, making it difficult, if not impossible, to obtain the requisite elastic parameters).

The transition elements form an interesting group of metals in that, with few exceptions, they have an identical number of valence electrons. Hence if the existing concepts of diffusion at low solute concentration are correct, it would be expected that the rates of diffusion of Ni^{63} into iron and into cobalt should be in close agreement with the rates of self-diffusion of these metals. To test the validity of this statement the rates of diffusion of Ni^{63} into iron and cobalt have been measured.

To further our knowledge of the concentration dependence of intrinsic diffusion coefficients, the rates of diffusion of nickel in two iron-nickel alloys, 6% and 16% Ni, have been measured. Because of the widespread use of nickel as an alloying element in steel, these results may eventually be of some practical use in interpreting the effect of nickel on the transformation properties of nickel-steels.

EXPERIMENTAL TECHNIQUES AND RESULTS

Part 1 - Characteristics of Ni^{63}

Diffusion measurements

Diffusion coefficients obtained by the use of radioactive tracers are measured most commonly by either of two methods, sectioning or surface activity techniques. In both methods a thin layer of radioactive material is deposited on the surface of a prepared metal disc. Then after a suitable period for diffusion at temperature, the diffusion coefficient is evaluated by determining the concentration and extent of the tracer's penetration into the disc.

In the sectioning technique the sample is mounted in a lathe and thin slices are machined off parallel to the active surface. After the specific activity of each slice is determined, a concentration-penetration curve can be drawn. The diffusion coefficient can be calculated from this curve using Equation (18). This technique has yielded the most dependable diffusion data.

In the surface activity technique the diffusion coefficient is calculated from the decrease in surface activity caused by diffusion of the active material into the specimen. This decrease results from the absorption of the radiation emitted from the active atoms located below the surface of the specimen.

A disadvantage here is that the shape of the concentration-penetration curve is not determined. However this method can be used to measure much smaller diffusion coefficients than the sectioning technique, as much smaller penetrations are required to obtain results of comparable accuracy.

The application of both methods depends on a knowledge of the counting characteristics of the tracer, particularly in the case of the surface activity technique. The following section deals with the preliminary experiments performed to obtain this information. For simplicity of presentation the relevant theory is presented in each individual section along with the experimental results.

Relative counting of a beta-emitting nuclide

When a radioactive source is placed under a counter only a fraction of the total number of disintegrations occurring in the source is detected. The counting rate, m, of a radioactive source is related to the actual number of disintegrations, D, occurring in the source by the expression[99]

$$m = D\,E\,f_{\tau}\,f_b\,f_w\,f_s \qquad (43)$$

where

E = Counter efficiency, which depends on its intrinsic sensitivity to beta-particles and the solid angle over which particles emitted from the source are detected.

f_τ = Correction factor for dead-time losses. The number of recorded counts will, in general, be smaller than the number of ionizing events occurring in the counter because of its inability to resolve closely spaced events.

f_b = Correction factor for backscattering. When a source is mounted on a thick backing, some particles emitted originally in a direction away from the counter are reflected back to the counter.

f_w = Correction factor for absorption in counter window, intervening gas, absorbers, etc.

f_s = Correction factor for self-absorption in the source.

The expression is simplified considerably when an internal source counter with a 2π geometry is used, as the factor $E\ f_w$ is a constant. By using source mounts which behave as infinitely thick backscatterers the factor f_b is also constant. Equation (43) then becomes

$$m = K\ D\ f_\tau\ f_s \qquad (44)$$

where

$$K = E\ f_w\ f_b$$

It is not necessary to know the value for K in determining the relative specific activity of a series of sources. Hence it is sufficient to determine the dead-time loss correction for the counter, and the self-absorption curve for the nuclide being counted.

Long-lived nickel isotopes

The active nickel used in this research was prepared by exposing three rods of spectrographically pure nickel metal to a thermal neutron flux. The metal was obtained from Johnson, Matthey and Company Limited, who supplied the analysis given in Table 5. The irradiation, of two weeks duration, was performed in the nuclear reactor at the Brookhaven National Laboratory. The two long-lived nickel isotopes produced by (n, γ) reactions are Ni^{63} decaying by the emission of a beta-particle, maximum energy 61.5 - 67 kev[100, 101], half-life 85 ± 20 years[101], and Ni^{59} decaying by K-electron capture with the emission of a Co K_α X-ray, half-life 7.5×10^{4} years[101]. In a predominantly thermal neutron flux, a minimum of iron and cobalt impurities is formed by (n, α) and (n,p) reactions respectively.

The activated material was stored for several months to permit any short-lived impurities and short-lived nickel isotopes to decay. After this period the sample continued to emit gamma radiation indicating the presence of a radioactive impurity. (Ni^{59} and Ni^{63} are known not to decay with the emission of gamma rays). Because of the long half-life of the impurity and the high purity of the nickel metal irradiated it was concluded

Table 5

Spectrographic Analysis of Nickel Rods

Element		Estimate of Quantity Present in Per Cent
Silicon		0.003
Magnesium		0.0005
Aluminum		0.0005
Iron		0.003
Copper		0.0002
Sodium	lines faintly visible	
Lead	lines barely visible	<0.001
Silver	detected by total combustion method	<0.0001

No lines of the following elements were observed:

As, Au, Bi, Cd, Co, Cr, Li, Mn, Sb, Sn, Ti, V, W, Zn, Zr.

that the impurity must have been formed by a nuclear reaction with one of the stable isotopes of nickel. The possible impurities, their modes of production, and the respective energies of the gamma rays emitted are shown in Table 6. The gamma spectrum of the material was determined using a NaI - Tl activated crystal scintillation spectrometer and an energy peak was found at 0.81 Mev. This tentatively identified the impurity as Co^{58}.

Table 6

Some Radioactive Impurities Formed From Nickel

Impurity	Reaction	Energy of the Gamma Rays Emitted-Mev
Fe^{55}	Ni^{58} (n,α) Fe^{55}	0.07
Fe^{59}	Ni^{62} (n,α) Fe^{59}	1.10, 1.30
Co^{58}	Ni^{58} (n,p) Co^{58}	0.805
Co^{60}	Ni^{60} (n,p) Co^{60}	1.115, 1.317

Purification procedure

The method chosen to separate the cobalt impurity from the active nickel was an anion exchange technique suggested by Moore and Kraus[102]. The separation is based on the fact that in concentrated hydrochloric acid solutions cobalt forms an anion complex $CoCl_3^-$, and nickel does not. Thus when a hydrochloric acid solution containing nickel and cobalt ions is passed through an anion exchange column, the cobalt is adsorbed on the resin, retarding its passage through the column, while the nickel passes directly through. The acid concentration range is critical, with best results obtained in a 9-M (molar) hydrochloric acid solution. This purification procedure has the additional advantage that any iron in the nickel solution is removed along with the cobalt.

The type of ion exchange apparatus used is illustrated in Figure 10. The column was 15 cm. long and had a 5 mm. bore. The lower 10 cm. was packed with Dowex-1, an anion exchange

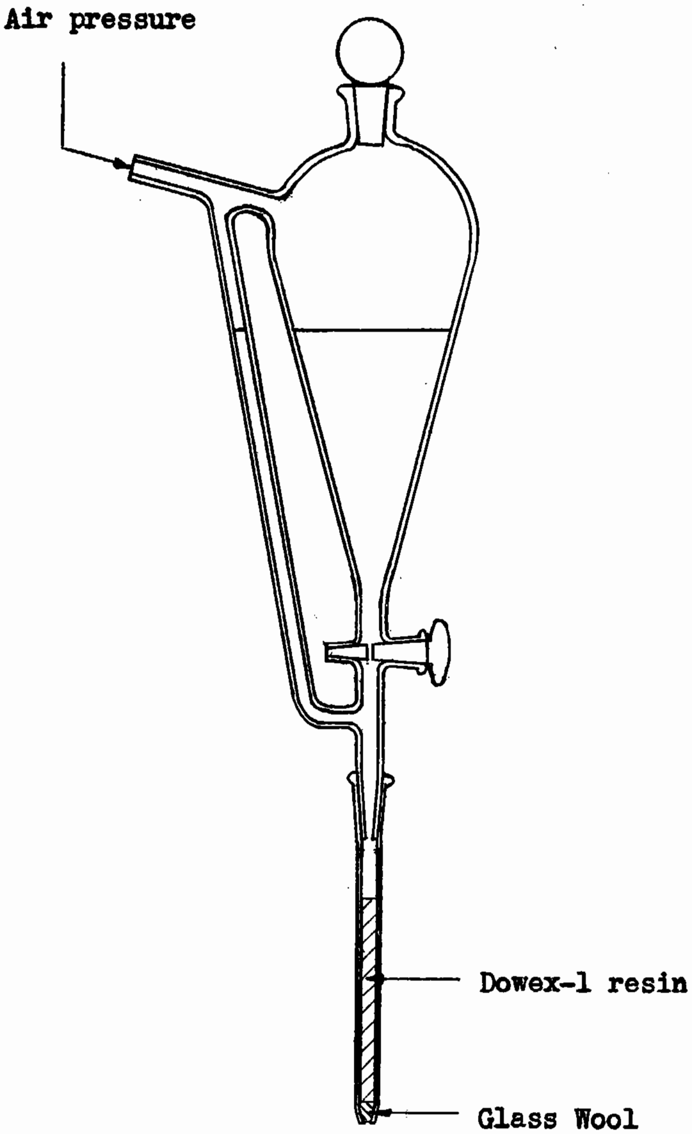

Figure 10. Anion Exchange Column

resin, the particle size of which varied from -200 to + 500 mesh. The use of this fine material made it necessary to apply air pressure - about 2 psi gauge - to force the solution through the column at reasonable rates. A 60-ml. separating funnel served as a reservoir for the impure solution. The stop-cock separating the reservoir from the column made it possible to pretreat the resin, and to remove adsorbed material from it without emptying the reservoir. The necessary reagents for these operations were added directly to the top of the column by breaking the joint connecting the column to the reservoir.

The purification of the active material was carried out in a "dry-box". A dry-box is a highly developed form of enclosed working space, access to which is provided by means of two long-sleeved rubber gloves, the cuffs of which are attached to special circular openings. This box is maintained at a negative pressure and the complete assembly protects the surroundings from contamination.

To perform a separation the nickel was first dissolved in hot concentrated hydrochloric acid. The resulting solution was evaporated to dryness, and the nickel chloride dissolved in sufficient 9-M HCl to form a 2-M $NiCl_2$ solution which was placed in the reservoir on top of the column. After the resin was prepared by acidifying it with 9-M HCl, a drop of inactive $CoCl_2$ solution was placed on top of the resin. This formed an intense blue band, which served as a visual marker to follow the descent of the cobalt complex. The stop-cock was then opened and the active solution was allowed to flow through the column.

For the column size specified, about 40 c.c. of active solution could be purified before the cobalt band had descended two-thirds of the length of the column. The stop-cock was then closed and the residual trace of active nickel was rinsed from the resin by passing successive additions of 9-M HCl down the column. The container holding the purified effluent was then removed and the adsorbed cobalt was eluted from the resin using distilled water.

Examinations of the purified nickel effluent showed no gamma radiation indicating that one pass through the column effected a complete separation.

Counting equipment

Ni^{59} decays by K-electron capture followed by the emission of a Co K_α X-ray to form the stable isotope Co^{59}. Ni^{63} decays to stable Cu^{63} by the emission of a β^--ray ($\sim$ 67 kev) which is so soft that it is completely absorbed in the window of a standard end window counter. For this reason an internal source proportional counter with a 2π geometry (AEP CFIS 2) was used throughout these experiments. The details of the counter are shown in Figure 11. The counter's chamber consists of a short

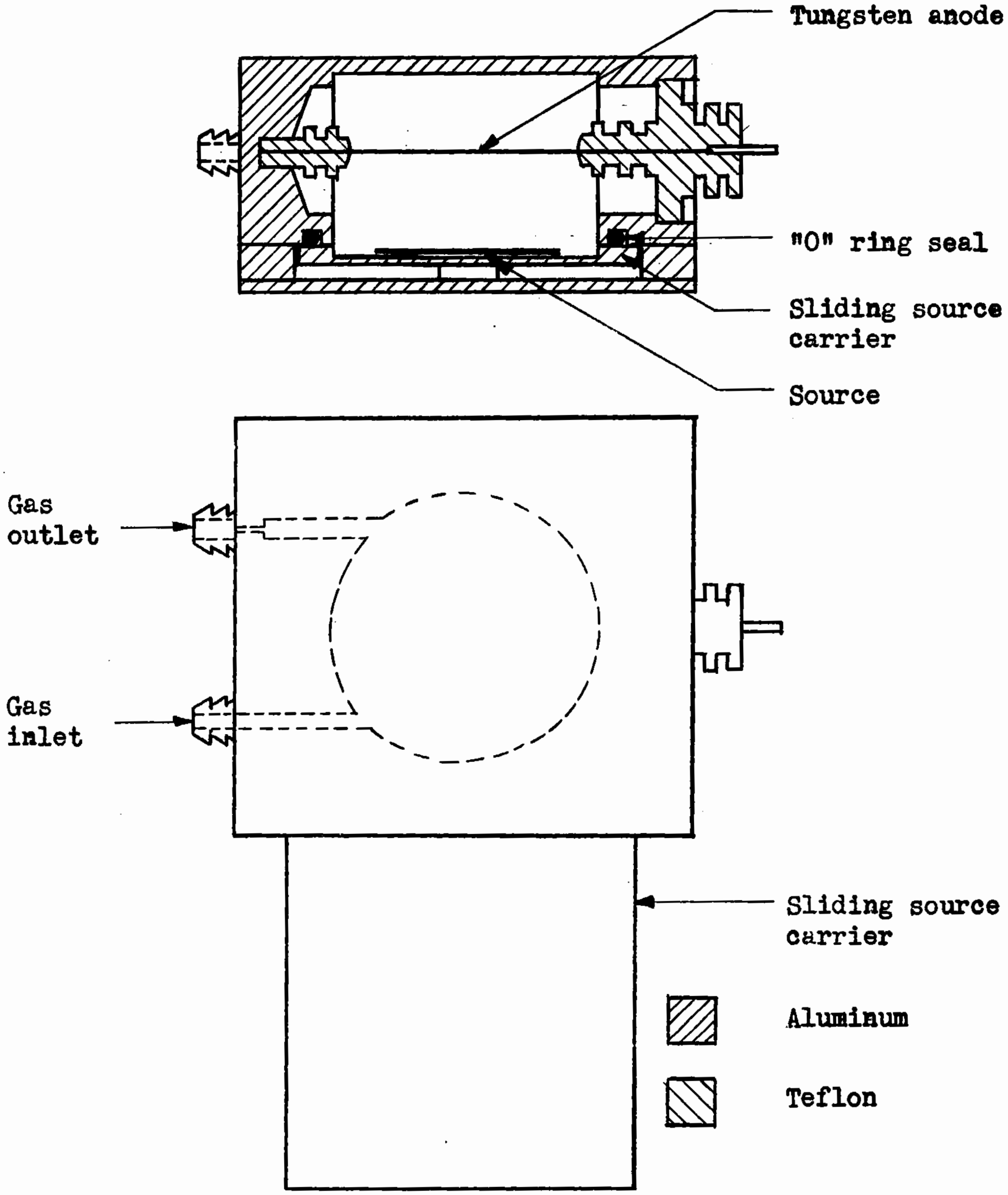

Figure 11. 2π Constant Flow Internal Source Proportional Counter

right cylindrical cavity with a horizontal tungsten anode stretched perpendicular to the axis of the cylinder. The source is introduced into the bottom of this cavity by a sliding aluminum plate which contains a depression for the source. Providing the source to anode distance is unaltered, a variety of counter bottoms can be used to accomodate different source sizes without changing the counter's characteristics.

The pulse from the counter was amplified (~2000) by an AEP-1448 amplifier-discriminator unit and then fed into a Marconi AEP-908 scale of 1000. The proportional chamber was mounted directly on the front panel of the amplifier-discriminator which plugged into the same base unit as the scaler. A Dynatron Radio Limited 4000 volt power supply (P 200 A) provided the anode potential. The counter gas used was C.P. methane dried with silica gel and flowed through the counter at a rate of two bubbles per second after an initial rapid preflushing period.

A proportional counter operates in what is known as the region of proportionality[99]. In this region, each electron produced by the primary ionizing event initiates an electron avalanche in the vicinity of the anode. As the avalanches are of similar size, the total charge, Q, collected at the anode, is proportional to the number of ions formed in the initial ionizing event which is dependent on the energy and type of radiation.

This charge produces a voltage pulse $V = Q/C$ (where C is the capacity of the anode to ground). As the potential across the chamber is increased the magnitude of V increases sharply. Eventually enough amplification is produced that even the weakest ionizing event produces a sizeable pulse. All pulses over a certain size trigger the associated electronic apparatus and are recorded on the scaler.

A beta-emitting nuclide emits electrons having a continuous energy spectrum, varying from a low energy to the maximum allowable for the transition. Hence as the voltage increases across the chamber, the most energetic particles are the first to produce a pulse large enough to trigger the scaler. With further increases a voltage is eventually reached where even the weakest beta-particles can be detected. Any further increase in voltage does not produce an increase in counting rate as all the beta-particles have already been detected. Thus a region, called the plateau, exists where the counting rate is very nearly independent of the applied anode potential. The length of the plateau indicates the useful range of voltage which may be used to operate the counter.

The position of the plateau in any counter is dependent on the energy of the beta-particles being counted. For this reason the high voltage characteristics of the proportional counter were determined using a Ni^{63} source, and are shown in Figure 12. The plateaus have negligible slopes, less than

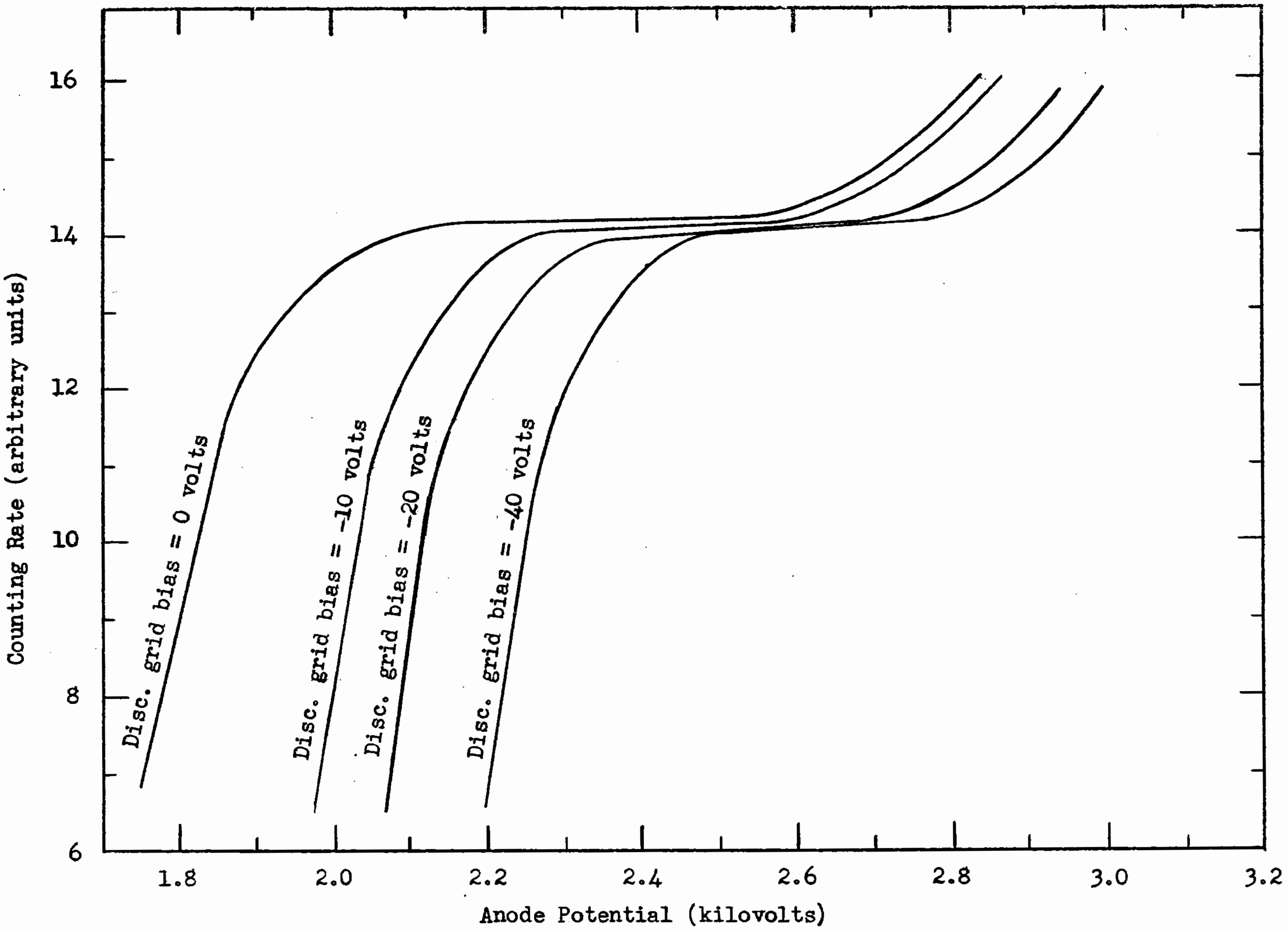

Figure 12. High Voltage Characteristics of the 2 π Proportional Counter for Ni^{63} Beta Radiation.

0.5%/100 volts, and are about 400 volts in length. Thus when the counter is operated 100 volts above the threshold of the plateau, small fluctuations in anode potential have a negligible effect on the counting rate. This also ensures that all ionizing particles are being counted.

The size of the voltage pulse required to trigger the scaling circuit may be increased by varying the negative bias applied to the grid of the input tube in the amplifier-discriminator. Other than shifting the position of the plateau, it can be seen that the only effect of increasing the grid bias is to decrease the counting rate slightly. This indicates that very few, if any, spurious counts are recorded due to stray electronic phenomena. Because of the flat plateau and the negligible effect caused by varying the grid bias, it may be assumed that the accuracy with which a particular source may be counted depends solely on counting statistics.

Counting statistics

The decay of a radioactive nuclide is a random phenomenon subject to the laws of statistics[99]. The statistical variations of a counting rate, R, are most commonly expressed in terms of the standard deviation σ. The standard deviation is defined by the expression

$$\sigma = \sqrt{R\ t} \qquad (45)$$

where

t = Total counting time.

The standard deviation is related to the probable accuracy of an individual measurement. The probability, P, that an individual counting rate lies within the following limits, expressed in terms of the standard deviation, σ, is given in the following tabulation.

Probability in per cent	Limits
68.3	± σ
90.0	± 1.65 σ
95.4	± 2.0 σ
99.7	± 3.0 σ

As it is clearly impossible to define an error limit, the common practice of expressing the confidence limits as ± σ has been followed in this research.

During the normal operation of a counter a certain background counting rate registers even in the absence of a source. This is due to cosmic radiation, and possibly from neighbouring sources. When an active source is counted this is included in the total activity and must be deducted to give the true activity. The standard deviation, σ_c , of the corrected counting rate is given by the expression

$$\sigma_a = \sqrt{\frac{c}{t_c} + \frac{b}{t_b}} \qquad (46)$$

where

c = Counting rate due to activity and background - c.p.m.

b = Background - c.p.m.

t_c = Counting time for source - minutes.

t_b = Counting time for background - minutes.

When the available counting time is limited, the above expression is minimized when the times taken to count the sample and to determine the background are related by

$$\frac{t_b}{t_c} = \sqrt{\frac{b}{c}} \qquad (47)$$

Dead-time loss correction

At low disintegration rates the number of recorded counts is equal to the number of ionizing events. At higher rates however, the number of recorded counts is lower because closely spaced events may not be resolved in either the chamber and/or the auxiliary electronic circuits. The magnitude of this coincidence loss was determined using the two source method. (See reference 99 for a complete description of the procedure). In this technique the sum of the measured activities of two single sources is compared to the measured activity of the two sources combined. The experimental results are summarized in Figure 13. When the coincidence loss is small, the accuracy with which it can be determined is quite low as it is obtained from the difference between two large numbers. However as the magnitude of the coincidence loss increases, the accuracy of its determination increases accordingly. Even at 10^5 c.p.m. the correction is less than two per cent. For counting rates below 10^4 c.p.m. the dead-time loss correction ($\leqslant \pm 0.6\%$) is negligible compared to the counting statistics generally employed ($\pm 1\%$) and has been neglected.

The dead-time can be calculated from the following equation[99]

$$R^{*} = \frac{R}{1 - R\tau} \qquad (48)$$

where

R^{*} = Number of ionizing events per second.

R = Recorded counting rate - c.p.s.

τ = Dead-time - sec.

The dotted line in Figure 13 was calculated from Equation (48) assuming a constant dead-time of 14 microseconds. The difference between this line and the one drawn through the experimental points may not be significant. If it is significant, it may be due to one or a combination of two factors.

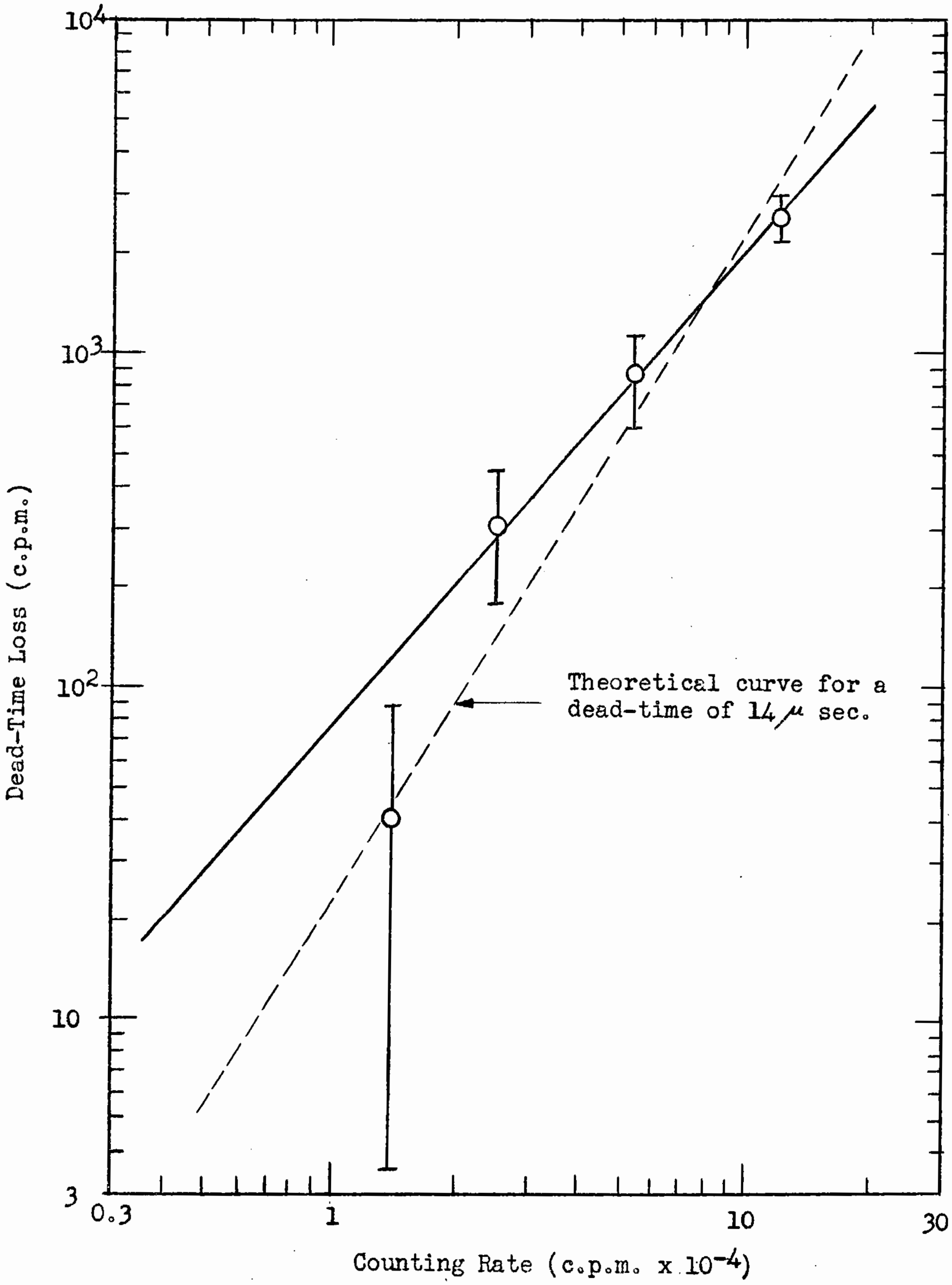

Figure 13. Dead-Time Loss Correction.

(1) Equation (48) does not adequately represent the conditions which cause this resolution loss. It is derived on the assumption that any event occurring during the period τ following the preceding event does not extend the dead-time. The validity of this assumption has been questioned[104].

(2) The dead-time is not a constant. It is commonly observed that the dead-time decreases with increasing counting rate.

Source mounting technique

All sources used in this work were prepared by electroplating active nickel onto one-inch diameter copper discs. The plating cells used are shown in Figure 14. To define accurately the area of the deposit, the polyethylene liners were made a force fit in the brass shells. However, the polyethylene tubing tended to contract with use, resulting in smaller deposits which were not always circular because the soft lining was no longer supported by the metal shell. This difficulty was overcome by placing the liners in warm water for 15 minutes before the cells were assembled. With this precaution the diameter of the deposits never varied by more than ± 0.005 inches, corresponding to errors in the area of the deposit of ± 1.5% (mean diameter of the deposit was 0.70 in.).

As the roughness of the source mount influenced the counting rate, all source mounts were cut from highly polished copper foil. This foil was visibly free from tarnish and the

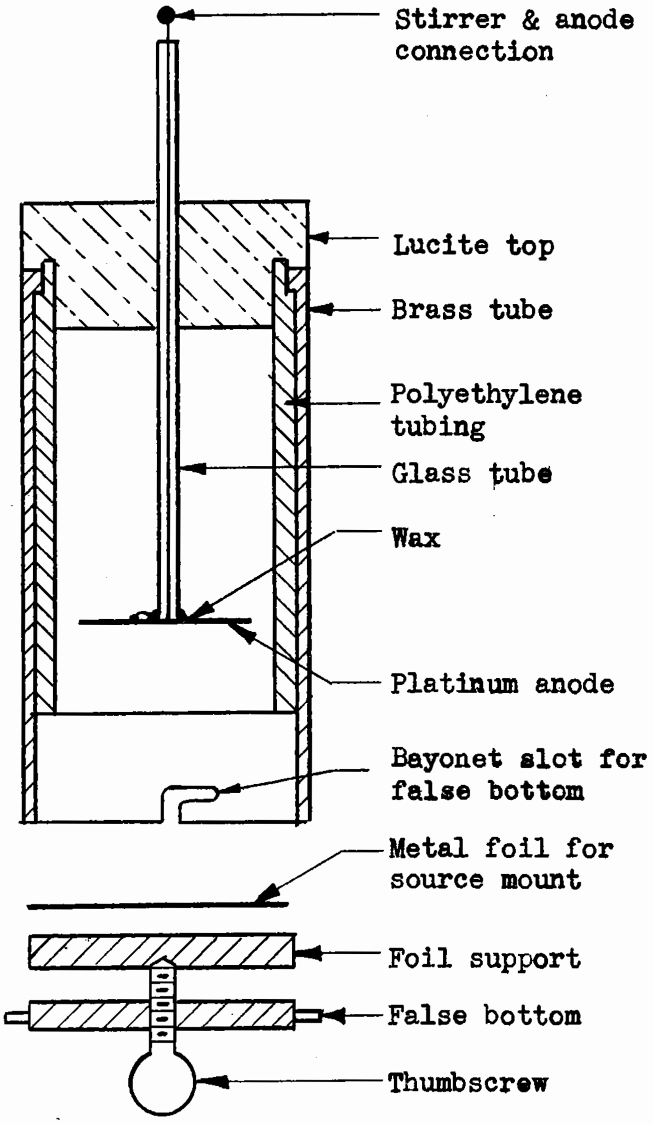

Figure 14. Electrolysis Apparatus

only precaution necessary to obtain adherent deposits was to remove any oil with carbon tetrachloride.

As an electrolyte the following stock solution was employed:

70 cc. conc. NH_4OH
30 cc. H_2O
10 gm. $(NH_4)_2SO_4$

Enough concentrated nickel chloride solution was added to this solution in the individual plating cells to prepare sources of the desired mass thickness. The nickel concentration was initially about 0.03 moles per liter. As this electrolyte readily attacks copper, it was essential that the anode and cathode be connected to the power supply before adding the plating solution.

The solution was stirred during deposition to remove bubbles formed by the considerable quantities of gas evolved at the anode and cathode. The minimum possible speed, about 60 r.p.m., was used as higher speeds tended to give a non-uniform deposit. Even at these low speeds the deposit on the periphery was several per cent thicker than in the center. The cell current density was 20 ma./cm^2.

External absorption curve for a nickel source

The absorption of beta and electromagnetic radiations generally obeys an exponential absorption law,

$$A_d = A_o e^{-\mu d} \tag{49}$$

where

A_o = The activity without an absorber.

A_d = The activity with an absorber.

d = The mass thickness of the absorber - mg./cm^2.

μ = The mass absorption coefficient - cm^2/mg.

For x-rays the value of μ depends only on the energy of the emitted radiation and the nature of the absorbing material. Thus it can be used as a means of identifying the decaying material. In the case of beta-radiation the exponential behaviour is a fortuitous result of the combined effects of scattering and the continuous energy spectrum of the radiation. At larger absorber thickness the exponential law breaks down and the beta-radiation exhibits a maximum range. This range is more commonly used to identify beta-emitters as it is less dependent on the geometrical arrangement of the source, counter and absorbers than is μ.

An external absorption curve was determined in order to confirm that the radioactive species in the active material were actually Ni^{59} and Ni^{63}, and to ascertain their relative counting rates. In addition to this essential information, the results permit an estimation of the maximum energy for Ni^{63} beta-particles, and an additional check on the radioactive purity of the material.

Referring to Figure 11 it can be observed that placing an aluminum foil layer over the active source transforms the counter into an end-window proportional counter. In addition to the reduction in counting rate caused by absorption of beta-particles in the absorber, further reductions are caused by absorption in the methane trapped between the foil and the source, and by scattering of beta-particles at the foil surface away from the chamber. These two latter effects can be eliminated by laminating the aluminum foil to the source with a thin layer of plastic.

The following procedure for this was found to be the most reliable. A 20 μ gm./cm^2. VYNS film was prepared on a wire frame as suggested by Pate and Yaffe[104]. The active side of the source was then wet with a thin layer of cyclohexanone, a solvent for VYNS resin. The source was passed slowly up through the film, and on contact the film over the source dissolved. This was repeated until the source no longer readily dissolved the film. Then the aluminum foil was smoothed on the coated source and it was put into an oven to dry at 120°C. When dry, the excess aluminum was trimmed and the source re-weighed to determine the mass thickness of the absorber. The advantage of using this laminating technique is that very thin uniform layers of plastic can be applied to laminate the aluminum foil to the source. For the thinnest foils employed the weight of aluminum was 0.225 mg./cm^2. and that of the plastic about 0.060 mg./cm^2. For thicker aluminum foils the ratio of aluminum to plastic increased accordingly.

Additional foils of various thicknesses were laminated onto the source to give the absorption curve shown in Figure 15. The laminating process apparently eliminated the scattering which usually occurs at the foil interfaces, because it was immaterial whether the thicker absorbers consisted of a single layer of thick foil, or one laminated from several thinner ones. The external absorption curve for Ni^{63} was obtained by subtracting the contribution of Ni^{59} from the total counting rate. This curve, shown in Figure 16, illustrates the commonly observed experimental fact that the absorption of beta-particles is an exponential phenomenon.

Referring to Figure 15 it can be seen that at zero absorber thickness, the ratio of the detected activities for Ni^{63} to Ni^{59} is 10^4. The half-thickness for Ni^{59} is approximately 9.0 mg./cm^2., indicating that no gamma background is present in the source. (When absorption is an exponential phenomenon the half-thickness is that thickness of absorber which reduces the observed activity by 50% and is equal to $0.693/\mu$). The calculated half-thickness for Ni^{63} is

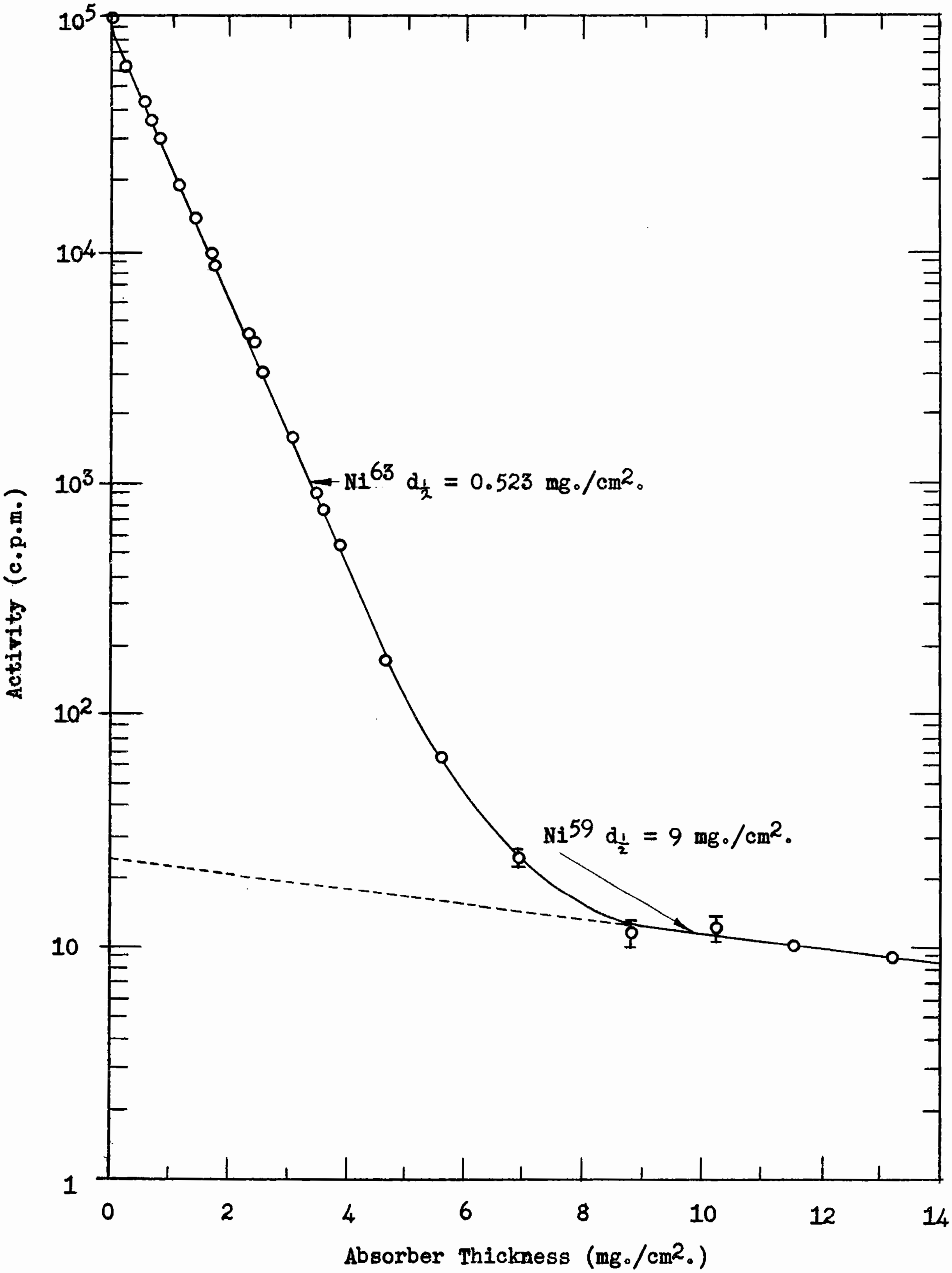

Figure 15. Absorption Curve for a Nickel Source in Aluminum (source thickness 1.40 mg./cm^2.)

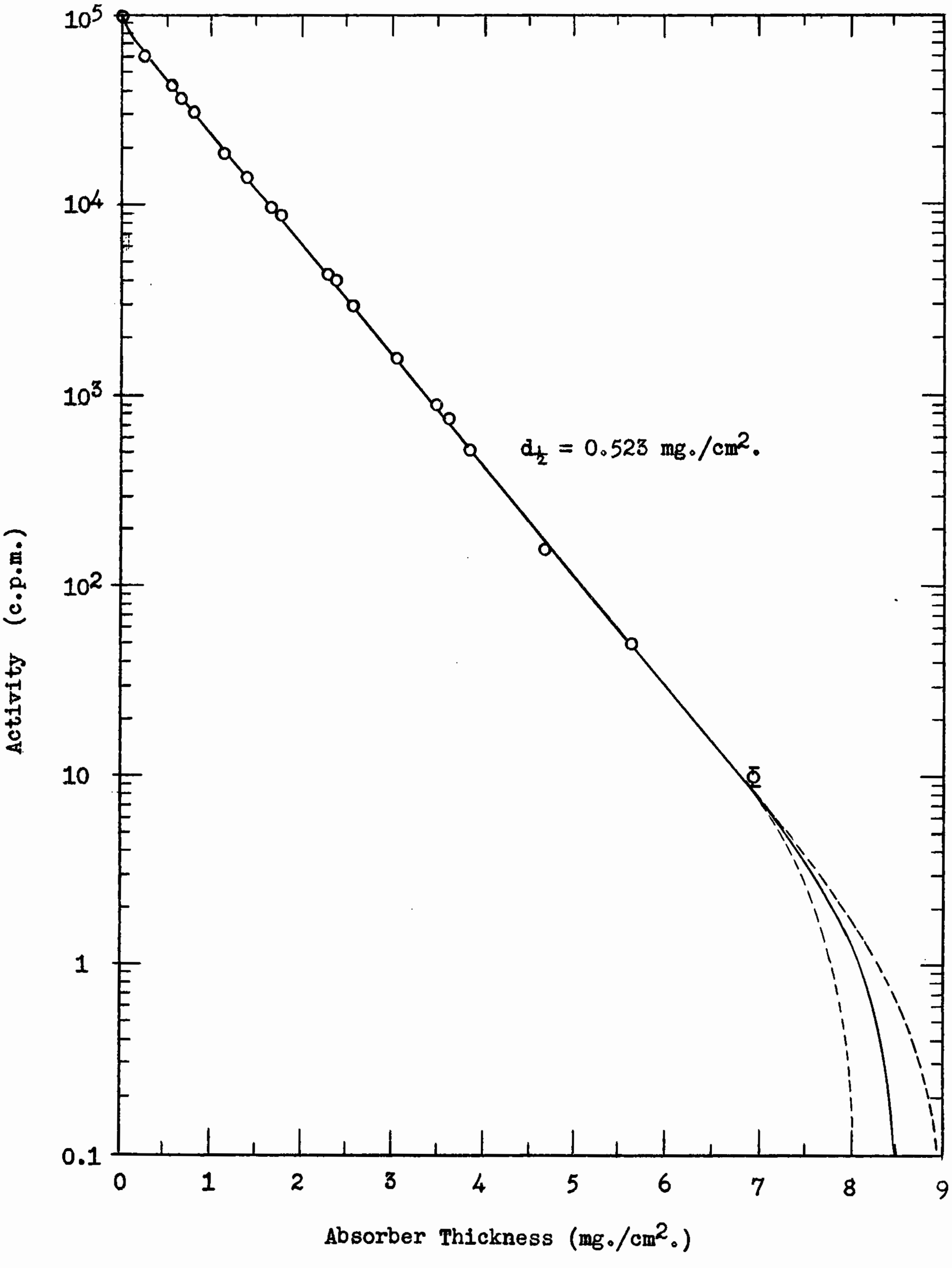

Figure 16. Absorption Curve for Ni^{63} in Aluminum

(source thickness 1.40 mg./cm^2.)

0.523 mg./cm^2. The maximum range for Ni^{63} in aluminum was determined visually as 8.5 ± 0.5 mg./cm^2. A Feather Plot[105] was not made because a standard in the same energy range is not yet available.

Self-absorption of Ni^{63} in nickel

With infinitely thin sources all the beta-particles emitted toward the counter are detected. However as the source thickness is increased, some of the beta-particles emitted by atoms lying beneath the surface are absorbed or scattered by the overlying layers of atoms. Thus the apparent specific activity of the material decreases as the source thickness is increased. If the activity, a, associated with a thin layer of atoms lying at a distance x beneath the surface is reduced to ae^{-kx} by absorption, it may be shown[99] that the counting rate for a source of thickness x is

$$A(x) = \frac{a_o}{k}(1 - e^{-kx}) \qquad (50)$$

where

$A(x)$ = Observed activity for a source of thickness x - c.p.m.

a_o = Specific activity of the source material - c.p.m. cm^2./mg.

k = Mass absorption coefficient - cm^2./mg.

x = Mass thickness of source - mg./cm^2.

The apparent specific activity of a source is $A(x)/x$, and for an infinitely thin source this is equal to the specific activity of the material a_o.

For thick sources Equation (50) reduces to

$$\underset{x \to \infty}{A(x)} = \frac{a_o}{k} \qquad (51)$$

Thus for thick sources the observed activity is directly proportional to the specific activity of the material. The required thickness, x, is somewhat less than the range determined in an external absorption experiment. The use of infinitely thick sources affords a simple method of determining relative specific activities of weak beta-emitters.

While Equation (50) has successfully interpreted the results of many investigations, it has been found that the value of k determined for any nuclide depends on the geometry of the counter. The greater the geometry the smaller the value of k associated with a given nuclide. Gora and Hickey[106] recently deduced an expression which gave identical k values for the self-absorption of C^{14}(β^- 0.156 Mev) in narrow and wide angle geometries.

Particles emitted at an angle Θ to a normal on the source surface traverse an effective thickness of source $x/\cos\Theta$ to reach the surface. Thus the activity of particles emitted at an angle Θ for a source of thickness x is

$$A(x, \Theta) = \frac{a_0 \cos\Theta}{k}\left(1 - e^{-\frac{kx}{\cos\Theta}}\right) \qquad (52)$$

The integrated values of this expression for a 2π geometry are plotted in Figure 17. The absorption effects arising from self-scattering in the source and from source mount backscattering are not included in this treatment. With the proper selection of k, a set of experimental results will coincide with the theoretical curve if they are consistent with the integrated form of Equation (52).

Gora and Hickey[106] also considered the case where a fraction, p, of the particles incident on the source mount are geometrically reflected back toward the counter. They were unable to extend this treatment to include the effects of back- and self-scattering in the source. Their integrated expression has been evaluated for $p = 0.5$, and for the hypothetical case $p = 1.0$ where all the particles incident on the source mount are backscattered into the counter. The effect of backscattering is to increase the apparent specific activity of the thin sources and to leave that of thick sources unchanged. As can be observed in Figure 17 the apparent specific activity initially decreases more rapidly when backscattering occurs. It will be noted that for convenience in Figures 17 and 18 the specific activity of the source material has been given the value unity and the values of the apparent specific activity adjusted accordingly.

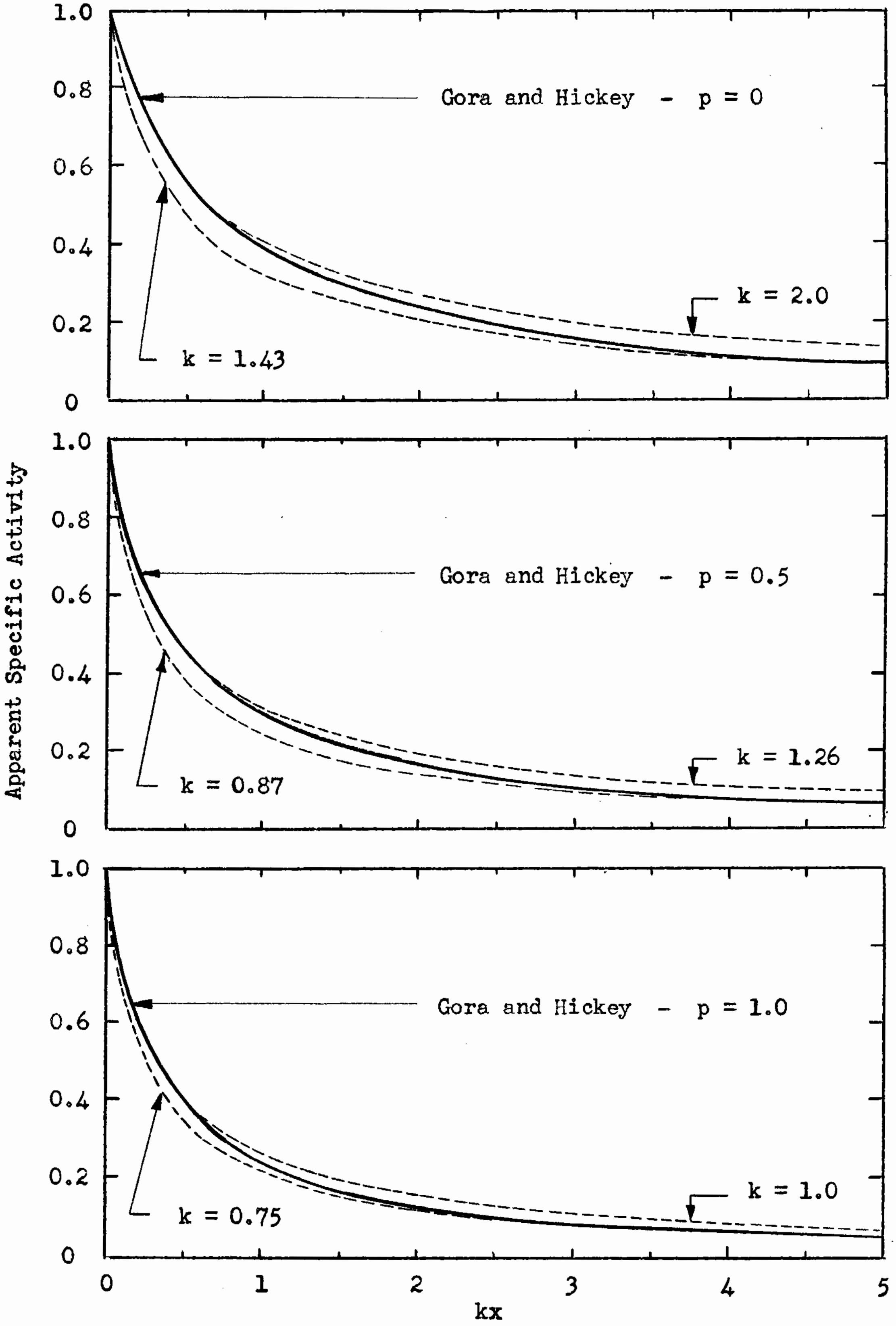

Figure 17. A Comparison of Self-Absorption of Ni^{63} with the Theoretical Curves by Gora and Hickey. Experimental Data for Ni^{63} Taken from Figure 18 and Shown as Dotted Lines for Various Values of k.

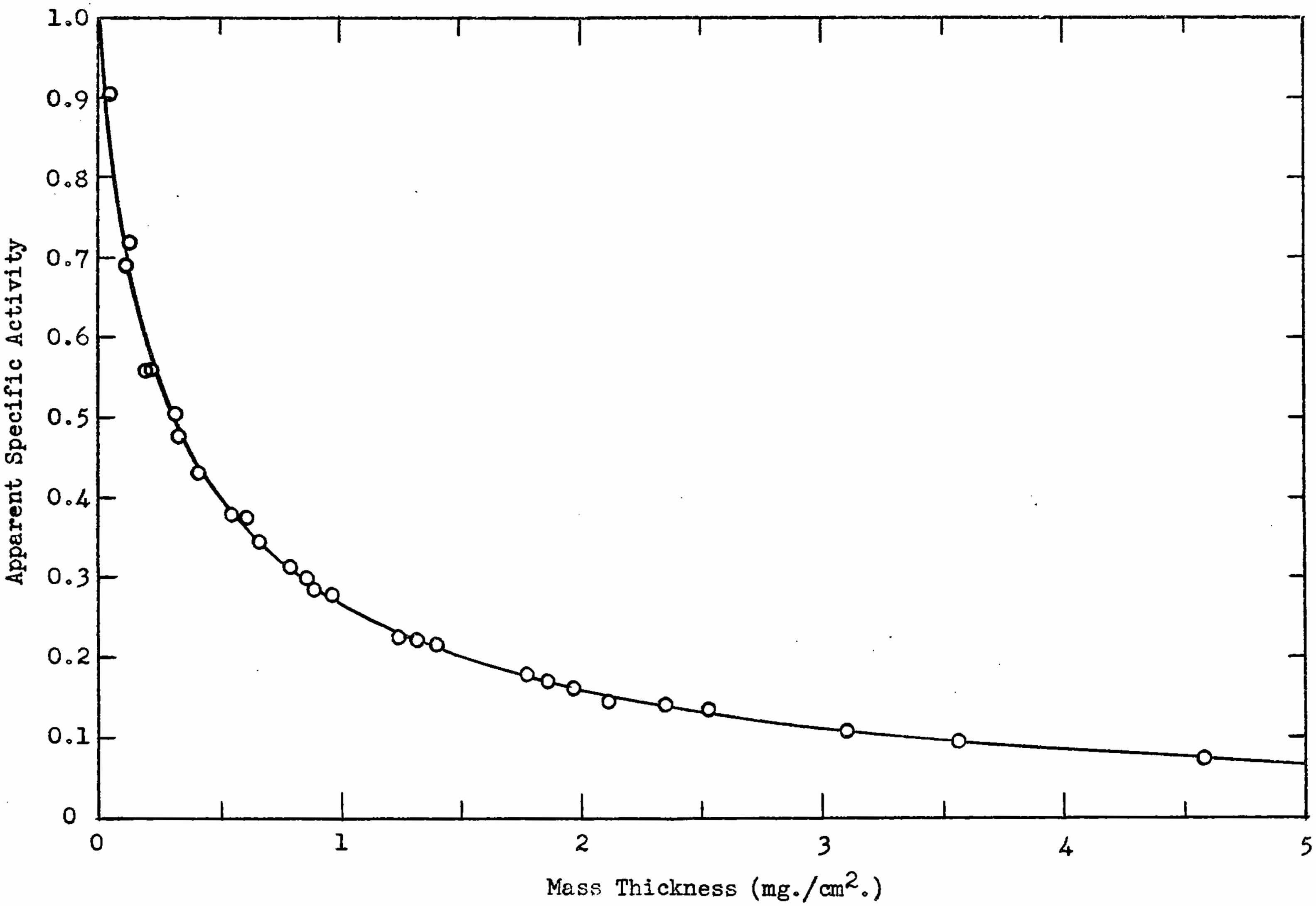

Figure 18. Self-Absorption Curve for Ni^{63} in Nickel - Apparent Specific Activity Plot.

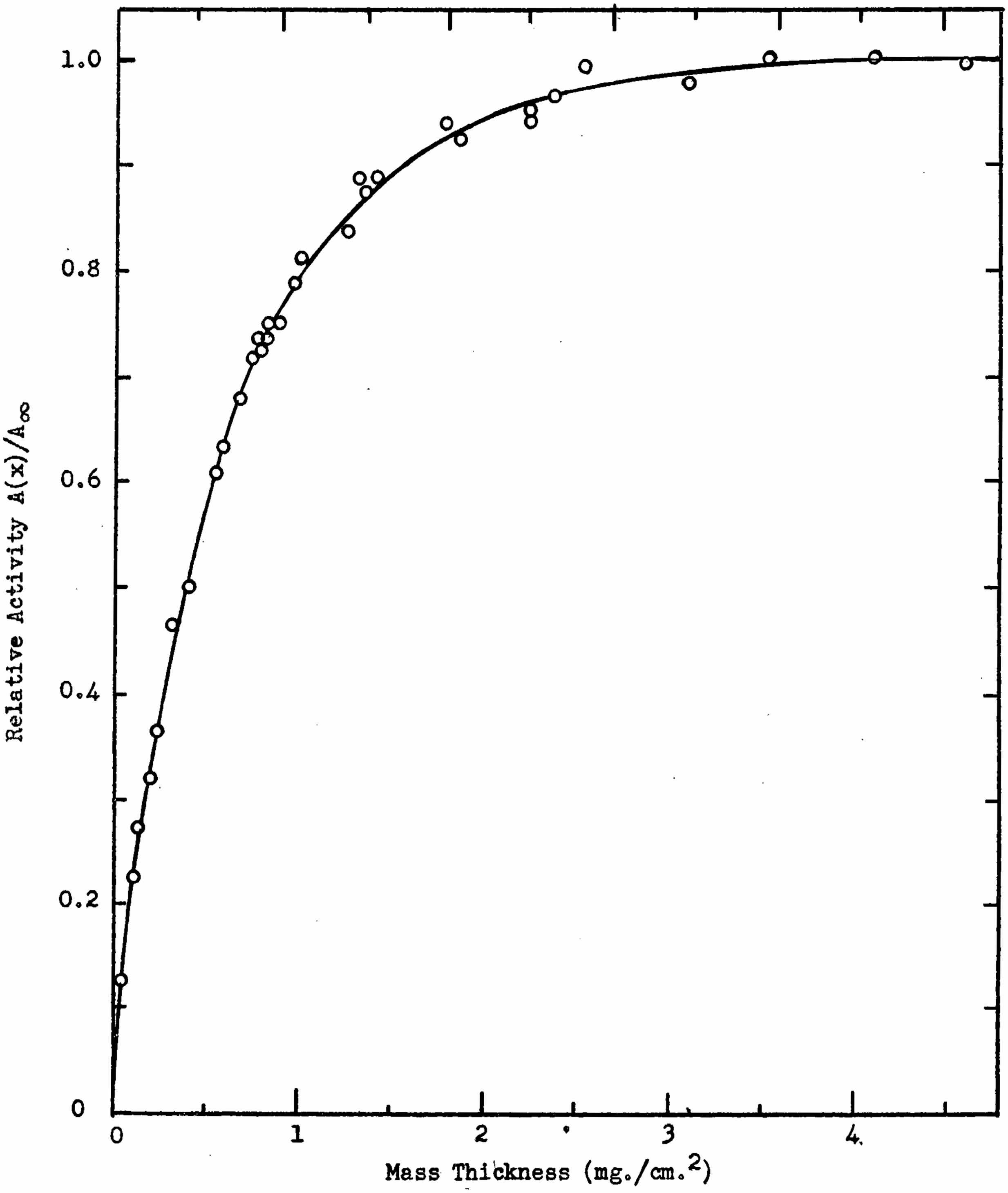

Figure 19. Self-Absorption Curve for Ni^{63} in Nickel - Saturation Plot.

To investigate the phenomenon of self-absorption, a series of active nickel sources of varying mass thickness was prepared by electrodeposition. All sources were prepared from material of the same specific activity. The range of source thickness investigated varied from 0.05 to 4.5 mg./cm^2. The source mounts were weighed on a five-place balance, sensitive to 0.005 mg., to determine the weight of the deposit. The deposits were checked for circular symmetry by measuring across various diameters and the mass thickness of the deposit was calculated from the mean of these diameters. All observed counting rates were corrected to correspond to the same area of active surface - a correction $\leqslant \pm 1.5\%$. The apparent specific activity of each source was calculated and is plotted against its mass thickness in Figure 18.

By selecting different values of the mass absorption coefficient, k, it was attempted to correlate the results shown in Figure 18 with the theoretical curves of Gora and Hickey plotted in Figure 17. As can be seen it is not possible to select a value of k for which the experimental and theoretical curves coincide over the whole range. The best agreement occurs with the Gora and Hickey expression for the limiting case, $p = 1.0$.

The counting rate of each source is plotted against its mass thickness in Figure 19. The results show the typical saturation behaviour expected. All sources thicker than 4.0 mg./cm^2. have a constant counting rate and are known as infinitely thick sources. The curve drawn through the experimental data was calculated from the following empirical expression

$$A(x) = A_\infty \left[0.194(1 - e^{-7.5x}) + 0.806(1 - e^{-1.35x})\right] \quad (53)$$

where

A_∞ = Observed counting rate for an infinitely thick source. This indicates that with a 2π geometry an absorbing layer of thickness x reduces the activity of Ni^{63} in proportion to

$$1.46\ e^{-7.5x} + 1.09\ e^{-1.35x} \quad (54)$$

The curve shown in Figure 19 can be used to correct the activity obtained for a source of thickness x to that which would be observed for an infinitely thick source. To check the probable error with which relative activities could be routinely determined using this curve, ten additional samples of mass thickness 2.0 to 4.5 mg./cm^2. were prepared. None of the corrected counting rates obtained differed from the mean value by more than ± 1.5%. Sufficient counts were taken to obtain counting statistics of ± 0.5% for this investigation.

DISCUSSION

Part 1 - Characteristics of Ni^{63}

External absorption curve for a nickel source

From the characteristics of the absorption curves given in Figures 15 and 16 it can be concluded that the active species present in the activated nickel metal are Ni^{59} and Ni^{63}. The external absorption curve given in Figure 15 indicates the presence of a low activity component with a half-thickness of 9.0 mg./cm^2. This value is in agreement with that given in x-ray tables[107] for the absorption of Co K α X-rays in aluminum of 9.4 mg./cm^2., and serves to identify this component as Ni^{59}. The soft component, Figure 16, has a half-thickness of 0.523 mg./cm^2. and a range of 8.5 ± 0.5 mg./cm^2., which are close enough to the values reported by Brosi, Borkowski, Conn and Greiss[101] of 0.6 mg./cm^2. and 6.6 mg./cm^2. respectively, to identify this component as Ni^{63}. Also, as there is no sign of a gamma ray background in Figure 15, it can be concluded that the anion exchange separation completely removed the radioactive impurity Co^{58}.

The value found for the range of Ni^{63} in these experiments is 8.5 ± 0.5 mg./cm^2. The "visual method" of estimating the range from the absorption curve, Figure 16, was employed because no suitable standard is as yet available in this energy range for a Feather[105] analysis. As the individual measurements made to obtain the external absorption curve for Ni^{63} can be accurately reproduced, the value 8.5 ± 0.5 mg./cm^2. is stated with confidence. This value is considerably greater than the values given by Wilson and Curan[108] of 6.0 mg./cm^2., and by Brosi et al[101] of 6.6 mg./cm^2.

Wilson and Curan give no information concerning their measurements, making it impossible to assess the accuracy of their results. However their failure to publish an absorption curve, and their rather high estimate of the maximum energy for Ni^{63} beta-particles (60 - 70 kev) corresponding to their value for the range (6 mg./cm^2.) gives the impression that their value is not very accurate and is probably low. Brosi et al determined their range using a Feather plot. Their failure to state which isotope they used as a standard in their Feather analysis makes their range determination of questionable worth. As they followed the absorption of Ni^{63} over only three decades of activity, the use of a standard having an energy spectrum different from Ni^{63} could result in an appreciable error in the estimated range. Furthermore a careful examination of their published absorption curve shows that they did not completely eliminate the scattering phenomenon which occurs when the first absorber is placed over the source. This could also account for their low value obtained for the range of Ni^{63}.

There are many empirical and semi-empirical expressions for relating the maximum energy of a beta-ray spectrum to the observed range of these particles in aluminum. However only two are recommended for use below 100 kev:

(1) Glendenin's[109] range-energy curve;
(2) Libby's[110] range-energy relation

$$R = 1/150\ E^{5/3} \tag{55}$$

where

R = Range - mg./cm^2.
E = Maximum energy - kev.

The maximum energy for Ni^{63} beta-particles obtained from relation (1) is 72.5 ± 2.5 kev and from relation (2) is 72.9 ± 2.5 kev using a range of 8.5 ± 0.5 mg./cm^2. These values are higher than the reported values of 67 ± 2[101], 63 ± 2[111] and 61.5 ± 2.5 kev[100], obtained directly using proportional counter beta-spectrometers. However these direct determinations may not be as free from error as might be desired. In two of the determinations[101,111] thick source mounts were employed, and in the other[100] a thick source. These conditions will result in an excess of soft electrons being observed in the beta-spectrum, and the resulting error in the slope of the Kurie[99] plot will cause the maximum energy to be underestimated.

Until a spectrometer measurement is made which is not subject to these limitations, it is proposed that 72.7 ± 2.5 kev be accepted as the value for the maximum energy of the Ni^{63} beta-spectrum.

In Figure 15, it can be observed that at zero absorber thickness the ratio of the detected disintegrations of Ni^{63} to Ni^{59} is 10^4 for a source of mass thickness 1.40 mg./cm^2. Using the appropriate corrections for self-absorption in the source, it is apparent that even for sources of superficial densities of 15 mg./cm^2. the ratio of detected disintegrations is 10^3. Hence it can be concluded that for the purposes of this research the active material consists of a single active species, Ni^{63}.

Self-absorption of Ni^{63}

The results for self-absorption of Ni^{63} given in Figure 18 are practically identical to those determined previously in a 2π geometry by Schweitzer, Stein and Nehls[112]. The agreement confirms the accuracy of both sets of data, which is important, as it is apparent with reference to Figure 17, that the experimental results for Ni^{63} self-absorption are not consistent with the theoretical expressions deduced by Gora and Hickey[106]. As can be observed the correlation is improved when a correction is made for source mount backscattering, with better correlation for the hypothetical case p = 1.0 than for p = 0.5. From this it may be concluded that for low energy beta-emitters the effects arising from self-scattering and backscattering are important enough to invalidate any description of self-absorption in a 2π system which ignores these processes.

When a value of the mass absorption coefficient, k, is selected to make the theoretical and experimental curves coincide for large source thicknesses, it is observed that the experimentally determined apparent specific activity decreases more rapidly than that predicted theoretically. This suggests that the backscattering processes in the source degrades the energy of the scattered particle, so that it is more easily absorbed in the overlying layers of atoms in the source. This is in agreement with the experimental work of Pate and Yaffe[113] who also suggest that the effect is more marked for wide angle geometries. In addition, their results show that the backscattering factor, p, for an infinitely thick source mount increases with decreasing energy of the beta-emitter. This probably accounts for the fact that Gora and Hickey could successfully interpret their results for self-absorption of $C^{14}(\beta^-\ 0.156)$, while the results for $Ni^{63}(\beta^-\ 0.072)$ are inconsistent with their equations.

It has been shown that the experimental results for self-absorption are satisfactorily expressed by an empirical equation involving two absorption coefficients

$$A(x) = A_\infty \left[0.194(1 - e^{-7.5x}) + 0.806(1 - e^{-1.35x})\right] . \quad (53)$$

Equation (53) suggests that eighty per cent of the emitted particles are absorbed by a process having an absorption coefficient of 1.35 cm^2./mg. which is practically identical to the value calculated from the external absorption experiments of 1.33 cm^2./mg. As the other twenty per cent are absorbed by a process having an absorption coefficient of 7.5 cm^2./mg., this is added confirmation that a certain portion of the beta-particles have their energy degraded by a scattering process.

Relative counting of Ni^{63} sources

The observed counting rate, m, is related to the disintegration rate, D, by

$$m = K\,D\,f_\tau\ f_s \qquad (44)$$

The correction factors for dead-time loss, f_τ, and self-absorption, f_s, have been evaluated for Ni^{63} radiation. Providing the mass thickness of the prepared sources are between 2.0 and 6.0 mg./cm^2., the relative specific activity of a sample can be determined to ± 1.5%. A close examination of the physical nature of the deposit reveals the presence of very small nickel crystals. Slight variations in plating conditions probably influence the size of these crystals, producing the observed fluctuations in counting rate.

EXPERIMENTAL TECHNIQUES AND RESULTS

Part 2 - Self-Diffusion in Polycrystalline Nickel Measured by a Sectioning Technique

Introduction

The experimental method chosen to measure the self-diffusion of nickel involves the preparation of short cylinders of high purity nickel, and the electrodeposition of a thin layer of radioactive nickel on to one end surface of the cylinders. The cylinders were machined to the closest tolerances possible so that the ends would approximate a plane surface. The prepared sample was placed in an electrically heated tube furnace, and brought to the required controlled temperature for a measured length of time to promote diffusion. After the introduction of the sample, the furnace was filled and swept with hydrogen during the whole period of diffusion to protect the sample from oxidation. After the diffused sample had cooled to room temperature, it was mounted in a precision lathe and thin slices turned off the end parallel to the active face.

The specific activity and the thickness of each of these slices were determined and from these data a concentration-penetration curve was drawn. The diffusion coefficient was then calculated from this curve. The above sequence of events will be followed in describing the experimental techniques and apparatus used in these measurements.

Sample Preparation

The diffusion specimens were machined from a one-inch diameter rod of high purity vacuum-melted nickel. This nickel was obtained from the National Research Corporation, Cambridge, Mass., and is identified as NIVAC-P. A typical analysis of this metal is given in Table 7. A microscopic examination of a polished and etched sample showed that this NIVAC-P had a fine equi-axed grain structure.

Sections of the nickel rod were annealed for twenty-four hours in a hydrogen atmosphere at 1300° C to remove all stresses and to promote grain growth. From this annealed material samples one inch in length were machined to 0.600 in. diameter for half their length, and 0.500 in. for the other half. The smaller end fitted the maximum collet size of the lathe, and the larger cross-sectional area of the other end gave a larger diffusion interface.

The sample then was annealed at 1400° C to obtain a very large grain size and to ensure that no further grain growth would occur during a diffusion experiment. The largest possible grain size is required to minimize the effect of grain boundary diffusion. The diameter of the grains after this anneal varied from

Table 7

Vacuum-Melted Ingot Nickel
Composition in Weight Per Cent

Nickel	99.9
Nitrogen	< 0.001
Oxygen	< 0.005
Hydrogen	< 0.0001
Aluminum	< 0.001
Calcium	< 0.001
Cobalt	< 0.02
Magnesium	< 0.001
Manganese	< 0.001
Silicon	< 0.001
Tin	< 0.001
Carbon	< 0.005
Copper	0.01
Iron	0.04

2 to 10 mm. A photomicrograph of this material at $2\frac{1}{2}$ diameters is shown in Figure 20.

Figure 20. Grain Size Obtained in Pure Nickel After a 24-Hour Anneal at 1400° C. 2.5x, Etchant Carapella's Reagent.

These prepared samples were faced using fine feeds and and shallow cuts to minimize the depth of the layer of disturbed metal. A spring-fit brass ring had been fitted to the 0.600 in. diameter section to prevent rounding of the faced surface during polishing. The flat surface was ground on a series of polishing papers, finishing on 4/0 grade.

The solution of the diffusion equation - Equation (18) - used to analyse the results of the research is based on the assumption that the tracer initially is contained in an infinitely thin layer on the surface of the specimen. In practice, a thick layer of tracer must be applied to have sufficient activity present to permit an accurate determination of the concentration-penetration curve. The low specific activity of the active nickel employed made it necessary to use a layer about 0.0001 cm. in thickness. The layer of active nickel was deposited from the stock solution previously used to prepare radioactive sources.

However to obtain meaningful results it was essential that the tracer be electrodeposited properly on the diffusion specimen. A layer of oxide between the tracer and the base metal will either prevent diffusion completely, or at least cause erroneous results by blocking the path of some of the tracer at the active surface.

Adherent deposits were obtained by the procedure recommended by the International Nickel Company[114]. First the sample was degreased with carbon tetrachloride and then sealed onto a lucite cylinder to form a plating cell as shown in Figure 21. An aqueous solution containing 25% sulphuric acid was added to the cell and the sample was given the following electrolytic treatment:

(1) anodic 30 ma./cm^2. for 5 minutes;
(2) anodic 150 ma./cm^2. for 1 minute;
(3) cathodic 30 ma./cm^2. for 3 seconds.

During the first portion of this treatment the anodic surface became polarized and a black layer of nickel oxide was formed;

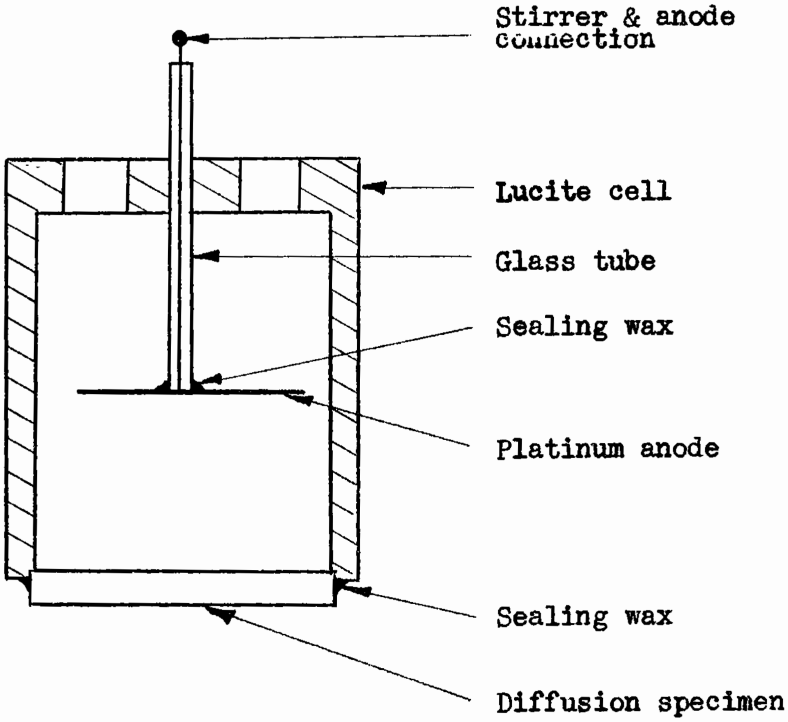

Figure 21. Plating Cell for Preparing Diffusion Specimens.

in the second stage this layer was detached by the violent evolution of oxygen at the anodic surface; the cathodic treatment removed all traces of oxides. After the cathodic treatment the cell was rinsed with distilled water, the nickel plating solution added and plating started as promptly as possible. The plating current used was 30 ma./cm^2. and the platinum anode was rotated to remove bubbles and to reduce the cathodic concentration polarization.

All the specimens were prepared in a regular fume hood in the radiochemistry laboratory. Rubber gloves were worn at all times and proper precautions taken to prevent contamination of the surroundings.

The samples were removed from the plating cell after 15 minutes and thoroughly washed to remove all non-adherent active nickel. The uniformity of the thickness of the deposited layer was determined by measuring the counting rate at nine positions on the active surface through a diaphragm with a 3/32-in. diameter opening. One count was taken at the center of the specimen and eight more at equal intervals near the periphery. These activity measurements were converted to mass thicknesses using the self-absorption curve for Ni^{63} - Figure 19 - and all samples showing variations in thickness greater than ± 3 per cent from the mean were rejected. Satisfactory specimens were mounted in the lathe and a thin layer machined from the cylindrical surface of the 0.600 in. diameter end to remove any active nickel. The machining was performed in a plastic box, to be described later, to prevent contamination of the lathe.

Temperature Measurements

All temperatures were measured with platinum - platinum 13% rhodium thermocouples which were calibrated against a laboratory standard, before each diffusion experiment. The cold junctions of the couples were maintained at 0° C in an ice bath, and the E.M.F.'s produced by the couples were measured with a Leeds and Northrup type K2 potentiometer. The potentiometer was sensitive to changes in temperatures of ± 0.05° C.

When temperatures were measured in the hydrogen atmosphere surrounding the diffusion sample, it was necessary to protect the couples against contamination from the products of reduced refractory oxides. For this purpose a Leeds and Northrup Fyrestan protecting tube was found to be satisfactory for temperatures up to 1400°C. The use of these tubes slightly reduced the accuracy with which the temperatures could be measured from heat conduction along the protecting tube. A calibration experiment using one unprotected couple and one protected couple, in an argon atmosphere, indicated that this difference amounted to less than 0.5° C over the range of temperatures used in the experiments. It is estimated that the measured temperatures are precise to ± 0.75°C, and accurate to ± 1.3°C.

The variation of the diffusion coefficient with temperature is given by

$$D = D_o e^{-Q/RT} \qquad (9)$$

Using a value of 70 kcal./mole for the activation energy, it can be shown that for one degree error in temperature at 1200^oC there is a 1.6% error in the diffusion coefficient. Thus it can be concluded that errors resulting from temperature measurements and from thermocouple calibrations can introduce a maximum error of ± 2% in the measured values of the diffusion coefficient.

Temperature control

A standard off-on potentiometrically controlled laboratory furnace cycles about ± 5^oC around the control temperature. This range is unsatisfactory for the precision demanded by these experiments. The circuits commonly used to obtain more precise temperature control are based on a.c. and d.c. Wheatstone bridges, with the temperature sensing arm being a resistance thermometer, or the furnace windings in the case of platinum-wound furnaces. It was decided to build a controller based on a d.c. bridge, since resistance thermometers become slightly capacitive above 900^oC, and additional elements must be introduced into the bridge to balance out this capacitance. The bridge itself consisted of a platinum resistance thermometer for a Sunvic temperature controller, a L. and N. d.c. Wheatstone bridge (4725) and galvanometer (2420a), and a 3-volt source of d.c. power.

A slit system was put in the galvanometer to collimate the light beam which was directed towards two phototubes. When the light was on one phototube the relay in the furnace power supply was opened, and when the beam shifted to the other phototube the relay was closed. This relay shunted a resistor in and out in the furnace power supply and gave a high-low current ratio of 0.70. The phototube amplifier and the relay circuit are part of a temperature control circuit proposed by Lutz and Wood[115].

By placing the phototubes about one inch apart and using a light beam 24 inches long, a change in the resistance of the sensing element equivalent to a temperature change of 0.2°C would move the light beam from one phototube to the other. With this arrangement a variety of tube furnaces was controlled to ± 0.5°C for varying periods and for temperatures of 900°C to 1300°C, by placing the resistance thermometer in intimate contact with the furnace winding.

The only objection found with the relay circuit was the moderate life of the phototubes - about one month of continuous operation. However this particular control system had other more serious disadvantages. Above 1050°C the resistance of the resistance thermometer drifted rapidly, necessitating frequent calibrations of the furnace temperature. Suspecting that the trouble was arising from the refractory cement used in the Sunvic resistance thermometer, a series of resistance thermometers were made by threading No. 30 gauge platinum wire through porcelain thermocouple insulators. This gave little improvement in performance and thus limited the use of the controller to a maximum of 1200°C.

The other temperature controller used was assembled from commercially available apparatus. The E.M.F. produced by a platinum-platinum 13% rhodium thermocouple was balanced at the desired control temperature by a L. and N. Students Potentiometer. A L. and N. microvolt amplifier (9835-B) was substituted for the galvanometer and this amplified the unbalance caused by the furnace drifting from the control temperature. The amplified difference in E.M.F. was fed into a L. and N. Speedomax type G recorder, with a -10 to +10 millivolt scale, which had a D.A.T. proportioning temperature control unit (10769-G). This unit shorted a resistance in-and-out in the power supply to give a high-low current ratio of 0.70. The short-time stability of the control unit was ± 0.1°C.

The long-time stability of the control unit depended on the stability of the thermocouple and the current supply for the student potentiometer. Changes in thermocouple calibration were observed above 1350°C, with the drift at 1400°C being about 0.25°C in 24 hours, and this was disregarded for diffusion times up to 24 hours. The current for the student potentiometer was supplied by three sets of No. 6 dry cells connected in parallel and placed in a carton filled with excelsior to eliminate the effects of sudden changes in the room temperature. After a week's operation the dry cells stabilized and the drift in 12 hours was less than the equivalent of 0.3°C.

With this assembly it was possible to maintain temperatures within ± 0.5°C for any length of time, at temperatures up to 1400°C, provided the following precautions were taken:

(1) above 1350°C the control thermocouple must be calibrated every 24 hours;

(2) the potentiometer current must be standardized at least every 10 hours;

(3) the cold junction temperature must be kept constant.

High temperature furnaces

For the diffusion experiments below 1200°C a wire-wound tube furnace of conventional design was constructed using Hoskins alloy No. 10 wire on a 2-inch I.D. alundum core (Norton RA98). The formed heating element was twenty inches in length and was located centrally on the 24-inch core. A survey along the tube of the operating furnace showed a marked temperature gradient from the ends to the center of the winding, and it was necessary to modify the current distribution in the winding to obtain a central zone with uniform temperature. Taps were provided so that a portion of the current flowing through the winding could be diverted from a seven-inch section in the center. The additional energy dissipated from the end sections of the windings made it possible, with careful adjustment, to obtain a uniform temperature, within ± 0.5°C, over a central tube zone five inches in length. As recommeded by Hoskins, the furnace windings were not cemented to the refractory core. The poor transfer of heat to the core limited the maximum continuous operating temperature of the furnace to 1200°C although the wire itself is recommended for use up to 1300°C.

The diffusion samples were supported in a one-inch I.D. mullite combustion tube thirty-six inches long, which passed through the refractory core. The temperature controller used with this furnace was the d.c. Wheatstone bridge type previously described.

At temperatures above 1200°C the diffusion specimens were heated in a molybdenum wire-wound tube furnace. Details of the furnace construction are shown in Figure 22. To reduce the hydrogen consumption necessary to protect the molybdenum winding from oxidation the furnace shell was made as impermeable as possible. All joints not subject to expansion in heating were sealed with a refractory cement composed of powdered talc and water glass. An expansion joint was necessary where the combustion tube entered the furnace shell, and as shown it was made

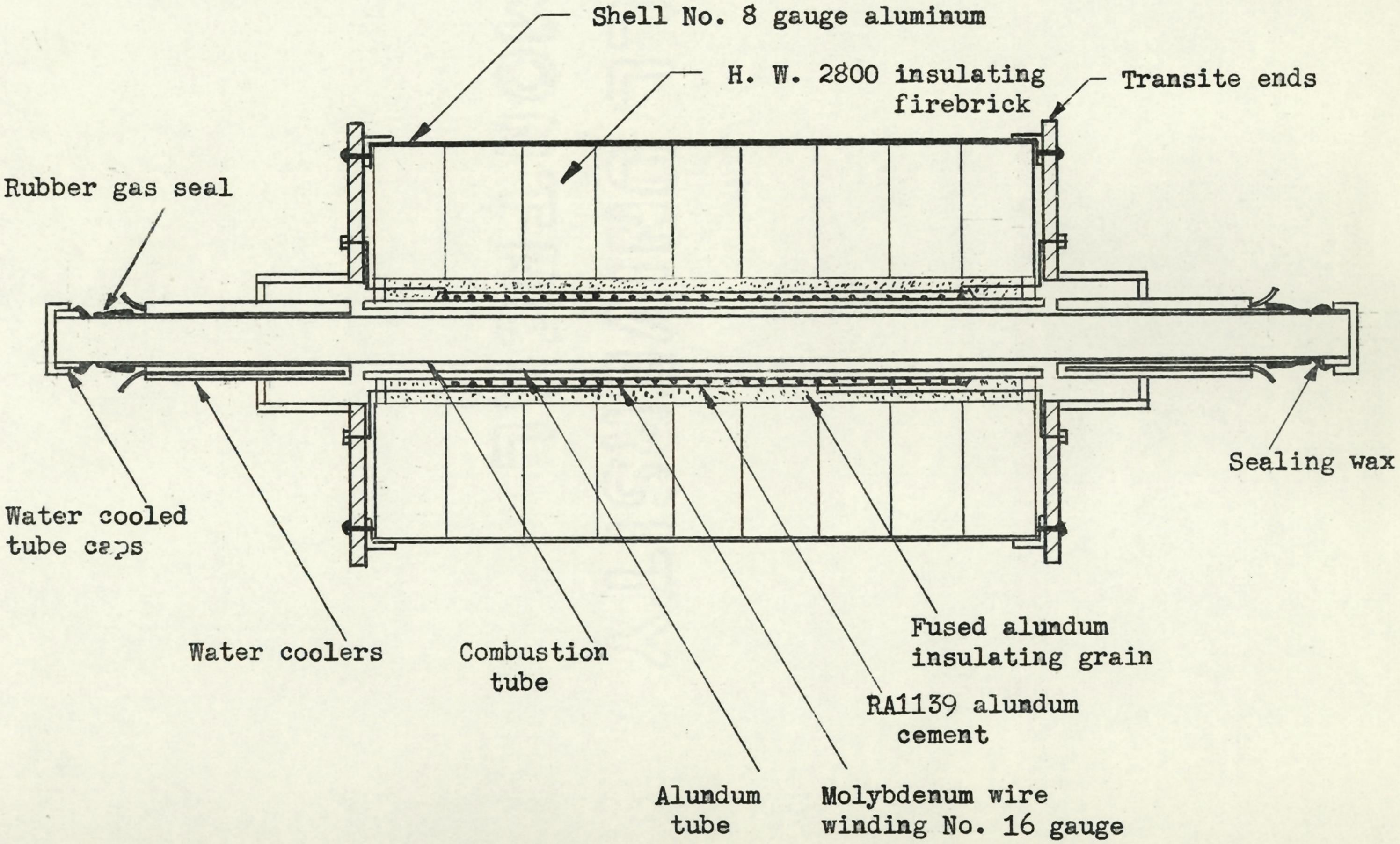

Figure 22. High Temperature Tube Furnace

with a piece of Gooch rubber tubing. Water jackets were installed at both ends of the furnace to cool the combustion tube sufficiently to prevent melting of the rubber. With these precautions the hydrogen consumption was limited to 35 cu. ft. per day.

The refractory core was twenty-four inches long and the molybdenum wire resistor was wound over the central twenty inches using the recommended 3/8 in. spacing between turns[116]. The winding was divided into three equal sections and by suitably shunting the central section it was possible to obtain a zone of temperatures constant to one degree over a four-inch length at 1400°C. The potentiometric controller was used on this furnace, with the control thermocouple inserted from one end of the combustion tube to reach the high temperature zone. The control thermocouple was protected by a Fyrestan tube.

Diffusion anneal

The diffusion specimens were protected from oxidation by annealing them in a pure hydrogen atmosphere. The hydrogen was purified by a system consisting of a palladium catalyst followed by an activated alumina drier. As hydrogen is known to reduce some of the refractory oxides in mullite, resulting in the formation of water vapour, it was necessary to sweep fresh hydrogen continuously through the combustion tube to maintain the proper atmosphere. The exit hydrogen was exhausted through a bubbler trap to prevent back diffusion of air.

The diffusion specimens were protected from contamination by reduced silicon from the combustion tube, by placing the samples in XN10 Triangle R.R. recrystallized alumina crucibles manufactured by Morgan, England. These crucibles of cylindrical shape had an I.D. of 0.75 in. and a length of 1 inch. All experiments were made in duplicate with the active faces of the two samples placed in intimate contact to prevent loss of the tracer by evaporation. The samples were charged into a cool end of a furnace that had been heated to the desired diffusion temperature. Then the open end of the combustion tube was sealed and the air was flushed out with a rapid steam of argon, followed by a rapid stream of hydrogen. After this flushing period the flow of hydrogen was reduced to one bubble per second, and then the samples were pushed slowly into the central zone by a nickel rod passing through a gas tight gland in the combustion tube cap. About ten minutes were required to charge or to remove samples from the furnace.

When an unusually long time was taken for the samples to come to temperature, a correction was made for diffusion taking place during this period by a method suggested by Ham, Parke and Herzig[117]. The mean effective diffusion time is given by

$$t_m = \frac{\int_o^t e^{-Q/RT}\,dt}{e^{-Q/RT_c}} \qquad (56)$$

where

t_m = Mean effective diffusion time.
T_c = Constant diffusion temperature.
T = Temperature of the diffusion sample at time t.

The maximum error in the length of the diffusion anneal occurs in those samples which are heated for the shortest time, in these experiments 24 hours. It is estimated that for these experiments, the diffusion time is accurate to ± 0.2%, introducing a maximum error of ± 0.2% in the measured value of the diffusion coefficient.

Standard sectioning procedure

A diffusion sample to be sectioned was placed in the collet attachment of a precision lathe. A dial gauge with 0.0001-inch divisions was mounted on the compound rest and adjustments made until the surface of the sample ran true to $\pm 5 \times 10^{-5}$ in. at the outer edge of the flat surface. During machining operations the turnings from the sample were collected in the plastic box shown in Figures 23a and 23b. A boring bar enters the box through a sliding bushing on one side, and the sample fits through a circular aperture at right angles to this. The degrees of freedom given by these sliding joints allowed the boring bar to be moved at right angles and parallel to the face of the specimen, which permitted facing and turning cuts to be

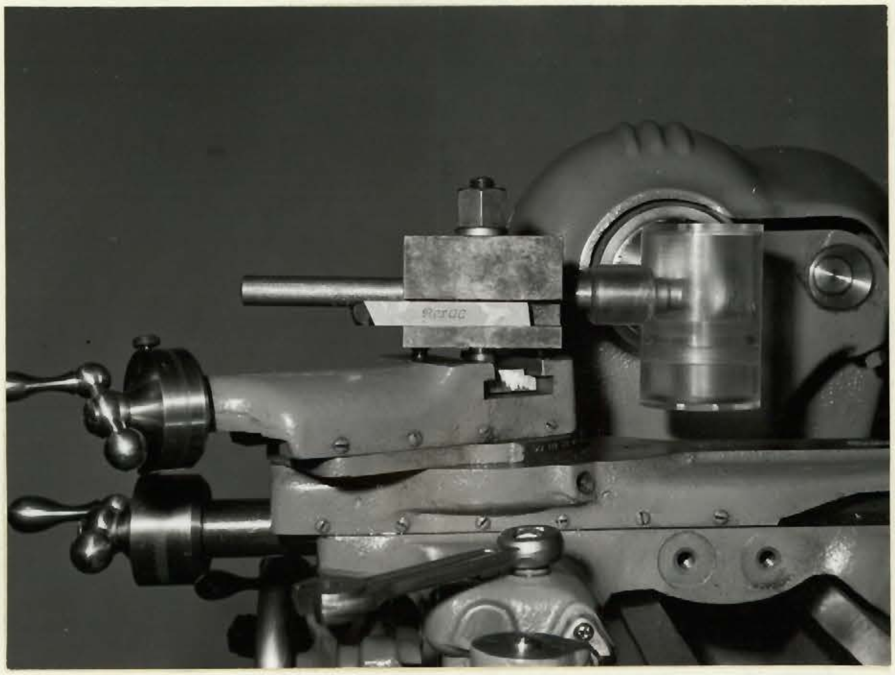

Figure 23a. Plastic Sectioning Box - Side View

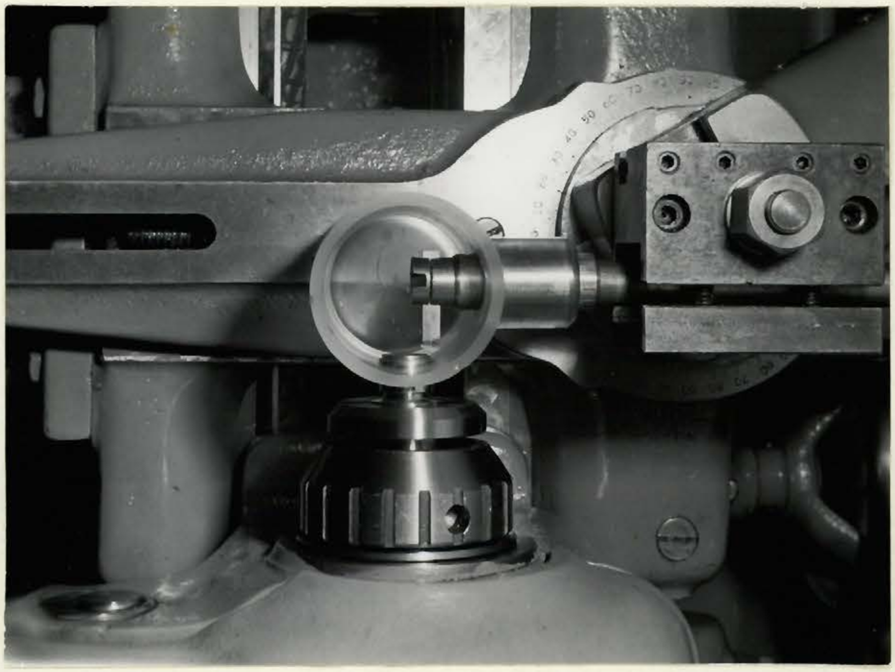

Figure 23b. Plastic Sectioning Box - Top View

made on the sample. The top of the box was removable to permit all turnings to be brushed into the lower third of the box; this lower section was removable to allow the turnings to be discarded or to be transferred to a numbered container for weighing and analysis.

Two different shapes of bits were employed to prepare and section the sample. A side cutting tool was used to reduce the diameter of the specimen to 0.550 in. to remove any metal affected by surface diffusion. For sectioning, best results were obtained using a sharp pointed tool with large back rake and side rake angles, no cutting oil, slow spindle speeds and a fine cross feed. Sections of 0.0025 to 0.0050 cm. in thickness were machined off depending on the depth of penetration of the tracer. The tool used is shown in Figure 23b.

The carriage of the lathe was locked during sectioning to ensure flat facing cuts. The depth of cut was set using the feed on the compound rest, though the actual thickness of the section was calculated from the weight of metal collected in the box. As a check on the accuracy of the sectioning procedure the total distance fed on the compound rest had to be in agreement with that calculated from the sum of the weights of all the sections. These two results always agreed indicating that no active material escaped from the sectioning box.

The solution to Fick's law corresponding to the diffusion of an infinitely thin layer of material into a semi-infinite medium, D assumed constant, is

$$\log C(x,t) = \log (C_0/\sqrt{\pi Dt}) - x^2/9.212\ Dt \qquad (18)$$

Since the diffusion coefficient can be calculated from the slope of log C(x,t) versus x^2, it is sufficient to employ some quantity which is directly proportional to C(x,t). In these experiments the quantity C(x,t) was taken as the relative specific activity of Ni^{63} contained in a section of thickness Δx, and the corresponding penetration distance $\bar{x}$ is taken as the distance to the center of the slice. The penetration distance, $\bar{x}$, was calculated from the weight of the individual sections, the density of nickel and the measured diameter of the diffusion couple. Individual sections averaged about 40.0 mg. in weight and were weighed to ± 0.05 mg. giving an estimated error in the penetration distance, $\bar{x}$, of ± 0.1%.

The turnings themselves, because of their bulk, do not constitute a suitable form of sample for measuring the concentration of Ni^{63} in a section. Suitable sources for counting were prepared by dissolving the turnings in the minimum amount of hydrochloric acid and the electrodeposition of the dissolved nickel on copper discs following the procedure previously described. The counting rate for each of these sources was corrected to that which would be observed for an infinitely thick source - Figure 19. These corrected counting rates were directly proportional to the specific activity of Ni^{63} contained in the section and were substituted for $C(x,t)$ in drawing the concentration-penetration curve. Sources from 2.0 to 6.0 $mg./cm^2$. in thickness were prepared which, as was previously observed, permitted the relative specific activity of the material in the source to be determined to ± 1.5% when sufficient counts were recorded to obtain statistics of ± 0.5%.

In general, the prepared sources counted at rates between a maximum of 300 c.p.m. and a minimum of 10 c.p.m. above background. Sources were counted until the first of the following possibilities ensued; either 10^4 counts were recorded; or counting had continued for one hour. With a background of 70 c.p.m., and employing the above limits for the counting time, sources with activities of 300 c.p.m. and 10 c.p.m. were measured, respectively, with standard deviations equivalent to ± 1.09% and ± 11.5%. These statistical fluctuations are indicated in the standard manner on the concentration-penetration curves given in the next section.

It is estimated that the errors introduced into the diffusion coefficient through the combined effects of counting statistics, source mounting errors, and errors in the determination of the thickness of the sections amounts to about ± 3.0%. In actual fact this may be an optimistic evaluation of the errors associated with the sectioning technique. Even with the finest possible lathe-feeds, a cutting tool with a sharp point leaves a fine series of machining spirals on the surface of the specimen. These grooves are about 0.0002 cm. deep under ideal conditions and are appreciable in relation to sections 0.0025 cm. thick. It has proved impossible to estimate what effect, if any, this has on the measured diffusion coefficient.

Another possible source of error in the sectioning technique is the assumption that the penetration distance, corresponding to the average specific activity of a slice, coincides with the distance measured to the center of the slice $\bar{x}$. For a system where D does not vary with composition the magnitude of this error can be calculated. The necessary analysis will be given as it is unavailable in the literature.

After a diffusion period of time, t, the concentration at a distance x is given by

$$C_x = \frac{C_o}{\sqrt{\pi Dt}} e^{-\frac{x^2}{4Dt}} \tag{17}$$

For a slice taken between distances x_1 and x_2 the average concentration $\bar{C}x$ is

$$\bar{C}_x = \frac{\int_{x_1}^{x_2} \frac{C_o}{\sqrt{\pi Dt}} e^{-\frac{x^2}{4Dt}} dx}{\int_{x_1}^{x_2} dx} \tag{57}$$

But this average concentration $\bar{C}_x$ occurs at some distance x_* in the section; therefore,

$$\overline{C_x} = \frac{C_o}{\sqrt{\pi Dt}} e^{-\frac{x_*^2}{4Dt}} \tag{58}$$

Combining equations (57) and (58) and evaluating for x_*^2 gives

$$x_*^2 = \frac{-4Dt \ln \sqrt{4\pi Dt}}{(x_2 - x_1)} \text{erf } y \Bigg]_{\frac{x_1}{2Dt}}^{\frac{x_2}{2Dt}} \tag{59}$$

where erf y = area under the normal curve of error between the ordinate y = o and the ordinate at y.

Selecting typical values of D and t for this research, the above expression was evaluated for the maximum thickness of sections employed, and the difference between x_* and the distance to the median of the section was found to be negligibly small. It can be concluded that, under these conditions, no error is introduced by taking sections of finite thickness, and using the median of the section as the penetration distance corresponding to the plane of average activity.

The uncertainties introduced into the value measured for the diffusion coefficient by,

errors in temperature measurements are ± 2.0%;
errors in the time of the diffusion anneal are ± 0.2%;
and errors in the sectioning procedure are ± 3.0%.

Thus errors as large as the total of the above, ± 5.2%, can be expected in the measured value of the diffusion coefficient.

Surface activity - sectioning technique

The very soft characteristics of Ni^{63} beta-radiation suggested that diffusion coefficients could be evaluated by a modified sectioning technique.

Referring to the self-absorption curve for Ni^{63} given in Figure 19, it can be seen that for an infinitely thick source, half of the total counts recorded came from the surface layer of nickel 0.38 mg./cm.^{2} or 0.43 x 10^{-4} cm. thick. For a diffusion specimen where the concentration of the tracer below the surface is decreasing as $e^{-x^2/Dt}$, over half of the counts detected at the surface come from a surface layer of this thickness. This is a negligibly small thickness compared to the thickness of a section 3.0 x 10^{-3} cm. and therefore the counting rate observed at the surface can be assumed to represent the surface activity of the material.

A concentration-penetration curve therefore can be determined by counting on the surface of the specimen before each section is removed. The penetration distance x corresponding to a determined activity is the total thickness of metal removed to that point. To investigate the accuracy of this surface activity-sectioning procedure, one of the duplicate nickel self-diffusion specimens was analysed using this technique and the results from this method compared with those determined by the standard sectioning technique. As an additional check the sections were saved and treated in the standard manner to give a duplicate concentration curve for the individual specimen.

In the presentation of the results, the curves determined by the modified technique will be designated as sample x, surface-sectioning, while those determined by the standard sectioning technique will be designated as sample x, sectioning.

Experimental results

Investigators have shown that, for polycrystalline materials, accurate volume diffusion coefficients are determined at temperatures where the quantity of material diffused along the grain boundaries is negligible compared to that diffusing through the grains. It was necessary first to determine the temperature above which the diffusion was primarily through the grains. As discussed in the introduction - short-circuiting paths in diffusion - the shape of the concentration curve indicates the type of diffusion that predominates. Volume diffusion predominates when the plot of log C(x,t) versus

x^{-2} is linear over the whole penetration range, and grain boundary diffusion predominates when the plot of log C(x,t) versus x is linear. It is obvious that there is a temperature range where both types of diffusion are effective.

The rate of nickel self-diffusion was investigated at 50 degree intervals over the temperature range 1050°C to 1400°C. Duplicate samples were used in each test and to prevent loss of active nickel by evaporation the active faces of the duplicate samples were placed in contact. This also insured that the conditions of treatment of the two specimens were identical. Four typical concentration-penetration curves obtained for diffusion temperatures of 1101°C, 1151°C, 1197°C and 1294°C are shown in Figures 24, 25, 26 and 27 respectively. The volume diffusion coefficients calculated from the slope of the curves, log C(x,t) versus x^{-2}, for all experiments are recorded in Table 8 under the heading $D_{20^\circ C}$.

A comparison of the curves given in Figures 24, 25, 26 and 27 showed that at temperatures above 1200°C the penetration of the tracer was characteristic of volume diffusion only, as log C(x,t) varied as x^{-2} for all penetration distances. The concentration-penetration curves for 1101°C, Figure 24, showed that for shallow penetrations log C(x,t) varied as x^{-2}, while for deep penetration log C(x,t) varied as $\bar{x}$. This was a definite indication that the Ni^{63}, penetrating deeply into

Table 8

Self-Diffusion Coefficients of Nickel

Sample Number	Sectioning Technique	Diffusion Coefficient x 10^{10}			Temp. Deg. C
		$D_{20^\circ C}$ cm^2./sec.	D_T cm^2./sec.	D cm^2./sec.	
1A	Standard	0.121	0.125	0.129	1051
1B	Standard	0.121			
2A	Standard	0.298	0.310	0.319	1101
2B	Standard	0.300			
3A	Standard	0.608	0.642	0.661	1151
3B	Standard	0.627			
3B	Surface	0.608	0.632	0.651	
4A	Standard	1.44	1.51	1.56	1197
4B	Standard	1.46			
4B	Surface	1.40	1.46	1.51	
5A	Standard	3.38	3.52	3.62	1251
5B	Standard	3.38			
5B	Surface	3.06	3.19	3.29	
6A	Standard	6.37	6.65	6.85	1294
6B	Standard	6.37			
6B	Surface	6.00	6.27	6.46	
7A	Standard	12.2	12.8	13.2	1353
8A	Standard	26.5	27.7	28.5	1399
8A	Surface	24.4	25.6	26.4	
8B	Surface	24.4			

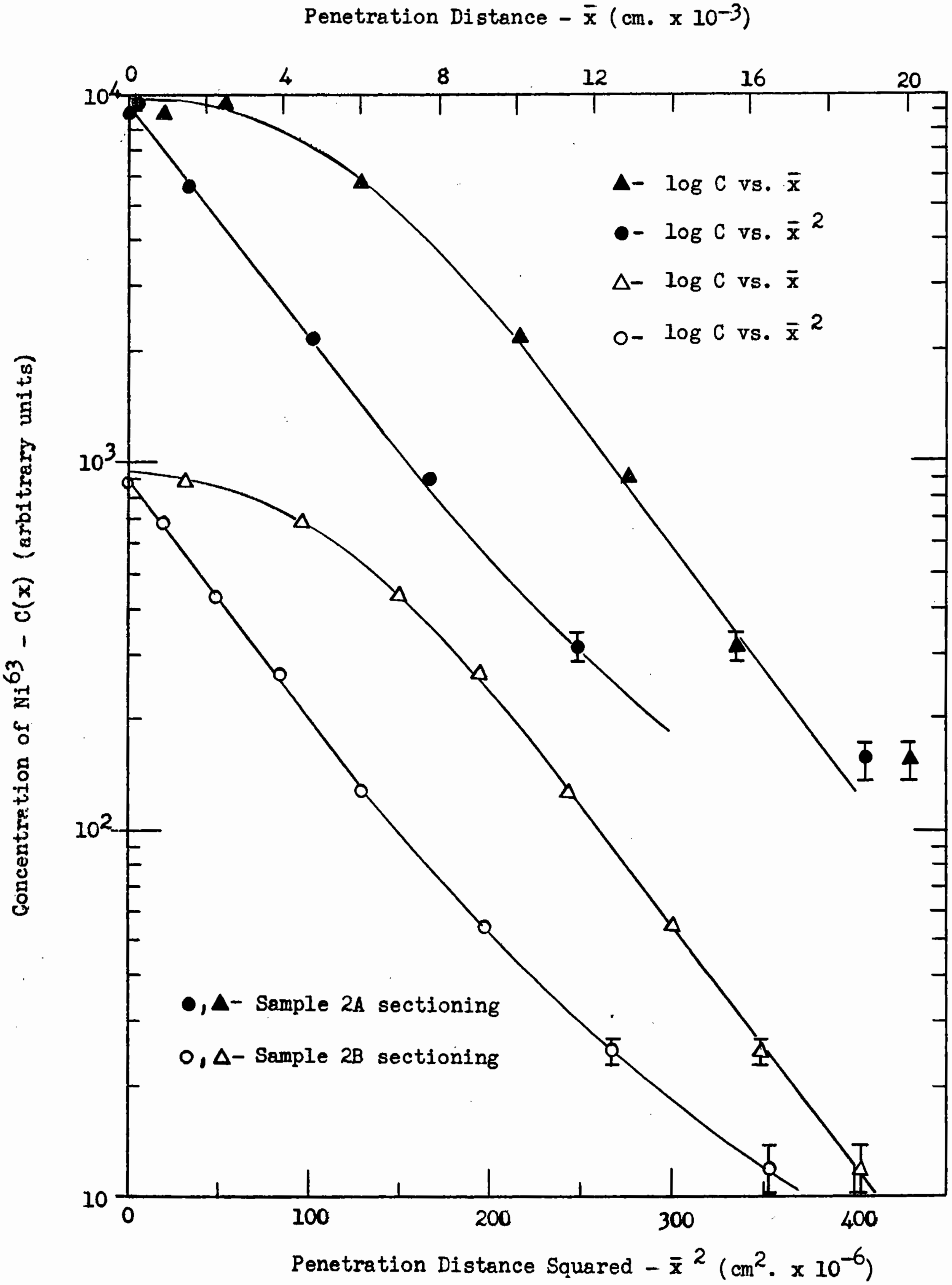

Figure 24. Concentration-Penetration Curves for Ni^{63} Self-Diffusion at 1101°C. Diffusion Time 154.5 hrs.

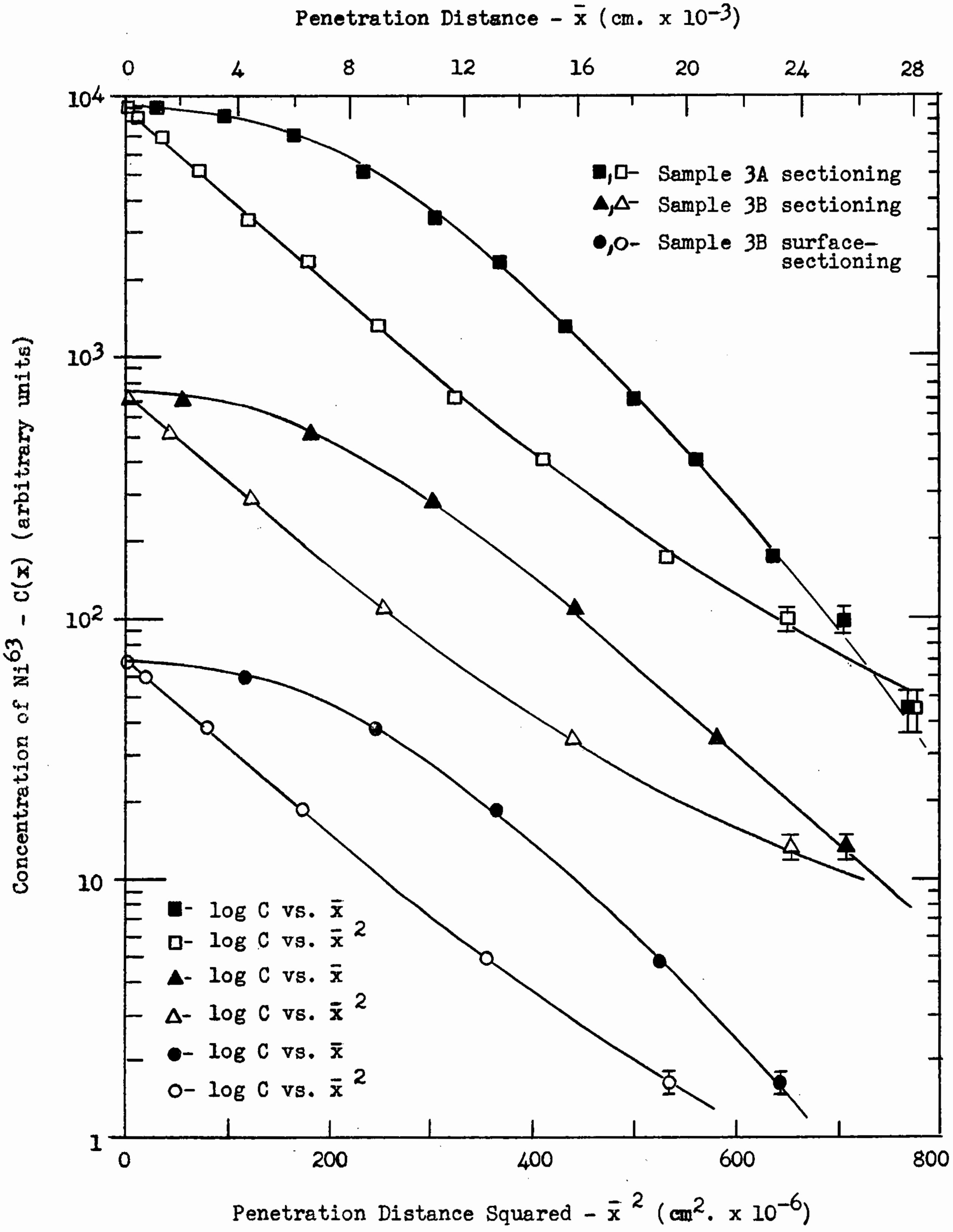

Figure 25. Concentration-Penetration Curves for Ni^{63} Self-Diffusion at 1151°C. Diffusion Time 145 hrs.

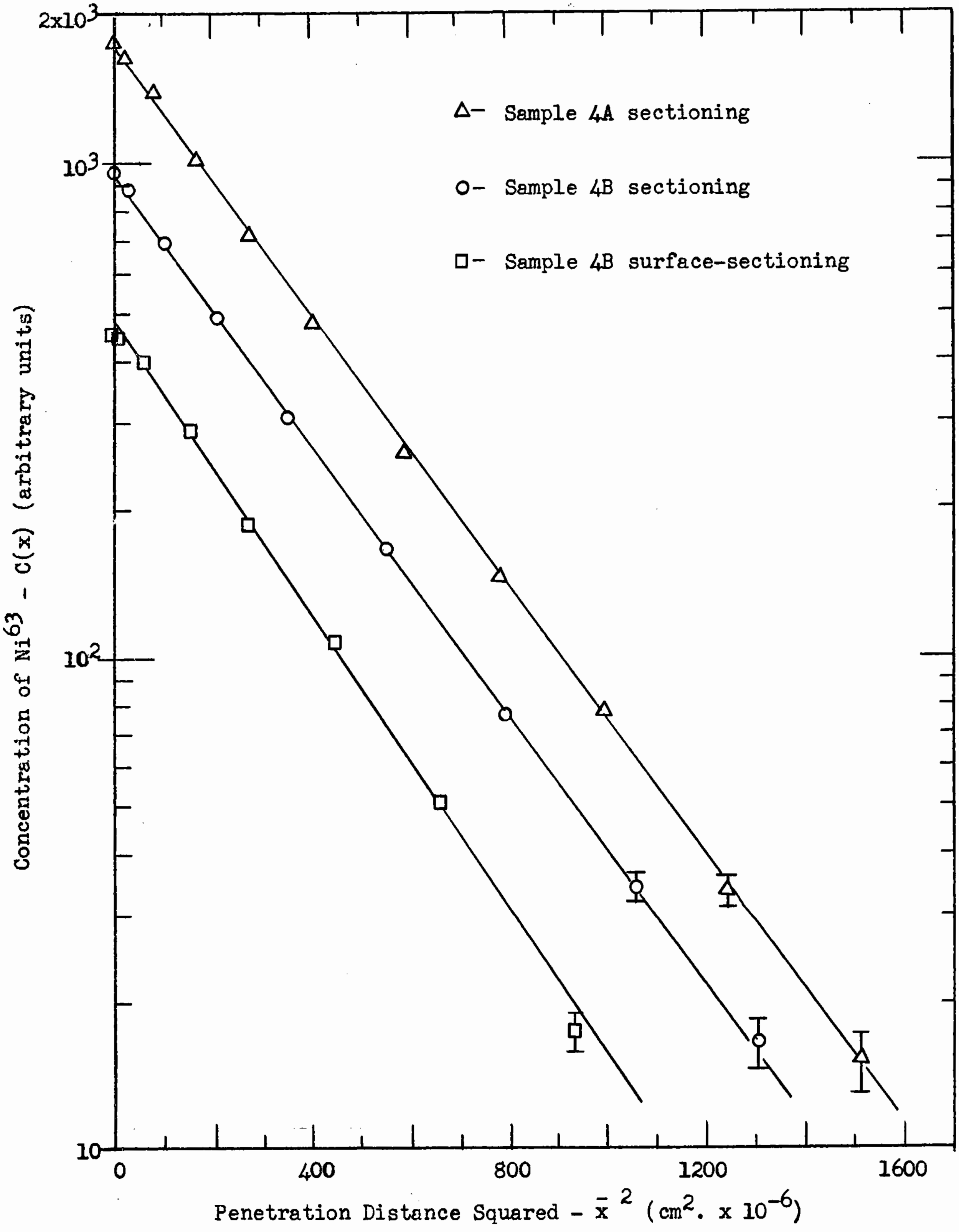

Figure 26. Concentration-Penetration Curves for Nickel Self-Diffusion at 1197°C. Diffusion Time 150.3 hrs.

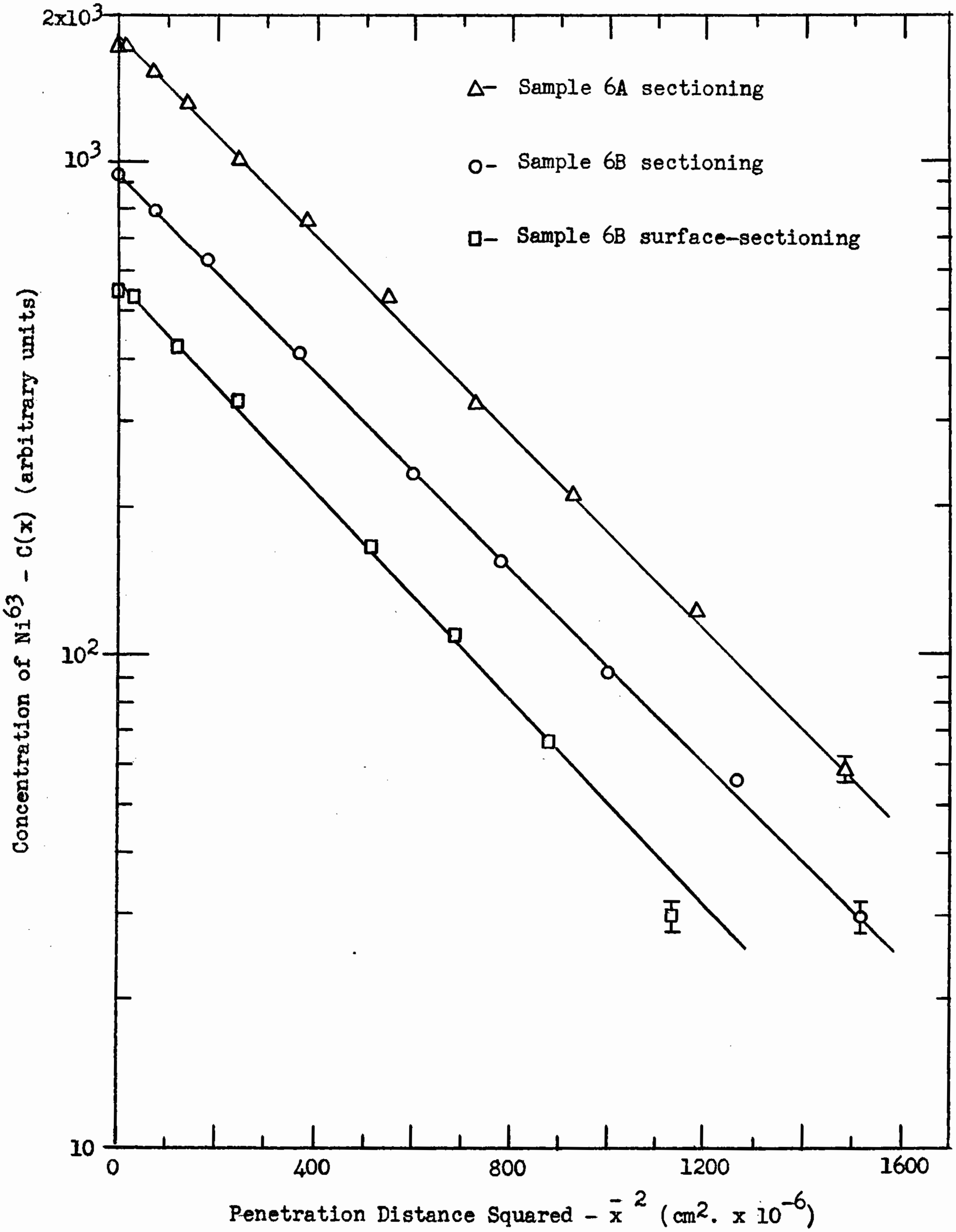

Figure 27. Concentration-Penetration Curves for Nickel Self-Diffusion at 1294°C. Diffusion Time 48.25 hrs.

the specimen, was transported there by grain boundary diffusion. An examination of the curves for 1151°C, Figure 25, showed that, while there was an indication of grain boundary diffusion, log C(x,t) was not linear with $\bar{x}$ at large penetration distances. This indicated that the results at 1151°C were more representative of volume diffusion than those obtained at lower temperatures.

In the penetration curves where volume diffusion predominated, the plotted points of the logarithm of concentration versus distance squared were located on or very close to a straight line relationship. The fact that the initial point always fell on this line made it apparent that none of the tracer was blocked at the surface by an oxide layer or lost by evaporation. If blocking occurred, the initial point would lie above the line, and if evaporation occurred, below the line.

The diffusion coefficients are calculated from the concentration-penetration curves using Equation (18). Because the distances plotted on the penetration curve refer to measurements made at 20°C, these coefficients must be corrected to the diffusion temperature. As this correction is slight the following equation adequately expresses the expansion of nickel with temperature.

$$l_T = l_{293} \left[1 + \alpha (T - 293) \right] \qquad (60)$$

where

α = Coefficient of linear expansion of nickel with temperature - $^{o}K^{-1}$.

Using a value of α equal to 17.3×10^{-6}, the diffusion coefficient at each temperature was corrected and recorded in Table 8 under the heading D_T.

Johnson[118] studied the rate of diffusion of the five stable isotopes of nickel into copper and found the rate of diffusion of each isotope was inversely proportional to the square root of its mass. As the mass of Ni^{63} is appreciably larger than the atomic weight of nickel, the coefficients were corrected by the relationship

$$D_{Ni} = D_{Ni^{63}} \sqrt{\frac{M_{Ni^{63}}}{M_{Ni}}} = 1.03\ D_{Ni^{63}} \qquad (61)$$

The corrected diffusion coefficients are recorded in Table 8 under the heading D.

An examination of the curves given in Figures 26 and 27 showed that the experimental data obtained with the surface activity-sectioning technique was not in good agreement with that obtained with the standard technique. The surface activity data gave steeper slopes than that obtained from the same sample using the standard technique. The excellent agreement between the results from the duplicate samples, when analysed in the standard technique, showed that this difference is real. The diffusion coefficients determined by both methods are compared in Table 9. It is apparent that the coefficients are about 5.6% lower, on the average, when determined by the surface activity method. It was considered that these differences arose from the use of sections of finite thickness or from contributions of Ni^{59} to the surface counting rate. Excessive section thickness could make the sectioning results too large and the presence of Ni^{59} could make the surface activity - sectioning results too low.

The error, introduced by using sections of finite thickness, was analysed mathematically and found to be negligible but an additional experiment was performed to confirm this conclusion. A pair of samples was held at the diffusion temperature, 1400°C, for twice the regular period of time. These samples were sectioned by both methods and no better agreement was found. From this it can be concluded that the section thickness is not the source of the error, as deeper penetrations should have improved the correlation.

The surface counting rate represents the specific activity of the active nickel on the surface only when there is a negligible amount of Ni^{59} in the active material. Ni^{59} has a much more penetrating radiation than Ni^{63}. When the surface activity of a diffused sample is determined at $x = 0$, the

Table 9

Comparison of Diffusion Coefficients Determined by Both Sectioning Techniques

Temp. Deg. C	Diffusion Coefficient x 10^{10}		Difference in Per Cent
	Standard cm^2./sec.	Surface cm^2./sec.	
1151	0.661	0.651	1.5
1197	1.56	1.51	3.2
1251	3.62	3.29	9.6
1294	6.85	6.46	6.0
1399	28.5	26.4	7.6

Average difference = 5.6 per cent

relative contributions of Ni^{59} to the total counting rate will be increased, as Ni^{59} will be detected from a much thicker portion of the diffused specimen than will Ni^{63}. As the sample is sectioned, it is apparent that the relative proportion of Ni^{59} to Ni^{63}, detected by surface counting, will decrease as the underlying layers of active material become thinner. The general effect will be smaller values for **the** determined diffusion coefficients. From a consideration of the absorption of Ni^{59} and Ni^{63}, the amount of tracer used and the relative proportions of Ni^{59} to Ni^{63}, it was estimated that the error from this source would be less than one per cent.

When beta-particles are absorbed in matter, there is a slight probability that some X-rays will be emitted from the absorbing material; this phenomenon is known as Bremsstrahlung. The X-rays, produced in this case by the absorption of beta-particles emitted from Ni^{63} atoms located well below the surface of the specimen, could cause an effect similar to that suggested for Ni^{59}. The total contribution of these penetrating radiations from Ni^{59} and Bremsstrahlung to the surface counting rate was checked in the following manner. The surface activity of a diffused specimen was measured with a 10 mg./cm^2. aluminum absorber placed over the active surface. This aluminum would absorb all the Ni^{63} radiation and about half the X-radiation emitted by the specimen. However the counting rate was found to be identical, within statistics, to the normal background for the counter, indicating that there were not enough X-rays being emitted to cause the observed deviations in the diffusion coefficient. No solution to this irregularity is offered.

The diffusion coefficients are usually related to the diffusion temperature by the Arrhenius equation

$$D = D_o e^{-Q/RT} \qquad (9)$$

The corrected diffusion coefficients from Table 8 have been plotted, in Figure 28, against the reciprocal of the temperature, to obtain the activation energy for nickel self-diffusion. The results from both the standard sectioning technique and the surface sectioning technique have been fitted separately by straight lines using least mean squares in the temperature range 1150° to 1400°C. In applying the least mean square method it has been assumed that the temperatures are accurate and that the observed deviations in the diffusion coefficients originate from other sources. In analysing the data for the standard sectioning technique, the diffusion coefficients determined at 1051°C and 1101°C have been omitted, as these values are suspect because of grain boundary diffusion.

The diffusion coefficient determined by standard sectioning technique is

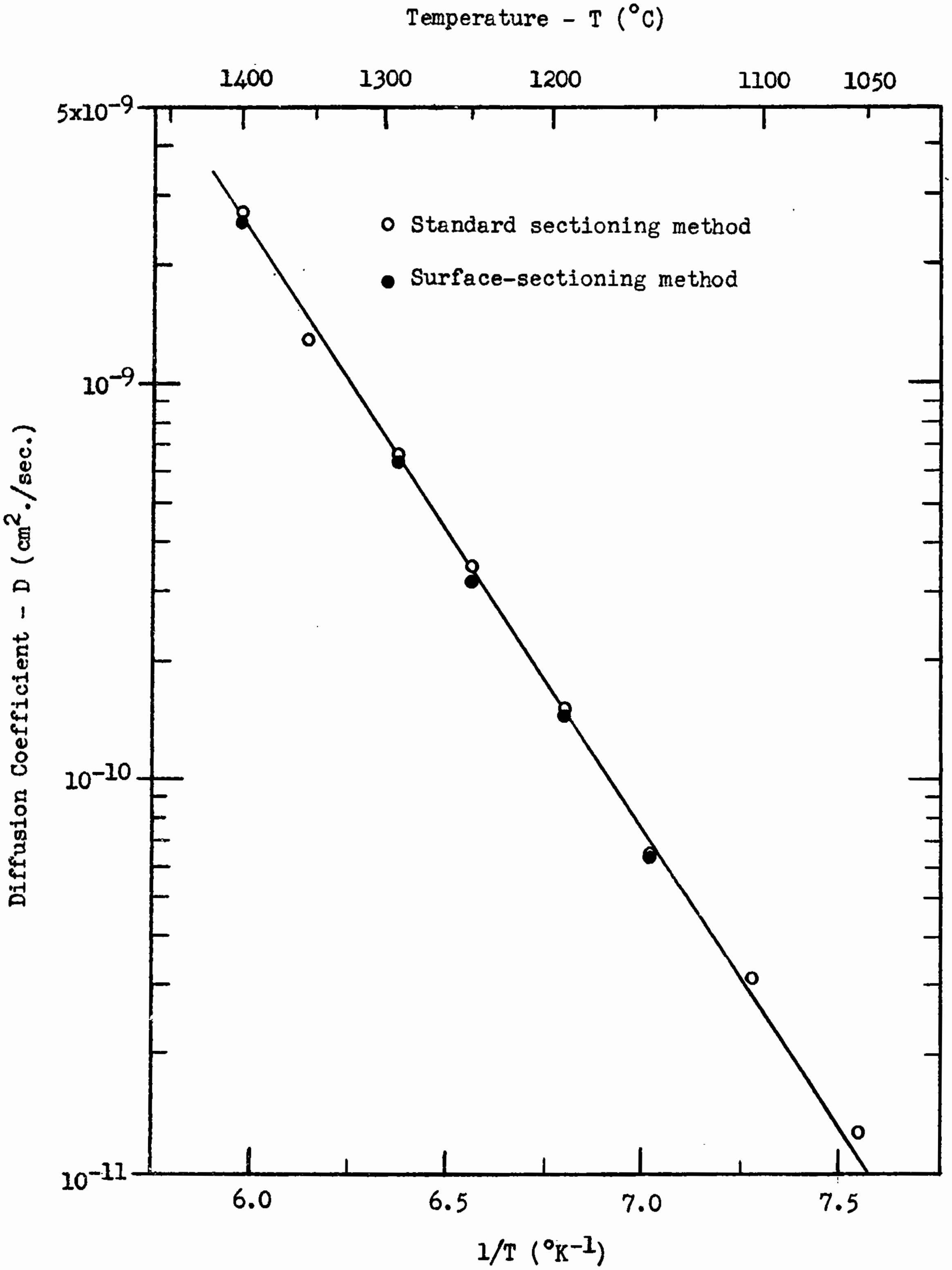

Figure 28. Activation Energy Plot for Nickel Self-Diffusion.

$$D_{Ni} = 3.77 \begin{matrix} +\ 2.72 \\ -\ 1.72 \end{matrix} e^{-\frac{70,000 \pm 1700}{RT}} \tag{62}$$

This gives an activation energy for nickel self-diffusion of 70 kcal./mole and a frequency factor of 3.77 cm^2./sec.

The diffusion coefficient determined by the surface activity-sectioning technique is

$$D_{Ni} = 3.13 \begin{matrix} +\ 0.78 \\ -\ 0.62 \end{matrix} e^{-\frac{69,500 \pm 600}{RT}} \tag{63}$$

This gives an activation energy for nickel self-diffusion of 69.5 kcal./mole and a frequency factor of 3.13 cm^2./sec.

EXPERIMENTAL TECHNIQUES AND RESULTS

Part 3 - Diffusion Studies with a Surface Activity Technique

Introduction

The surface activity-sectioning technique was developed to facilitate the determination of the rate of diffusion of Ni^{63} into other metals. Its successful application is dependent on the ease with which a sample, which has been removed from the lathe to determine its surface activity, can be replaced and realigned. Preliminary experiments, using this technique to determine the rate of diffusion of Ni^{63} into iron and cobalt, were not successful, because specimens of these metals changed shape during diffusion, making it difficult to realigne them in the lathe. The distortion of these samples occurs as a result of the allotropic transformations taking place when iron or cobalt specimens are heated to and cooled from the diffusion temperature.

However the results of the surface-activity sectioning experiments for nickel self-diffusion showed that the specific activity of the material at the surface of a diffusion specimen was given by the counting rate observed at the surface. This suggested the use of the following method to obtain diffusion coefficients. The solution to Fick's law corresponding to the diffusion of an infinitely thin layer of material into a semi-infinite medium, D assumed constant, is

$$C(x,t) = \frac{C_o}{\sqrt{\pi Dt}} e^{-x^2/4Dt} \qquad (17)$$

For the limiting case of x = 0, Equation (17) becomes

$$C(0,t) = \frac{C_o}{\sqrt{\pi Dt}} \qquad (64)$$

Thus by measuring C_o, the quantity of tracer initially deposited on the surface, and by measuring the variation of surface activity **with** time, the diffusion coefficient can be evaluated.

Diffusion specimens

The samples used in this part of the research were high-purity nickel, iron and cobalt, and two iron-nickel alloys. The nickel, iron and cobalt were obtained from the National Research Corporation, Cambridge, Mass. and are identified as NIVAC-P, FERROVAC and COVAC. Their respective analyses are shown in Tables 7, 10 and 11, The two iron-nickel alloys were prepared from electrolytic iron and nickel in a vacuum-melting furnace by H.V. Kinsey, Bureau of Mines, Ottawa, Ontario. The analyses of these alloys are given in Table 12. Discs 0.650

Table 10

Gas Free High Purity Iron

Composition in Weight Per Cent

All values except for iron are less than the amount given

Iron	99.91
Nitrogen	0.0005
Oxygen	0.02
Hydrogen	0.0005
Aluminum	0.002
Arsenic	0.0001
Carbon	0.005
Chromium	0.002
Cobalt	0.007
Copper	0.01
Lead	0.0001
Manganese	0.007
Mercury	0.0001
Molybdenum	0.002
Nickel	0.015
Phosphorus	0.001
Silicon	0.007
Sulphur	0.003
Tin	0.005

Table 11

Vacuum-Melted High-Purity Cobalt

Composition in Weight Per Cent

Cobalt	99.5
Nitrogen	< 0.0001
Oxygen	< 0.01
Hydrogen	< 0.0001
Calcium	trace
Carbon	< 0.01
Iron	0.15
Magnesium	trace
Nickel	0.3
Silicon	0.05

Table 12

Iron-Nickel Alloys

Analysis in Weight Per Cent

	Alloy 1	Alloy 2
Nickel	5.79	14.88
Iron	94.19	85.11
Carbon	0.036	0.020

inches in diameter and about 0.15 inches in thickness were machined from the five materials to prepare the diffusion specimens.

The iron, cobalt and the two alloys all differ from nickel in that, while they have a face-centered cubic structure at diffusion temperatures, they transform, either partially or entirely, into other structures when cooled to room temperature. However by annealing the samples at a high temperature - 1400°C - for 24 hours, a large prior grain size was attained. As the transformation structures are crystallographically oriented with respect to this original structure, the large prior grain structure was rapidly reattained when the specimens were reheated to the diffusion temperature. Thus the preliminary treatment assured that no grain growth occurred during most of the diffusion anneal and a very large grain size was attained very rapidly, to minimize the effect of grain boundary diffusion.

Samples of the above four materials were examined under the microscope to estimate the prior grain size. The grain diameter of the iron and cobalt was 6 to 10mm, and of the iron-nickel alloys 2 to 4 mm.

The specimens were then carefully faced on a lathe, using fine feeds and shallow cuts to minimize the depth of the layer of disturbed metal. This flat surface was ground on a series of polishing papers, finishing on 4/0 grade. The samples were then prepared anodically for electroplating, using the technique previously described, and an equal amount of radioactive nickel was electroplated onto each specimen, the layer of active material being 0.0001 cm. thick. All samples were checked for the uniformity of the electroplated layer and those showing variations in thickness greater than ± 3 per cent from the mean were rejected.

Diffusion anneal

To minimize the effects of evaporation, the experiments were made in duplicate, with the active faces of the two samples placed in contact. A suspension of fine alumina powder in ethyl alcohol was used to wash the samples before diffusion. The slight deposit of alumina left on the specimens separated them sufficiently to prevent welding during the diffusion anneal. Ten specimens, a pair for each metal investigated, were placed in an alumina crucible and annealed together at the chosen diffusion temperature. The same precautions and techniques as previously employed were followed to accurately maintain the specimens at the chosen diffusion temperature and to determine the length of the diffusion anneal. A purified hydrogen atmosphere was used to protect the samples and no signs of oxide were found on any of the specimens after diffusion.

Results

Diffusion coefficients were determined at five temperatures in the range 1150°C to 1400°C. The surface activity of each specimen was measured at least four times, after varying periods of diffusion, to obtain a curve of $C(0,t)$ versus $1/\sqrt{t}$. The diffusion periods were selected to give equal intervals on a $1/\sqrt{t}$ axis, for example, 4, 16, 36 and 64 hours. The surface activities were measured using a diaphragm with a 0.55-in. diameter opening over the active surface, to minimize edge effects arising from surface diffusion.

The error in the diffusion coefficient, calculated from Equation (64), is twice the experimental error involved in measuring C_o, the quantity of tracer deposited on the specimen. The following procedure was selected as giving the best value for C_o. The two nickel specimens, diffused at 1209°C, were sectioned by the surface activity-sectioning technique and the area under the resulting curve of $C(x,t)$ versus x was integrated to give a value for C_o. The values of C_o for the two samples agreed within one per cent. Using the mean value of C_o, the diffusion coefficients calculated for these samples from Equation (64) were in good agreement with those calculated from the sectioning data using Equation (18). This confirmed that this surface activity method gives results in agreement with those obtained with the sectioning techniques.

The experimental curves for all specimens, at the diffusion temperature of 1209°C, are given in Figure 29 and are typical of those obtained at all temperatures. It can be seen that for surface activities below 4500 c.p.m. the curves are all linear, conforming to Equation (64). However the curves for the diffusion of nickel into iron, cobalt and the two iron-nickel alloys are all curved in the region corresponding to small amounts of diffusion. This curvature indicates either a variation of the diffusion coefficient with time - a concentration effect - or a failure to satisfy the boundary conditions of Equation (64). The curve given in Figure 30 shows that the plot of $C(0,t)$ versus $1/\sqrt{t}$ for nickel self-diffusion at 1150°C is linear for all diffusion times. This confirms that the curvature observed in the experimental curves for the other specimens - Figure 29 - corresponds to a variation of the diffusion coefficient with composition - a result of not using an infinitely thin layer of tracer.

It can also be observed in Figure 29 that all the curves, when extrapolated to infinite diffusion time, pass through the origin, indicating that none of the active nickel was blocked at the surface. This showed that the procedure used to electroplate the tracer on the various specimens was satisfactory and no errors were introduced by blocking of the tracer at the surface.

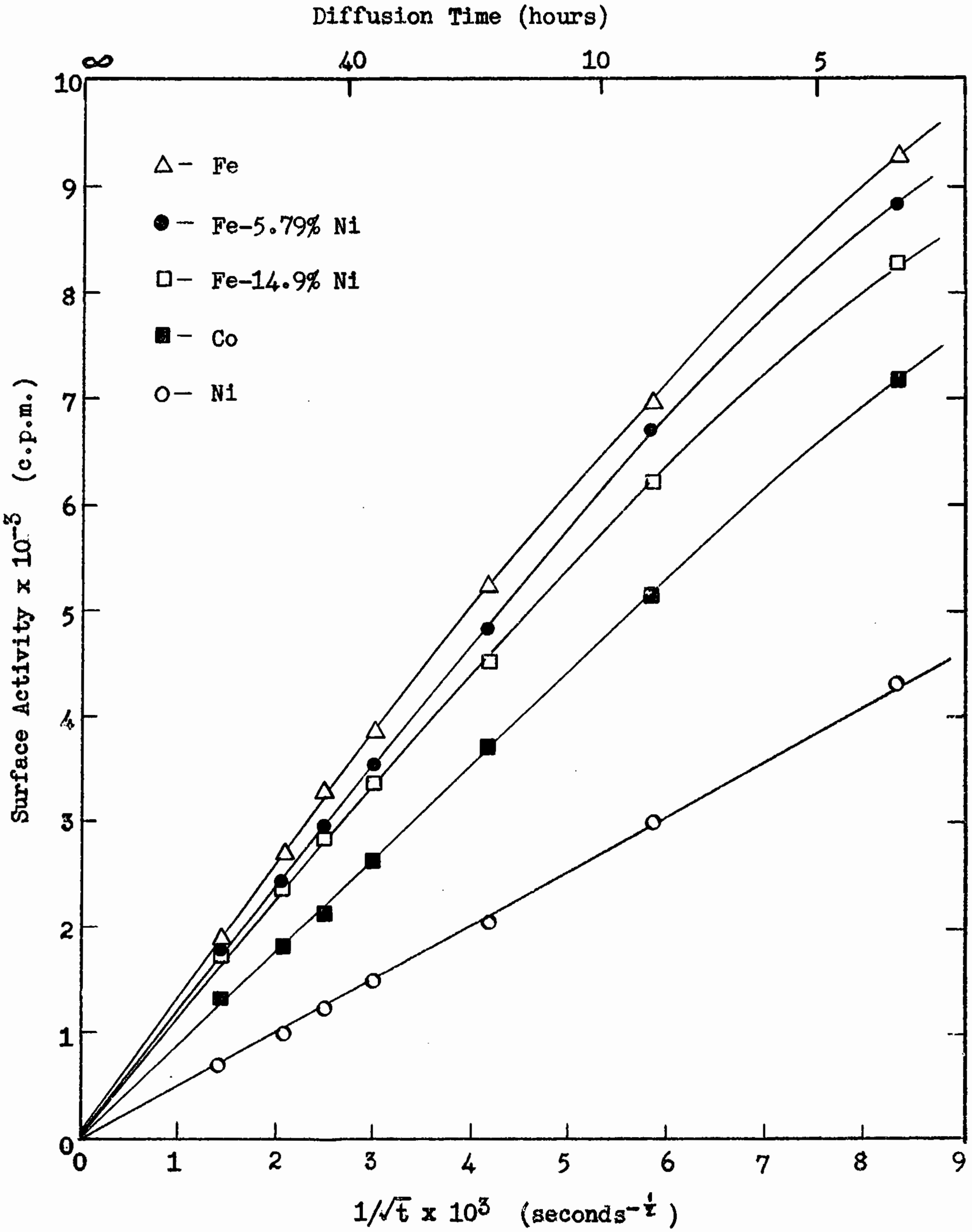

Figure 29. Variation of Surface Activity with Diffusion Time for Ni^{63} Diffusing into Various Metals and Alloys at 1209°C.

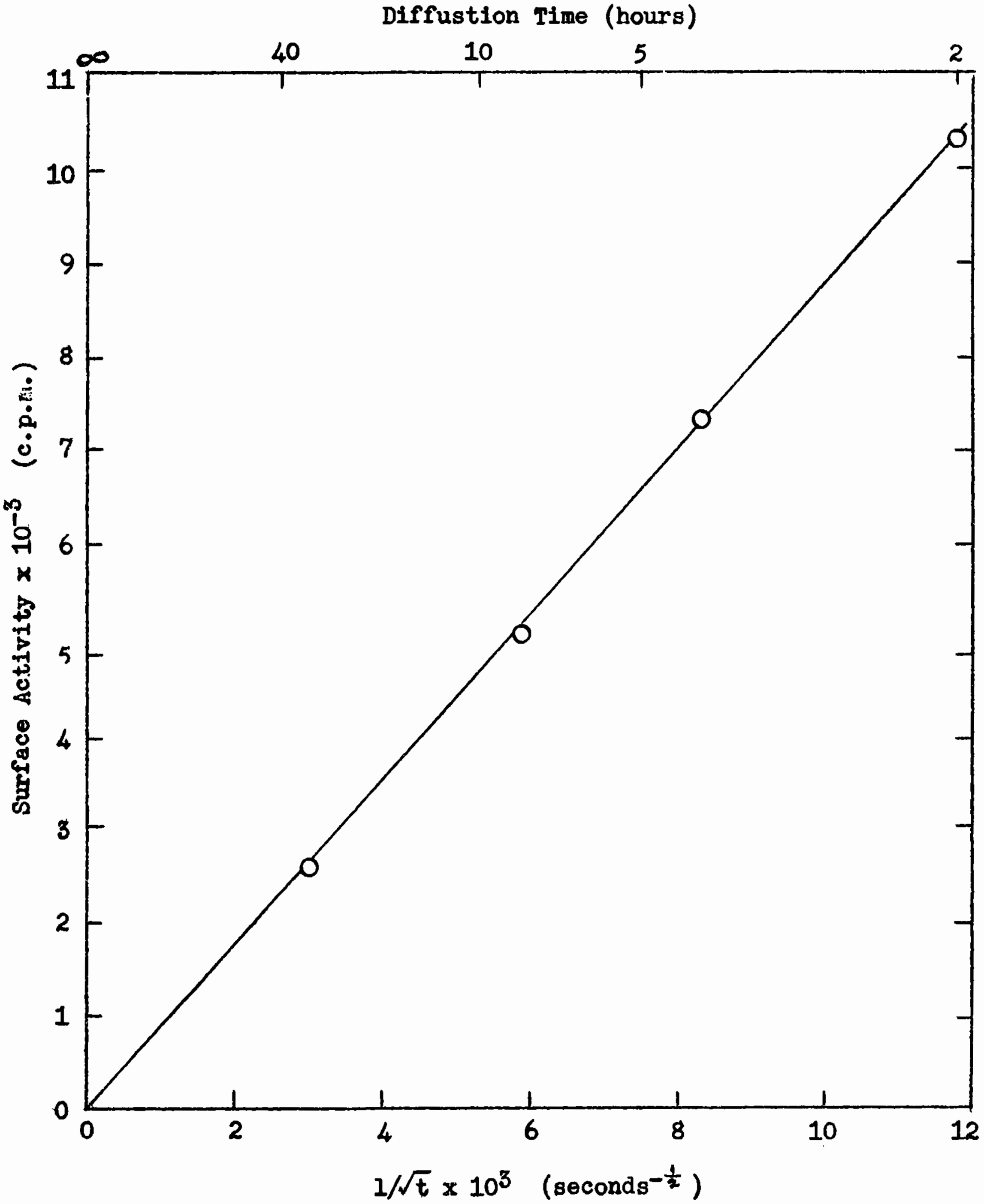

Figure 30. Variation of Surface Activity with Diffusion Time for Nickel Self-Diffusion.

The diffusion coefficients obtained by a surface activity technique have larger errors, introduced by evaporation of the tracer from the active surfaces, than the sectioning technique. The following experiment was performed to determine if active material did evaporate from the diffusion specimens at temperature and, in the event that evaporation occurred, how successful was the experimental procedure of placing the active faces of a pair of specimens in contact, to reduce the loss of the tracer. Two nickel discs were prepared in the usual manner but active nickel was applied to the face of only one of the discs. The discs were placed together, with the active surface between them, and annealed at 1200°C for 12 hours in a hydrogen atmosphere. After this period activity was found on the surface of the inactive disc, indicating that evaporation and condensation of nickel had occurred in the gap between the specimens. No trace of activity was found on the surface of the supporting crucible, however, which indicated that the loss of activity from the interface was quite small. Thus while evaporation of the active nickel did occur during diffusion, it would appear that a negligibly small quantity was lost from the surfaces, and the resulting error in the diffusion coefficients was small.

The diffusion coefficients were calculated in each experiment from the linear portions of the curves $C(0,t)$ versus

$1/\sqrt{t}$. It is apparent that since the diffusion coefficient was constant in this region, the calculated coefficients are representative of the rate of diffusion of nickel at low solute concentrations, in the case of iron and cobalt, and of the rate of nickel self-diffusion in a homogeneous alloy, in the case of the iron-nickel alloys.

The diffusion coefficients were corrected, as before, for lattice expansion and the isotopic mass effect. The results are summarized in Table 13 and the activation energy plot given in Figure 31. The equations for the diffusion coefficients were determined using least mean squares, on the assumption that the measured temperatures are correct, and are for nickel self-diffusion

$$D = 5.28 \begin{matrix} +\ 2.80 \\ -\ 1.77 \end{matrix}\ e^{-\frac{71{,}000 \pm 1800}{RT}} \qquad (65)$$

diffusion of nickel into cobalt at low solute concentrations

$$D = 1.29 \begin{matrix} +\ 0.72 \\ -\ 0.475 \end{matrix}\ e^{-\frac{72{,}100 \pm 1400}{RT}} \qquad (66)$$

diffusion of nickel into iron at low solute concentrations

$$D = 7.13 \begin{matrix} +\ 6.70 \\ -\ 3.45 \end{matrix}\ e^{-\frac{77{,}600 \pm 2000}{RT}} \qquad (67)$$

Table 13

Diffusion Coefficients for the Diffusion of Ni^{63} into Certain Metals and Alloys

Temp. Deg. Cent.	Diffusion Coefficients, $cm^2. sec^{-1}. \times 10^{11}$ for the Diffusion of Nickel into				
	Nickel	Iron 14.9% Ni	Iron 5.9% Ni	Iron	Cobalt
1152	6.36	1.33	1.25	0.882	2.22
1209	19.5	3.69	3.35	2.81	6.22
1271	49.7	9.94	8.37	6.97	16.2
1327	103	26.3	19.1	16.9	35.8
1400	276	67.5	61.8	55.3	99.1

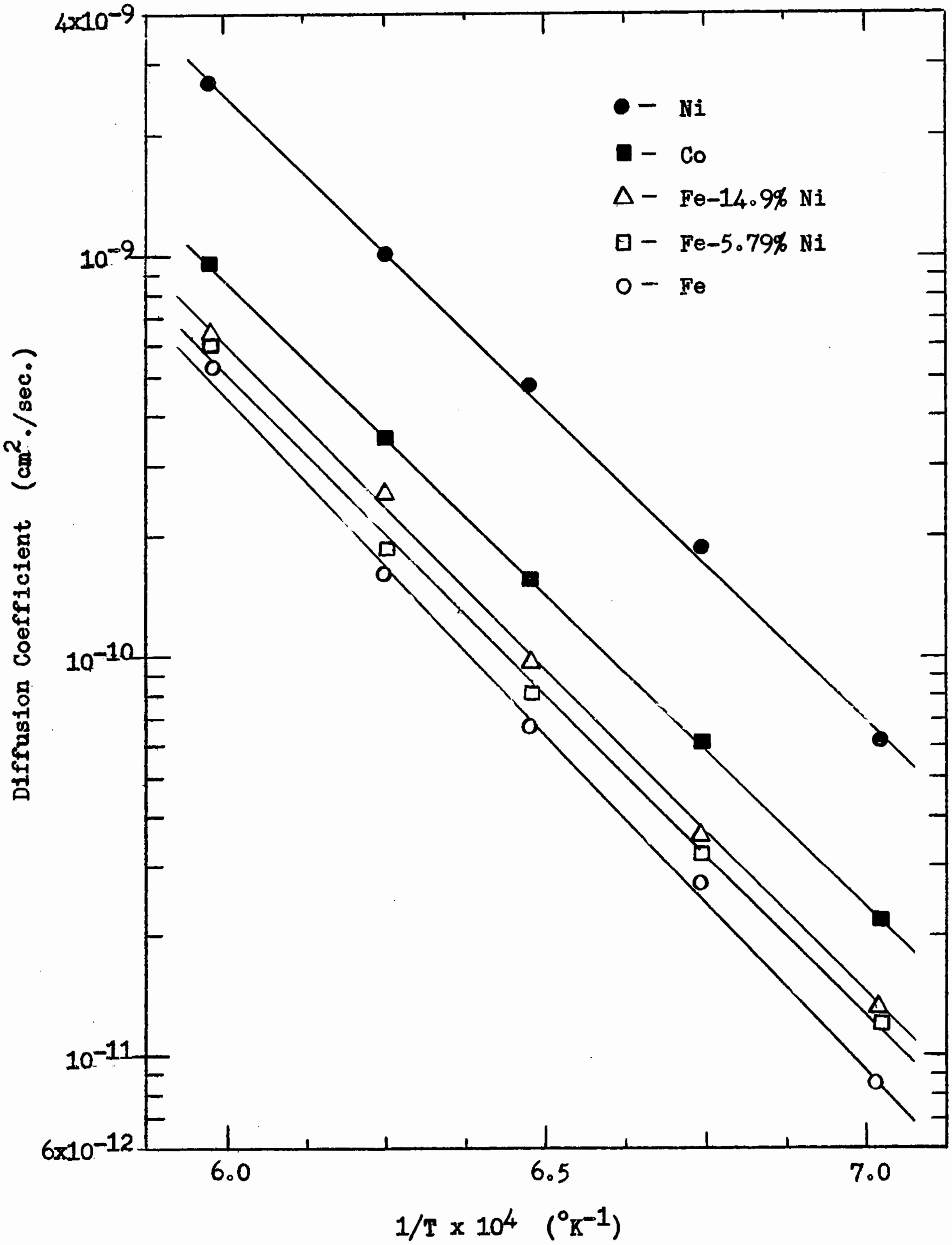

Figure 31. Activation Energy Curves for Nickel Self-Diffusion and Diffusion of Nickel into Various Metals and Alloys.

self-diffusion coefficient for nickel in an iron-5.8% nickel alloy

$$D = 2.17\begin{matrix}+\ 2.11\\-\ 1.09\end{matrix}\ e^{-\frac{73{,}500 \pm 2000}{RT}} \qquad (68)$$

and the self-diffusion coefficient for nickel in an iron-14.88% nickel alloy

$$D = 5.14\begin{matrix}+\ 2.58\\-\ 1.70\end{matrix}\ e^{-\frac{75{,}600 \pm 1200}{RT}} \qquad (69)$$

The corresponding activation energies and frequency factors are shown in these equations.

DISCUSSION

Parts 2 and 3a - Self-Diffusion of Nickel

Results

The rate of nickel self-diffusion, in polycrystalline material, was measured in this research over the temperature range 1050°C to 1400°C. Above 1150°C it was found that the measured rate of diffusion was equal to the rate of volume self-diffusion. Below 1150°C, diffusion occurred in a non-homogeneous manner, with both grain boundary and volume diffusion occurring simultaneously. The diffusion coefficients determined at 1050°C and 1100°C gave results that were erroneously high on a volume diffusion basis. The high results were shown to be due to the rapid migration of a portion of the tracer, Ni^{63}, along the grain boundaries.

Three experimental methods were used to measure the rate of nickel self-diffusion in the range 1150°C to 1400°C. The results obtained by these three methods are, for the standard sectioning method

$$D = 3.77 \begin{array}{l} + 2.72 \\ - 1.72 \end{array} e^{-\frac{70,000 \pm 1700}{RT}} \qquad (62)$$

for the surface activity-sectioning method

$$D = 3.13^{+0.78}_{-0.62} \, e^{-\frac{69,500 \pm 600}{RT}} \qquad (63)$$

and for the surface activity method

$$D = 5.28^{+2.80}_{-1.77} \, e^{-\frac{71,000 \pm 1800}{RT}} \qquad (65)$$

These equations all agree within the accuracy given for each and show that the measurements have been made with good precision for a high temperature diffusion study. The two special techniques, developed to take advantage of the very soft characteristics of Ni^{63} beta-radiation, the surface activity-sectioning method and the surface activity method, gave as precise results as the standard sectioning technique.

The results of the three methods of investigation are summarized in the equation

$$D = 3.97 \, e^{-\frac{70,100}{RT}} \qquad (70)$$

It therefore can be concluded that the activation energy for nickel self-diffusion is 70.1 kcal./mole and the frequency factor is 3.97 cm^2./sec.

After this research was started, a short note was published by Burgess and Smoluchowski[118], who proposed a value between 61.0 and 65.0 kcal./mole for the activation energy for nickel self-diffusion. Their results were obtained by a surface activity technique, not specified in detail, below a maximum temperature of 1250°C. While the surface activity method is less sensitive to the errors introduced by grain boundary diffusion than is a sectioning method, it is highly probable that their proposed value is too low on account of the effect of grain boundary diffusion, which in this research became appreciable below 1150°C. No value was given for the frequency factor which further suggests that their results are only tentative. A recent review article has indicated that nickel self-diffusion has been investigated by Hoffman, Pikus and Ward[119] but no results are available to date.

It has been found by other investigators that the rate of diffusion of solute atoms, at low solute concentrations, is of the same order of magnitude as the rate of self-diffusion of the solvent atoms, when the solute and solvent atoms have similar properties. Cobalt, manganese and nickel are transition elements with many similarities in properties and it would be expected that their rates of diffusion into nickel would be similar to the rate of self-diffusion of nickel. The values of D_o and Q determined by Ruder and Birchenall[73], for the rate of diffusion of Co^{60} into nickel, are 1.46 cm^2./sec. and 68.3 kcal./mole and those determined by Swalin and Martin[120], for the rate of diffusion of manganese into nickel, are 7.5 cm^2./sec. and 67.1 kcal./mole. The similarity between these results and those of this investigation for nickel self-diffusion can be considered as evidence of the accuracy of the present work.

Elastic parameters of nickel

In the introduction, certain formulae were given to relate the values of D_0 and Q for a self-diffusion measurement to the elastic properties of the lattice. In particular, the required parameters are the temperature coefficient of Young's modulus, μ', and the three elastic moduli, C_{11}, C_{12} and C_{44}. The temperature variation of Young's modulus for nickel was measured by Koster[121] and by Siegel and Quimby[122]. The data obtained are shown respectively in Figures 31a and 31b. It is apparent that above the Curie point the temperature variation of Young's modulus for paramagnetic nickel is linear, indicating the absence of viscous slip at the grain boundaries[86]. The values calculated from these curves for the ratio of the temperature coefficient of Young's modulus, μ', to the value of Young's modulus extrapolated to $0^\circ K$, μ_0, are respectively 2.90 and $2.83 \times 10^{-4}\ {}^\circ K^{-1}$. As these values were calculated from the linear portion of the curves above the Curie temperature, it is evident that they are representative of paramagnetic nickel and can be used in interpreting diffusion measurements in paramagnetic nickel.

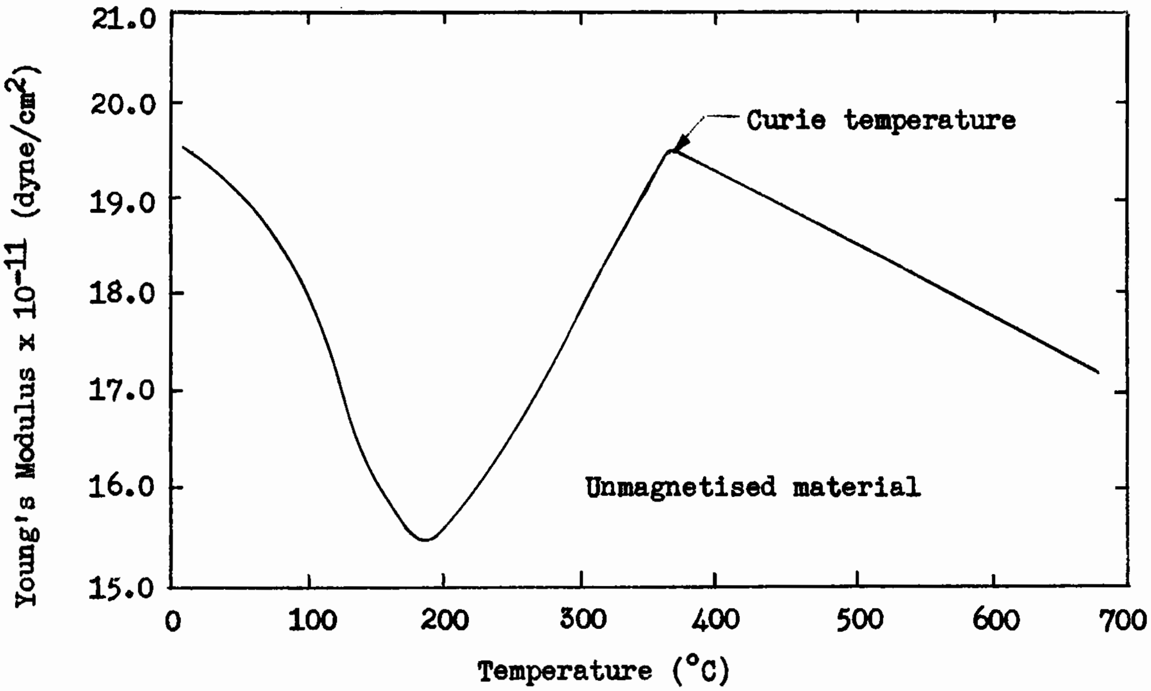

Figure 31a. Temperature Variation of Young's Modulus for Nickel
Koster 121

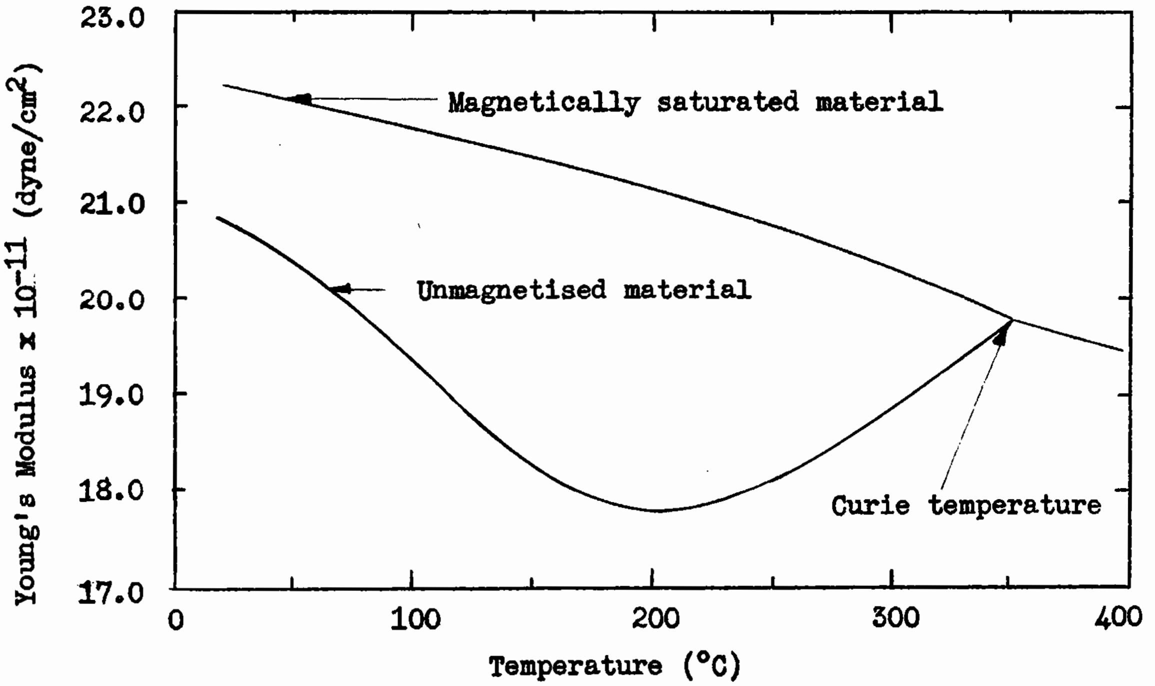

Figure 31b. Temperature Variation of Young's Modulus for Nickel
Sidney, Seigel and Quimby 122

The elastic moduli, C_{11}, C_{12} and C_{44} were measured in ferromagnetic nickel by Bozworth, Mason, McSkimin and Walker[123] at room temperature. No values are available for paramagnetic nickel. It is apparent from Figures 31a and 31b that the elastic properties suffer an abrupt, though slight, change when nickel transforms from paramagnetic nickel, the form existing above the Curie temperature, to ferromagnetic nickel, the form existing below the Curie temperature. It can be observed in Figure 31b that when the ferromagnetic nickel is magnetically saturated, its behaviour is typical of a non-ferromagnetic material with only a slight break occurring in the curve at the Curie point. It can be calculated that the value found for Young's modulus in a non-saturated sample is 6.7% lower than that found for a saturated sample at room temperature. This indicates that the difference between the elastic properties of ferromagnetic nickel, at room temperature, and those expected if the material were still paramagnetic at room temperature is quite small. Therefore the values C_{11}, C_{12} and C_{44} measured experimentally at room temperature will be taken as the appropriate values for paramagnetic nickel.

Using the above sources of data the average value for μ'/μ_0 is 2.87×10^{-4} $^{\circ}K^{-1}$ and the value of Young's modulus, E_{211}, calculated for the <211> direction in nickel is 57.0 kcal./cm^3. at 0°K. These values are specified because Kurtz, Averback and Cohen[124] have employed values of μ'/μ_0 equal to 2.43×10^{-4} °K^{-1} and E_{211} equal to 54.0 at 0°K in their paper on the rate of self-diffusion of gold in the gold-nickel system. As they give the identical references for the source of their elastic data, and do not mention that any adjustment of values was made, no apparent reason exists for this discrepancy. While it is of no importance to this research, anyone comparing the calculations made in this research to those in any other investigation should check to see that the comparison is made using the same values of μ'/μ_0 and E_{211}.

Brooks' macroscopic calculation for the activation energy

In the introduction the details of a macroscopic calculation made by Brooks[91] for the activation energy for self-diffusion in face-centered cubic lattice metals were given. The results of his calculations were summarized in Table 4 and compared to selected diffusion data. It was indicated that his theoretical values were 1.84 times as large as the experimental values he quoted. This table is repeated in Table 14, with the main difference being that most of the reasonable self-diffusion data are now included, not only selected data. The values marked with an asterisk are closest to the average experimental values originally quoted. The theoretical values for the activation energy were calculated from Equations (40) and (42).

Table 14

Comparison of Experimental Values of the Activation Energy for Self-Diffusion to Values Calculated from Macroscopic Considerations

Metal	Experimental Activation Energy Q $\frac{\text{kcal.}}{\text{mole}}$	Theoretical Activation Energy $f_s + f_v$ $\frac{\text{kcal.}}{\text{mole}}$	Ratio $\frac{\text{Theory}}{\text{Experimental}}$	Reference
Pb	27.4*	49.3	1.80	66
	24.2		2.04	67
	25.7		1.92	68
Ag	45.9*	83.7	1.82	44, 55
	45.5*		1.84	69
Cu	46.5	88.0	1.89	125
	49.0*		1.80	28
	46.8		1.88	29
Au	51.0*	92.2	1.81	70
	53.0		1.74	71
	45.6		2.02	72
Ni	70.1	121.8	1.72	

It is apparent that using a slightly wider selection of self-diffusion data has rather reduced the consistency of the correlation. The ratio calculated for nickel is 1.72 which is lower than any of the other values included in the tabulation. However this discrepancy is no greater than for most of the additional self-diffusion data in the table.

Assuming that Brooks' equations are valid, the ratio of 1.72 for nickel indicated that either the experimental activation energy determined for nickel, in the present research, is too large, or that the use of the elastic moduli for ferromagnetic nickel in Brooks' calculation has resulted in a value too low for the theoretical activation energy. Alternatively, assuming that all the diffusion data is valid, it is possible that the ratio of the theoretical activation energy to the experimental value varies with temperature. The metals gold, silver and copper melt in the range 950°C to 1100°C, while lead melts at 327°C and nickel at 1453°C. On this basis, Table 14 suggests that the correlation ratio decreases with increasing temperature and that Brooks' equations must be regarded as approximations. There is not sufficient evidence at present to decide which of these suggested reasons accounts for the discrepancy.

LeClaire's theoretical expressions for D_0 and Q

Le Claire's expressions - Equations (34) and (35b) - have been used in the manner suggested by him to calculate the correlation coefficients k_1 and k_2 for the self-diffusion data recorded in Table 15. The order of calculations is first to determine k_1 from Equation (35b) for all the data. Then with the average value of k_1 calculate the value of k_2 from Equation (34). Constant values for the coefficients k_1 and k_2 are taken as evidence that the experimental self-diffusion data for the face-centered cubic metals are consistent with the assumptions made to derive the theoretical expressions. All the data recorded in Table 15 are identical to that used to test Brooks' correlation and the data selected by LeClaire are marked with asterisks. The average values given by LeClaire for k_1 and k_2 are respectively 0.215 and 0.215. It should be emphasized that a high degree of correlation should not be expected, as values for D_o as shown in Table 15, generally show no greater accuracy than those obtained in this research, for example

$$3.77 \begin{matrix} + 2.72 \\ - 1.72 \end{matrix} \text{ cm}^2\text{./sec.}$$

An examination of Table 15 shows that the diffusion data selected by LeClaire gave values of k_1 between 0.201 and 0.228 and values of k_2 between 0.176 and 0.245. The values, found for nickel of k_1 and k_2 equal to 0.200 and 0.188 respectively, are in good agreement with the range of values obtained for the selected data, though slightly lower in both cases than the average values. An examination of the rest of the data recorded in the table indicates that most of it is in

Table 15

A Correlation of Diffusion Data with LeClaire's Theoretical Expressions

Metal	Q $\frac{\text{kcal.}}{\text{mole}}$	D_o $\frac{\text{cm}^2.}{\text{sec.}}$	k_1	k_2	Ref.
Pb	27.4*	4.02	0.214	0.221	66
	24.2	0.281	0.362	0.180	67
	25.7	1.17	0.282	0.199	68
Ag	45.9*	0.895	0.217	0.218	44, 45
	45.5	0.724	0.229	0.215	69
Cu	46.5*	0.178	0.228	0.176	125
	49.0	0.60	0.117	0.191	28
	46.8	0.32	0.164	0.178	29
Au	53.0*	0.157	0.201	0.245	71
	51.0	2.1	-0.139	0.231	70
	45.6	0.625	-0.101	0.191	72
Ni	70.1	3.97	0.200	0.188	

poor agreement with LeClaire's selected data.

On the assumption that LeClaire's correlation is valid, it can be concluded that the values of D_o and Q obtained in this research are in good agreement with some of the self-diffusion data determined for other metals.

Buffington and Cohen's theoretical expressions for D_o and Q

As noted in the introduction, Buffington and Cohen's approach, while similar to LeClaire's, resulted in slightly different expressions for D_o and Q. In their expressions the correlation coefficients are λ and K_{211}. The data included in Table 16 is, with few exceptions, that originally considered by Buffington and Cohen in testing the validity of their expressions. The values of λ and K_{211} were calculated from Equations (37) and (38). Buffington and Cohen suggested that all data be compared to the values of K_{211} and λ calculated from the precisely reproduced experimental data for silver self-diffusion. The nickel results of K_{211} equal to 0.473 and λ equal to 0.710 are in as good agreement with those of silver as are most of the other data. However it should be pointed out that the value of K_{211} is lower than the average for the table, which suggests that the activation energy determined for nickel is too low, while Brooks' correlation suggests that the value is too high.

In summary it can be stated that the values of D_o and

Table 16

A Correlation of Diffusion Data with Buffington and Cohen's Theoretical Expressions

Metal	Q $\frac{\text{kcal.}}{\text{mole}}$	D_o $\frac{\text{cm}^2.}{\text{sec.}}$	K_{211}	λ	Ref.
Pb	27.4	4.02	0.0516	0.642	66
	24.2	0.281	0.0456	0.440	67
	25.7	1.17	0.0483	0.560	68
Ag	45.9	0.895	0.0519	0.660	44, 45
	45.5	0.724	0.0515	0.637	69
Cu	46.5	0.178	0.0486	0.593	125
	49.0	0.60	0.0512	0.788	28
	46.8	0.32	0.0490	0.701	29
Au	51.0	2.1	0.0587	1.24	70
	53.0	0.157	0.0610	0.650	71
	45.6	0.625	0.0525	1.09	72
Ni	70.1	3.97	0.0473	0.710	

Q found for nickel self-diffusion are in reasonable agreement with the existing theories. However it is apparent that more accurate diffusion data and more accurate values for the physical constants of the metals are needed to ascertain the validity of the various lattice strain theories.

Activation energy to form a vacancy in nickel

These three theories all permit an estimation of the activation energy required to form a vacancy in nickel. The values calculated from each are listed in Table 17. A direct experimental determination of the activation energy required to form a vacancy has not been satisfactorily completed as yet. The values published to date have varied from 30 to 50 per cent of the total activation energy for diffusion, which is consistent with the estimates in Table 17.

Table 17

Estimated Activation Energies for Vacancy Formation in Nickel

Theory	Experimental Activation Energy Q $\frac{\text{kcal.}}{\text{mole}}$	Activation Energy to form a Vacancy f_v $\frac{\text{kcal.}}{\text{mole}}$	Ratio $\frac{f_v}{Q}$
Brooks	70.1	29.9	0.427
LeClaire	70.1	20.2	0.288
Buffington & Cohen	70.1	20.3	0.290

DISCUSSION

Part 3b - Diffusion Studies with a Surface Activity Technique

The rate of diffusion of Ni^{63} into five different polycrystalline materials, nickel, iron, cobalt, iron-5.79% nickel and iron-14.88% nickel, was measured in this research by a decrease in surface activity technique over the temperature range 1150°C to 1400°C. The results were corrected for the isotopic mass effect to represent the average rate of diffusion of nickel into the various materials. Coefficients for the diffusion of nickel into the five materials are given in the following tabulation and are for 1270°C. The calculated ratios of diffusion coefficients apply approximately to the whole temperature range investigated.

Solvent	$D \times 10^{11}$ cm^2./sec.	$\frac{D_{Ni}(\text{solvent})}{D_{Ni}(\text{self})}$
Ni	46.0	1.00
Co	15.5	0.34
Fe-14.88% Ni	10.0	0.22
Fe-5.79% Ni	8.71	0.19
Fe	6.92	0.15

The above results are consistent with the general rule that the higher the melting point of the solvent the lower the observed rate of diffusion in the solvent.

Time dependence of the diffusion coefficient

The common method of determining diffusion coefficients, using radioactive tracers, is to measure the rate of penetration of a thin layer of tracer into a semi-infinite medium. It has been commonly accepted that, even when the tracer is a different element than the solvent, the diffusion coefficient is independent of concentration. The only experimental evidence that this supposition is incorrect was given by Martin, Johnson and Asaro[96], who studied the rate of diffusion of gold into copper, using Au^{198}. They observed that at 1000°C the diffusion coefficient varied with the time of anneal, decreasing steadily for the first thirty hours and then assuming a constant value for longer diffusion times. No noticeable improvement was observed when the thickness of the layer of Au^{198} was decreased by a factor of fifty. This made it difficult to attribute the effect to a variation of the diffusion coefficient with composition. As an alternative, Martin et al suggested that an excess of vacancies was formed initially at the interface of tracer and solvent, and higher rates of diffusion were to be expected until the concentration of vacancies returned to normal. This suggestion implied that the same effect could be noticed in self-diffusion experiments as it was apparently independent of concentration. This was not confirmed by Tomizuka and Lazurus[126] who investigated the effect by studying silver self-diffusion for varying diffusion times. They concluded that the measured self-diffusion coefficient is independent of the time of anneal.

A similar effect was noticed in the present experiments. For the diffusion of nickel into iron, cobalt and the two iron-nickel alloys, it was observed that the diffusion coefficients decreased with time during the initial portion of the anneal. This phenomenon was not observed in the nickel self-diffusion experiments and thus confirms that the concentration gradient existing across the "mixed" diffusion couples results in an initial variation of the diffusion coefficient with time. In these experiments the diffusion coefficient became constant when sufficient diffusion had occurred to decrease the concentration of nickel at the active surface to about four per cent of the initial value.

Diffusion of nickel into cobalt at low solute concentration

The rate of diffusion of nickel into cobalt, at low nickel concentration, was found to be approximately one-third of the rate of nickel self-diffusion over the temperature range investigated. The diffusion coefficients obtained for the diffusion of nickel into cobalt are represented by the equation

$$D = 1.29 \begin{matrix} + 0.72 \\ - 0.47 \end{matrix} e^{-\frac{72,100 \pm 2000}{RT}} \qquad (66)$$

If the existing concepts of diffusion at low solute concentration are correct, it would be expected that these results would be similar to those obtained for the rate of cobalt self-diffusion. Cobalt self-diffusion has been investigated by Ruder and Birchenall[73], Gruzin[127], Mead and Birchenall[76] and Nix and Jaumont[128]. The results obtained in the latter two investigations are respectively

$$D = 0.83\ e^{-67,700/RT} \qquad (70)$$

and

$$D = 0.367\ e^{-67,000/RT} \qquad (71)$$

A comparison of Equations (66), (70) and (71) shows that the activation energy for nickel diffusing into cobalt is about 5 kcal./mole higher than the results for cobalt self-diffusion. Despite this discrepancy in the values found for the activation energy, it can be observed, with reference to Figure 32, that the results for the values of the measured coefficients for cobalt self-diffusion are in good agreement with those obtained in this research. Thus it can be concluded that these measurements support the concept that the rate of diffusion of solute at low solute concentration is close to the observed rate of solvent self-diffusion.

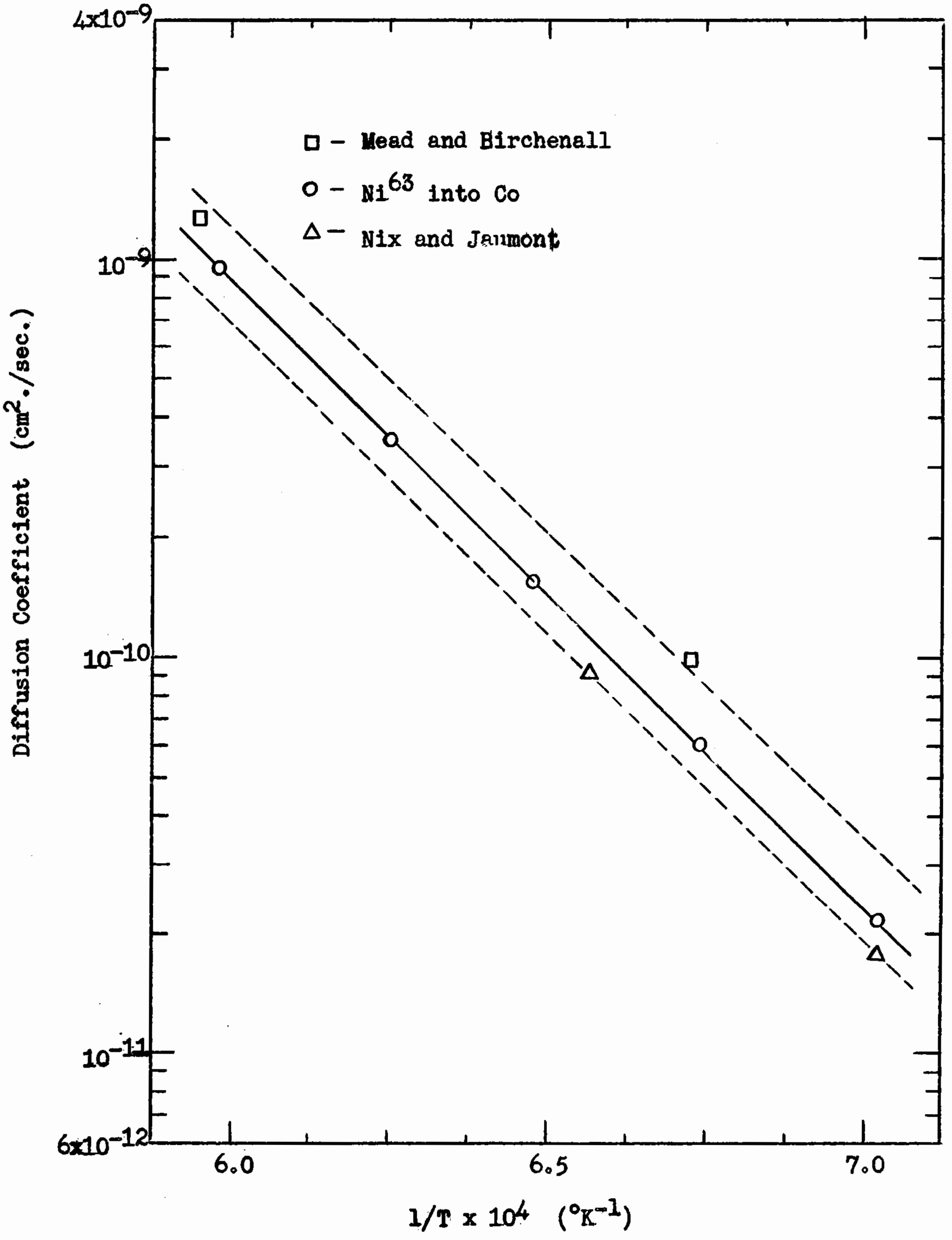

Figure 32. A Comparison of the Rate of Nickel Diffusing into Cobalt at Low Solute Concentration with the Rate of Cobalt Self-Diffusion.

Diffusion of nickel into iron at low solute concentration

The rate of diffusion of nickel into iron, at low nickel concentration, was found to be approximately one-sixth the rate of nickel self-diffusion over the temperature range investigated. The diffusion coefficients obtained for the diffusion of nickel into iron are represented by the equation

$$D = 7.13^{+6.70}_{-3.45}\ e^{-\frac{77,600 \pm 2000}{RT}} \qquad (69)$$

Iron self-diffusion has been investigated by Birchenall and Mehl[129] and Buffington, Bakalar and Cohen[130] who obtained the following results, respectively

$$D = 5.8\ e^{-74,200/RT} \qquad (72)$$

and

$$D = 0.58\ e^{-67,900/RT} \qquad (73)$$

An examination of Equations (69), (72) and (73) would suggest that the present results are in better agreement with those obtained by Birchenall and Mehl. However the curves in Figure 33 indicate that the magnitude of the diffusion coefficients obtained for the diffusion of nickel into iron are lower than those obtained for iron self-diffusion by a factor of two to three, over the temperature range investigated. Therefore it must be concluded that the results for the diffusion of nickel

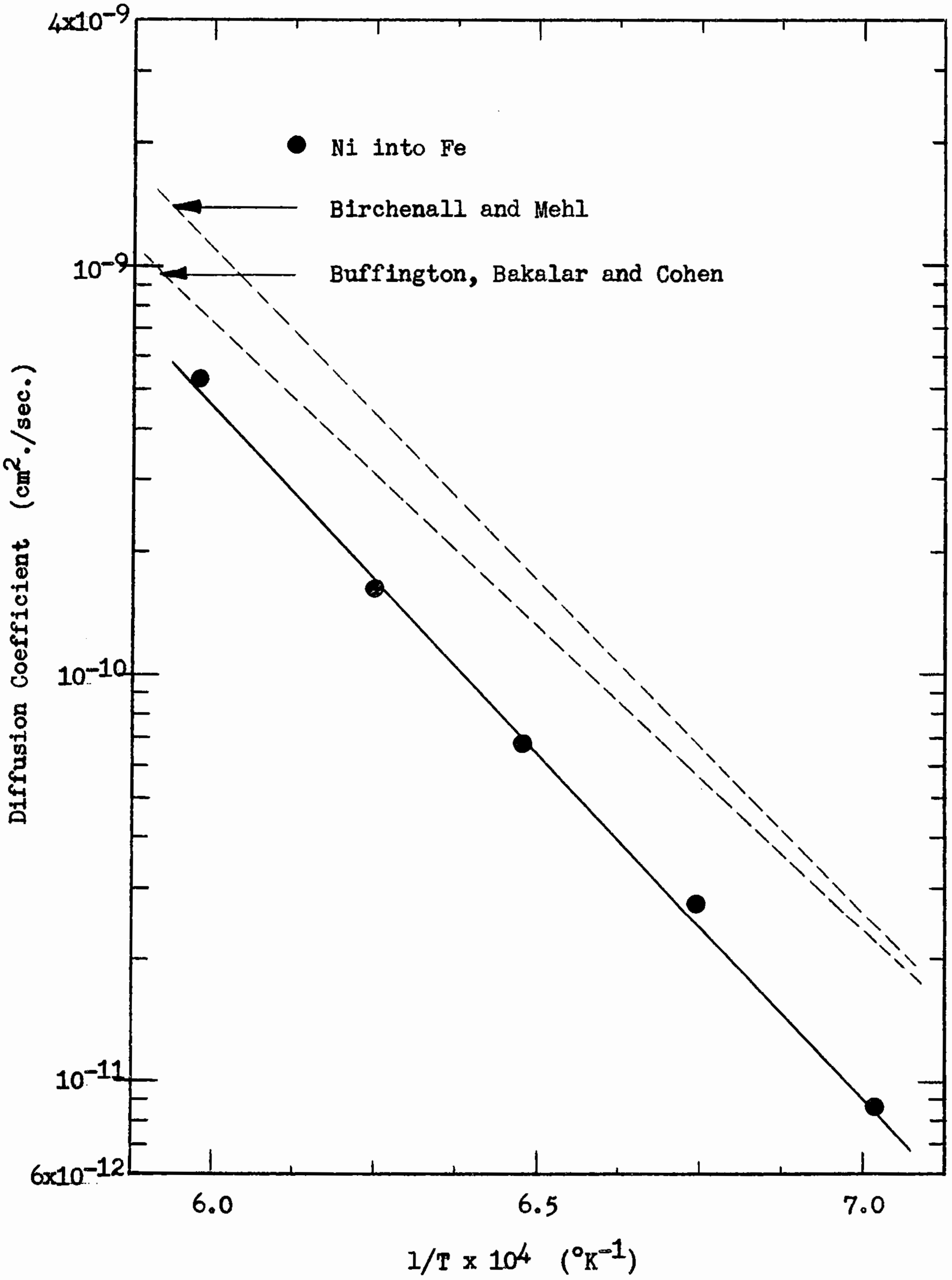

Figure 33. A Comparison of the Rate of Nickel Diffusing into Iron at Low Solute Concentration with the Rate of Iron Self-Diffusion.

into gamma iron at low solute concentration are not consistent with the measured rate of self-diffusion in gamma iron. The present results suggest that the nickel atoms are bound more tightly to the iron lattice than the iron atoms themselves. This is reflected by the high activation energy obtained and the low observed rate of diffusion of nickel into iron.

In summary it is concluded that the rate of diffusion of a solute at low concentration is not always equal to the rate of solvent self-diffusion.

Self-diffusion of nickel in the iron-nickel system

The rates of nickel self-diffusion were measured in pure nickel and two iron-nickel alloys, of 5.79 and 14.88 per cent nickel respectively.

Combining the above results with the measured rate of diffusion of nickel into iron, at low solute concentration, an approximation to the variation of the self-diffusion coefficient of nickel with composition can be obtained for the iron-nickel system. The activation energy plot for these results was given previously in Figure 31. A summary of the results are given in the following tabulation.

Alloy Weight Per Cent	Frequency Factor Do $cm^2./sec.$	Activation Energy Q kcal./mole
Pure Ni	3.97	70.1
Fe-14.88% Ni	5.14	75.6
Fe-5.79% Ni	2.27	73.5
Pure Fe	7.13	77.6

As can be observed there is an indication of a trend towards lower activation energies and frequency factors as the nickel content is increased.

The chemical diffusion coefficient, D_c, is related to the intrinsic diffusion coefficients for a binary system by Equation (12), in particular

$$D_c = N_{Fe} D_{Ni} + N_{Ni} D_{Fe} \qquad (12)$$

The intrinsic diffusion coefficient, D_{Ni}, is related to the self-diffusion coefficient, D^*_{Ni}, by Equation (11)

$$D_{Ni} = D^*_{Ni} \left(1 + \frac{\partial \log \gamma_{Ni}}{\partial \log N_{Ni}}\right) \qquad (11)$$

Iron and nickel form a thermodynamically ideal solid solution in the gamma region[131,132] and therefore Equation (11) becomes

$$D_{Ni} = D^*_{Ni} \qquad (74)$$

Combining Equations (12) and (74) gives

$$D_c = N_{Fe} D^*_{Ni} + N_{Ni} D^*_{Fe} \qquad (75)$$

While it is necessary to know D_c, D^*_{Ni} and D^*_{Fe} over the whole range of compositions to make a complete comparison, it is of interest to compare the variation of the self-diffusion coefficient for nickel in the iron-nickel system to the results obtained by other investigators for the variation of the chemical diffusion coefficient. The variation of the chemical diffusion coefficient, D_c, with composition, in the iron-nickel system, was investigated at 1300°C by Wells and Mehl[133] and by Seith and Kottman[134] at 1310°C. A comparison with the results of this investigation are made in Figures 34a, 34b and 34c.

In comparison to the results of Wells and Mehl[133] - Figure 34a - the variation of D^*_{Ni} with composition is about one-half the variation obtained for D_c. It is interesting to note in the high iron region that log D varies approximately with the atomic fraction of nickel present in the alloy. The results of Seith and Kottman for D_c, though a factor of three higher than D^*_{Ni} across the range, show about the same variation with composition, if the minimum in the region of four per cent nickel is neglected. Actually the effect was exaggerated by the use of a log scale and the replotted results in Figure 34c give a more representative impression of the magnitude of this anomalous effect.

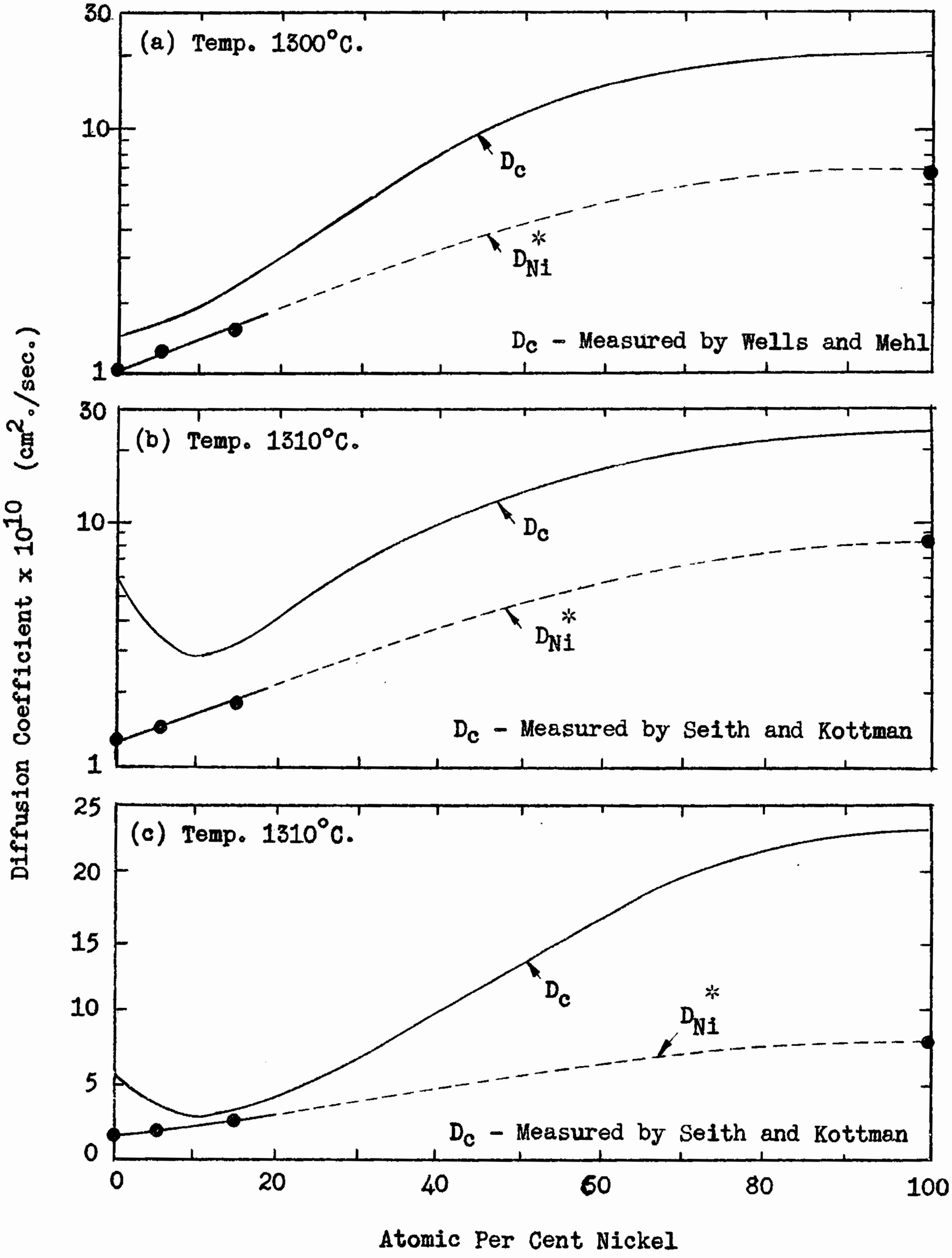

Figure 34. Variation of the Diffusion Coefficients with Composition in the Iron-Nickel System.

Seith and Kottman[134] suggest that the minimum observed in Figures 34b and 34c is not a real effect, as a microscopic examination of this region showed marked porosity. Porosity is one of the manifestations of the Kirkendall effect[35] and on observing this porosity Seith and Kottman concluded that iron and nickel diffuse at different rates. Porosity is a result of incomplete shrinkage of the lattice in the region where a net flux of atoms is flowing out. Theoretically the excess number of vacancies flowing into the region is supposed to be absorbed there by dislocations, but this latter process is never completely effective and some porosity always occurs as a result of the Kirkendall effect.

Thus it is apparent that the iron atoms are diffusing out of this region faster than the nickel atoms are diffusing in. This is in agreement with the present results which indicate that the rate of nickel self-diffusion in iron-nickel alloys is slower than the rate of chemical diffusion across the whole concentration range. With reference to Equation (75) it is apparent that D_{Fe}^{*} must be greater than D_{Ni}^{*} because D_c is greater than D_{Ni}^{*}. This implies that when a vacancy is adjacent to both an iron and a nickel atom it is more probable that the iron atom will exchange positions with the vacancy than will the nickel atom. Thus while these results represent only a preliminary investigation of diffusion in the iron-nickel system, it can be concluded that iron atoms must diffuse more rapidly than nickel atoms in the iron-rich portion of the iron-nickel system.

CONTRIBUTIONS TO KNOWLEDGE

(1) The characteristics of Ni^{63} beta-radiation have been investigated to permit its use as a tracer in diffusion studies. Suitable counting techniques have been developed so that the relative specific activity of Ni^{63} contained in a series of samples can be determined to ± 1.5 per cent.

(2) The maximum range in aluminum of Ni^{63} beta-particles has been measured. This value has been more carefully determined than those of previous workers, and is considerably larger than those found previously. The range determined in the present experiments indicates that the accepted values for the maximum energy of the Ni^{63} beta-spectrum are slightly low.

(3) The self-absorption of Ni^{63} radiations in metallic nickel sources has been investigated in a counter having a 2π geometry. The results have been used to test Gora and Hickey's theoretical expressions for self-absorption of beta-emitting nuclides. These expressions have been shown to be inadequate to interpret the results obtained for a low energy beta emitter.

(4) The rate of nickel self-diffusion was measured in polycrystalline materials over a temperature range of 1150°C to 1400°C. Measurements were made by three different techniques,

the standard sectioning technique and two other techniques developed to take advantage of the soft nature of Ni^{63} beta radiation. The values determined by the three methods are consistent. The results of this research, the first obtained for nickel self-diffusion, have been used to test the existing lattice strain theories and were found to be in as good agreement as most measurements of self-diffusion in other face-centered cubic metals.

(5) Original measurements have been made for the rate of diffusion of nickel into cobalt at low solute concentration. The measurements were found to agree closely with the rate of cobalt self-diffusion.

(6) Original measurements have been made for the rate of diffusion of nickel into iron at low solute concentrations. These results are much lower than for the rate of iron self-diffusion. This was taken as an indication that nickel is more tightly bound to the iron lattice than are the iron atoms.

(7) A preliminary study has been made of the rate of nickel self-diffusion in the iron-nickel system. These original results suggest that the rate of self-diffusion of nickel in iron-rich alloys is slower than the rate of iron self-diffusion. These results confirm Seith and Kottman's observation of a Kirkendall effect in the iron-nickel system.

(8) A dependence of the diffusion coefficient upon the time of anneal was observed for all systems studied, except for self-diffusion in pure nickel. This confirms the previous findings that a concentration effect is noticed when studying the rate of diffusion of a thin layer of tracer into a dissimilar medium.

APPENDIX 1

This appendix includes a fuller discussion of some of the assumptions necessary to derive a theoretical expression for the diffusion coefficient.

Correlation of the successive jumps of a radioactive tracer atom

The rate of self-diffusion of a metal is commonly determined by measuring the rate of mixing of a radioactive tracer electroplated onto the surface of a metal disc. If the successive jumps of the tracer are completely random in direction and uncorrelated, then the tracer's diffusion coefficient, D_T, is equal to the self-diffusion coefficient of the material, D_{AA}. This question has been examined in detail by Bardeen and Herring[135]. They found that when the concentration of vacancies is low, a tracer atom which has just changed places with a vacancy has a greater probability of rechanging positions with the vacancy than of moving off in some unrelated direction. This will slow down the rate of mixing so that D_T is smaller than the actual self-diffusion coefficient D_{AA}. Their analysis shows that for a face-centered cubic lattice

$$D_T = 0.902 \, D_{AA} \qquad (76)$$

As this correction is within the experimental error of most diffusion experiments, it has always been neglected.

Order of magnitude calculation for ΔS_1

Both LeClaire[41] and Buffington and Cohen[42], in deriving theoretical expressions for the diffusion coefficient, neglect the contribution of ΔS_1, the change in entropy on forming a vacancy, as being small compared to ΔS_2, the strain entropy.

The presence of a vacant lattice site causes a decrease in the vibrational frequency of the surrounding atoms, which is responsible for the positive value of ΔS_1. Also the presence of a vacancy will cause a change in the local values of the elastic properties. The local values of μ_0 and μ'/μ_0 will be numerically less than the bulk values, μ_0^* and μ'/μ_0. In actual fact, the local values of μ_0 and μ'/μ_0 should be used in the lattice strain equations. Referring to Equation (35b) it is apparent that decreasing the value of ΔS_1 will increase k_1, while increasing μ'/μ_0 will decrease k_1. An order of magnitude calculation by LeClaire[41] suggests that ΔS_1 and the elastic properties are so related that, by neglecting ΔS_1 in the above expression and using the bulk values of the elastic properties, the resulting value of k_1 will be unaffected.

If using the normal bulk values, $(\mu'/\mu_0)^*$, instead of the local values, μ'/μ_0, in Equation (35b) completely compensates for neglecting ΔS_1, then it can be written that

$$\Delta S_1 - (Q - k_1L_s)(\mu'/\mu_o - \rho'/\rho_o) = -(Q - k_1L_s)\left[(\mu'/\mu_o)^* - \rho'/\rho_o\right] \quad (77)$$

or that

$$\Delta S_1 = (Q - k_1L_s)\,\frac{\partial \Delta \log \mu}{\partial T} \quad (78)$$

The free energy change, ΔG_1, on forming a vacancy[43] is

$$\Delta G_1 = \Delta H_1 + Z\,R\,T \log \nu/\nu^* \quad (79)$$

where

Z = Number of neighbouring atoms. (Z = 12 for f.c.c.)

ν^* = Frequency of vibration of an atom in a normal lattice site.

ν = Reduced frequency of vibration in the radial direction of each of the Z neighbours of a vacancy.

The change in entropy, ΔS_1, is

$$\Delta S_1 = -Z\,R \log \nu/\nu^* \quad (80)$$

but

$$\Delta S_1 = \left(\frac{\partial \Delta G_1}{\partial T}\right)_P$$

so from Equation (79)

$$\frac{\partial \Delta H_1}{\partial T} = -Z\,R\,T\,\frac{\partial \Delta \log \nu}{\partial T} \quad (81)$$

The frequency of vibration, ν, in one crystalline direction is related to the shear modulus, μ , in that direction[136] by

$$\nu \propto \mu^{\frac{1}{2}} \qquad (82)$$

or

$$\Delta \log \nu = \tfrac{1}{2} \Delta \log \mu \qquad (82a)$$

Combining Equations (33), (78), (81) and (82a) gives the following estimate for ΔS_1.

$$\Delta S_1 = - \frac{(Q - k_1 L_s)\ 2k_1}{Z\ R\ T} \frac{\partial L_s}{\partial T} \qquad (83)$$

Using the rough values available for $\partial L_s / \partial T$ for the face-centered cubic metals, values for ΔS_1 of about 1 cal./mole/degree are obtained.

An independent estimate of ΔS_1 may be obtained by assuming that when a vacancy is formed, the space previously available for 13 atoms is now occupied by 12 atoms. If V is the volume per atom, then a change in log V of log 13/12 takes place on forming a vacancy. The frequency of vibration of atoms in a solid is related to the space they occupy in the Grüneisen theory[137] by

$$\frac{\partial \log \nu}{\partial \log V} = - \gamma \qquad (84)$$

where γ is Grüneisen's constant. Therefore we can calculate ΔS_1 by substituting Equation (84) into Equation (80). Thus

$$\Delta S_1 = - Z R \gamma \Delta \log V \qquad (85)$$

For a face-centered cubic metal Z = 12, therefore

$$\Delta S_1 = 1.87 \gamma$$

Calculated values of ΔS_1 are recorded in the following table for some face-centered cubic metals. The results show that

$$\Delta S_1 \sim 4\text{-}5 \text{ cal./mole/}^{\circ}\text{K}$$

Calculation of ΔS_1 from Grüneisen's Constant

Metal	γ	ΔS_1 cal./mole/$^{\circ}$K
Cu	1.96	3.7
Ag	2.40	4.5
Au	3.03	5.7
Al	2.17	4.1
Pb	2.73	5.1
Ni	1.88	3.5
Pd	2.23	4.2
Pt	2.54	4.8
		ΔS Av. ~ 4.5

It is therefore apparent that, on the basis of the order of magnitude calculations, it was not completely valid to neglect the contribution of ΔS_1 to the total entropy change, ΔS, for diffusion. However the use of bulk elastic properties does partially compensate for this approximation.

Shear moduli and their temperature coefficients

To evaluate the entropy of strain, ΔS_2, it is necessary to know the temperature coefficient of the particular elastic modulus. Unfortunately the appropriate quantities have not been measured. However the temperature variation of Young's modulus, E, has been measured for a large number of polycrystalline materials. For an isotropic medium the shear modulus, μ, Young's modulus, E, and Poisson's ratio, σ, are connected by the equation

$$\mu = \frac{E}{2(1 + \sigma)} \qquad (86)$$

As the temperature variation of Poisson's ratio is much smaller than that of Young's modulus, to a first approximation

$$\mu'/\mu_0 = E'/E_0 \qquad (87)$$

This assumption may be open to question and cannot be answered until the temperature dependence for all the individual moduli are available. The only data available for the face-centered cubic metals is for aluminum[138]. A comparison shows

$$E'/E_o = -3.75 \times 10^{-4}/^{o}K$$

and

$$\mu'/\mu_o = -5.05 \times 10^{-4}/^{o}K$$

Though these values are different it is impossible to state what effect this variation will have on the correlation until results are available for additional metals.

Young's modulus, E, for any direction in a crystalline material can be calculated from the following expression.

$$1/E = S_{11} - 2S\Gamma' \qquad (88)$$

where

$$S = S_{11} - S_{12} - \tfrac{1}{2} S_{44}$$

$$\Gamma = \alpha^2\beta^2 + \alpha^2\gamma^2 + \beta^2\gamma^2$$

S_{11}, S_{12} and S_{44} are the elastic coefficients for the metal and α, β and γ are the direction cosines with respect to the principle crystal axis.

APPENDIX 2

This appendix contains the equations for evaluating the physical constants which are substituted in Equations (40) and (41). For a complete description the reader is referred to the original article[91]. However if the following expressions are used then the values obtained by Brooks in Table 4 can be reproduced. Because an atomic surface has more surface area exposed than a plane surface, Brooks reduced the macroscopic value for the specific surface free energy, γ', obtained from tables, by a factor of 1.225 before using the value in Equation (40). When a value for γ could not be found, he took one-sixth of heat of sublimation per surface atom for the specific surface energy. For Equation (40) the rigidity modulus, G', is calculated from

$$1/G' = \frac{0.6}{c_{44}} + \frac{0.4}{\frac{1}{2}(c_{11} - c_{12})} \qquad (89)$$

For Equation (41) the value for r_s/ r_o is

$$r_s/r_o = 1/(\sqrt{3} - 1) \qquad (90)$$

Actually this value for r_o is easily evaluated if reference is made to Figure 8. The radius of the sphere which will just slip between the barrier atoms without displacing them is r_o. The value for the shear modulus, G", for any direction in a crystalline material is

$$G'' = 4/3 \left[3/2\,(c' - c)(\alpha^4 + \beta^4 + \gamma^4 - 3/5) + (3/5\,c + 2/5\,c') \right] \qquad (91)$$

where

$c' = c_{11} - c_{12}$

$c = c_{44}$

BIBLIOGRAPHY

1. Spring, W. Z. phy. Chem. 15 : 65. 1894.
2. Farady, M. and Stodart, J. Quart. J. Sci. 9 : 319. 1820.
3. Roberts-Austen, W. Philos. Trans. 187A : 393. 1896.
4. Fick, A. Ann. phys. Lpz. 94 : 59. 1855.
5. Grube, G. and Jedele, A. Z. Electrochem. 38 : 799. 1932.
6. Matano, C. Jap. J. Phys. 8 : 109. 1933.
7. Uller, K. Phys. Z. 32 : 892. 1931.
8. Darken, L.S. Trans. A.I.M.E. 150 : 157. 1942.
9. Birchenall, C.E. and Mehl, R.F. Trans. A.I.M.E. 171 : 141. 1947.
10. Darken, L.S. Trans. A.I.M.E. 175 : 184. 1948.
11. Onsager, L. and Foss, R.M. J. Phys. Chem. 36 : 2689. 1932.
12. Dehlinger, U. Z. Phys. 102 : 633. 1936.
13. Le Claire, A.D. Progress in Metal Physics. 1st ed., Chapter 7, Diffusion of Metals in Metals. Interscience Publishers, Inc., New York. 1949.
14. Tamman, G. and Schönert, K. Ztsch. anorg. Chem. 27 : 122. 1922.
15. Weiss, H. and Henry, P. Compt. Rend. 171 : 108. 1920., 173 : 146. 1921.
16. v'ant Hoff, J.H. Etudes de Dynamique Chemique. F. Muller and Company, Amsterdam. 1884.
17. Arrhenius, S. Z. physik. Chem. 4 : 226. 1889.
18. Dushman, S. and Langmuir, I. Phys. Rev. 20 : 113. 1922.

19. Frenkel, I. Z. Phys. 35 : 652. 1926.

20. Wagner, C. and Schottky, W. Z. phys. Chem. 11 : 163. 1930.

21. Seitz, F. Acta Cryst. 3 : 346. 1950.

22. Huntington, H.B. and Seitz, F. Phys. Rev. 61 : 315. 1942.

23. Huntington, H.B. Phys. Rev. 61 : 325. 1942.

24. Huntington, H.B. Phys. Rev. 76 : 1728. 1949.

25. Seitz, F. Phase Transformations in Solids. Chapter 4, Fundamental Aspects of Diffusion in Solids. John Wiley & Sons, Inc., New York. 1951.

26. Steigman, J., Shockley, W. and Nix, F.C. Phys. Rev. 56 : 13. 1939.

27. Rollin, B.V. Phys. Rev. 55 : 231. 1939.

28. Maier, M.S. and Nelson, H.R. Trans. A.I.M.E. 147 : 39. 1942.

29. Raynor, C.L., Thomassen, L. and Rouse, L.J. Trans. A.S.M. 30 : 313. 1942.

30. Zener, C. Acta Cryst. 3 : 346. 1950.

31. Seith, W. and Kiel, A. Z. phys. Chem. 22 : 350. 1933.

32. Johnson, W.A. Trans. A.I.M.E. 147 : 331. 1942.

33. Kirkendall, E.O. Trans. A.I.M.E. 147 : 102. 1942.

34. Kirkendall, E.O. Trans. A.I.M.E. 133 : 186. 1939.

35. Smigelskas, A.D. and Kirkendall, E.O. Trans. A.I.M.E. 171 : 130. 1947.

36. Correa Da Silva, L.C. and Mehl, R.F. Trans. A.I.M.E. 191 : 155. 1951.

37. Buckle, H. and Blin, J. J. Inst. Metals. 80 : 385. 1951.

38. Barnes, R.S. Proc. Roy. Soc. B65 : 512. 1952.

39. Seith, W., Hermann, T. and Kottmann, A. Naturwiss. 39 : 41. 1952.

40. Seith, W. and Kottmann, A. Ange. Chem. 64 : 376. 1952.

41. Le Claire, A.D. Acta Met. 1 :438. 1953.

42. Buffington, F.S. and Cohen, M. Acta Met. 2 : 660. 1954.

43. Mott, N.F. and Gurney, R.W. Electronic Processes in Ionic Crystals. Chapter 2. Oxford University Press. 1951.

44. Hoffman, R.E. and Turnbull, D.J. J. Appl. Phys. 22 : 634. 1951.

45. Seitz, F. Acta Cryst. 3 : 355. 1950.

46. Nowick, A.S. Phys. Rev. 82 : 340. 1951.

47. Nowick, A.S. Phys. Rev. 88 : 925. 1952.

48. Ke, T.S. J. Appl. Phys. 19 : 285. 1948.

49. Le Claire, A.D. Phil. Mag. 42 : 673. 1951.

50. Le Claire, A.D. and Childs, B.G. Acta Met. 2 : 718. 1954.

51. Nowick, A.S. Phys. Rev. 82 : 551. 1951.

52. Meechan, C.J. and Eggleston, R.R. Acta Met. 2 : 681. 1954.

53. Abeles, F. Compt. Rend. 237 : 796. 1953.

54. Hoffman, R.E. and Turnbull, D. J. Appl. Phy. 22 : 634. 1951.

55. Johnson, W.A. Trans. A.I.M.E. 143 : 107. 1941.

56. Fisher, J.C. J. Appl. Phys. 22 : 74. 1951.

57. Wajda, E.S. Acta Met. 2 : 184. 1954.

58. Shirn, G.A., Wajda, E.S. and Huntington, H.B. Acta Met. 1 : 513. 1953.

59. Nickerson, R.A. and Parker, E.R. Trans. Amer. Soc. Metals. 42 : 376. 1950.

60. Achter, R.M. and Smoluchowski, R. J. Appl. Phys. 22 : 1260. 1952.

61. Yukawa, S. and Sinnott, M.J. Trans. A.I.M.E. 203 : 996. 1955.

62. Burgers, J.M. Proc. Roy. Acad. Sci. Amsterdam. 42 : 293, 378. 1939.

63. Burgers, J.M. Proc. Phys. Soc. Lond. 52 : 23. 1940.

64. Hendrickson, A.A. and Machin, E.S. Trans. A.I.M.E. 200 : 10, 35. 1954.

65. Nachtreib, N.H. and Handler, G.S. Acta Met. 2 : 797. 1954.

66. Seith, W. and Kiel, A. Z. Metallk. 25 : 104. 1933. Values of D_o and Q recalculated by Le Claire; see reference 41.

67. Nachtreib, N.H. and Handler, G.S. J. Chem. Phys. 23 : 1569. 1955.

68. Okkerse, B. Acta Met. 2 : 551. 1954.

69. Slifkin, L., Lazarus, D. and Tomizuka, C.T. J. Appl. Phys. 23 : 1032. 1952.

70. McKay, H.A.C. Trans. Faraday Soc. 34 : 845. 1938.

71. Zagrubski, A.M. Bull. Acad. Sci. U.S.S.R. (Phys.) 6 : 903. 1937.

72. Gatos, H.C. and Kurtz, A.D. Trans. A.I.M.E. 200 : 616. 1954.

73. Ruder, R.C. and Birchenall, C.E. Trans. A.I.M.E. 191 : 142. 1951.

74. Nix, F.C. and Jaumont, F.E. Phys. Rev. 82 : 72. 1951.

75. Mead, H.W. and Birchenall, C.E. Trans. A.I.M.E. 203 : 994. 1955.

76. Birchenall, C.E. and Mehl, R.F. Trans. A.I.M.E. 188 : 144. 1950.

77. Buffington, F.S., Bakalar, I.D. and Cohen, M. Discussion in reference 76.

78. Selected Values of Thermodynamic Properties. Nat. Bur. Stand. Cir. 500. Washington, D.C. 1952.

79. Riemann-Weber. Differentialgleichungen der Physik. 7th ed., Vol. 2, p. 203. Braunschweig. 1927.

80. Stearn, A.E. and Eyring, H. J. Phys. Chem. 44 : 955. 1940.

81. Glasstone, S., Laidler, K.J. and Eyring, H. Theory of Rate Processes. McGraw Hill, New York. 1941.

82. Wert, C.A. and Zener, C. Phys. Rev. 76 : 1169. 1949.

83. Zener, C. J. Appl. Phy. 22 : 372. 1951.

84. Zener, C. Imperfections in Nearly Perfect Crystals. Chapter 11. John Wiley and Sons, Inc., New York. 1952.

85. Wert, C.A. Phys. Rev. 79 : 601. 1950.

86. Ke, T.S. Phys. Rev. 72 : 41. 1942.

87. Mott, N.F. Proc. Roy. Soc. 215A : 1. 1952.

88. Boas, W. and Mackenzie, J.K. Progress in Metal Physics, Vol. 2. Chapter 3, Anistropy in Metals. Pergammon Press Ltd., London. 1950.

89. Koster, W. Z. Metallkunde. 39 : 1. 1948.

90. Siegel, S. and Quimby, S.L. Phys. Rev. 49 : 663. 1936.

91. Brooks, H. Impurities and Imperfections. Chapter 1, Lattice

Vacancies and Interstitials in Metals. American Society for Metals, Cleveland, Ohio. 1955.

92. Rhines, F.N. and Mehl, R.F. Trans. A.I.M.E. 128 : 185. 1938.

93. Johnson, R.P. Phys. Rev. 56 : 814. 1939.

94. Nowick, A.S. J. Appl. Phy. 22 : 1182. 1951.

95. Barnes, R.S. Proc. Phys. Soc. B65 : 512. 1952.

96. Martin, A.B., Johnson, R.P., and Asaro, F. J. Appl. Phy. 25 : 369. 1954.

97. Sonder, E., Slifkin. L. and Tomizuka, C. Phys. Rev. 61: 315. 1942.

98. Lazarus, D. Impurities and Imperfections. Chapter 5, Impurities and Imperfections in Metallic Diffusion. American Society for Metals, Cleveland, Ohio. 1955.

99. See any standard text on radiochemistry, for example: Bleuler, E. and Goldsmith, G.J. Experimental Nucleonics. 1st. ed. Rinehart & Company, Inc., New York. 1952.

100. Kobayashi, Y., Miyamoto, G. and Mori, S. J. Phys. Soc. Japan. 8 : 684. 1953.

101. Brosi, A.R., Borkowski, C.J., Conn, E.E. and Greiss, J.C. Jr. Phys. Rev. 81 : 391. 1951.

102. Moore, G.E. and Kraus, K.A. J. Am. Chem. Soc. 73 : 9. 1951; 74 : 843. 1952.

103. Schiff, L.I. and Evans, R.D. Rev. Sci. Inst. 7 : 456. 1936.

104. Pate, B.D. and Yaffe, L. Can. J. Chem. 33 : 15. 1955.

105. Feather, N. Proc. Cambridge Soc. 34 : 599. 1938.

106. Gora, E.K. and Hickey, F.C. Anal. Chem. 26 : 1158. 1954.

107. Henry, N.F.M., Lipson, H. and Wooster, W.A. The Interpretation of X-Ray Diffraction Photographs. MacMillan and Co. Ltd., London. 1951.

108. Wilson, H.W. and Curan, S.C. Phil. Mag. 40 : 631. 1949.

109. Glendenin, L.E. Nucleonics 2 : 12. 1948.

110. Libby, W.F. Anal. Chem. 19 : 2. 1947.

111. Wilson, H.W. Phys. Rev. 79 : 1032. 1950.

112. Schweitzer, G.K., Stein, B.R. and Nehls, J.W. J. Phys. Chem. 56 : 692. 1952.

113. Pate, B.D. and Yaffe, L. Can. J. Chem. 33 : 1656. 1955.

114. Wesley, W.A. and Prine, W.H. Practical Nickel Plating. The International Nickel Co., Inc. New York. N.Y.

115. Lutz, B.C. and Wood, J.H. Can. J. Research 26A : 145. 1948.

116. The Construction of Electric Furnaces for the Laboratory. Norton Company, Worcester, Mass.

117. Ham, J.L., Parke, R.M. and Herzig, A.J. Trans. Am. Soc. Met. 31 : 877. 1943.

118. Burgess, H. and Smoluchowski, R. J. Appl. Phy. 26 : 491. 1955.

119. Hoffman, R.E., Pikus, F.W. and Ward, R.A. To be published.

120. Swalin, R.A. and Martin, A.E. Phys. Rev. 96 : 840A. 1954.

121. Koster, W. Z. Metallkunde 39 : 1. 1948.

122. Siegel, S. and Quimby, S.L. Phys. Rev. 49 : 663. 1936.

123. Bozorth, R.M., Mason, W.P., McSkimin, H.J. and Walker, J.G.

Phys. Rev. 75 : 1954. 1949.

124. Kurtz, A.D., Averback, B.L. and Cohen, M. Acta Met. 3 : 442. 1955.

125. Kubaschewski, O. Trans. Far. Soc. 46 : 713. 1950.

126. Tomizuka, C.T. and Lazurus, D. J. Appl. Phy. 25 : 1943. 1954.

127. Gruzin, P.L. Doklady Akad. Nauk. SSSR 86 : 289. 1952.

128. Nix, F.C. and Jaumot, F.E. Phys. Rev. 82 : 72. 1951.

129. Birchenall, C.E. and Mehl, R.F. Trans. A.I.M.E. 188 : 144. 1950.

130. Buffington, F.S., Bakalar, I.D. and Cohen, M. Trans. A.I.M.E. 188 : 1374. 1950.

131. Kubaschewski, O. and Goldbeck, O. Trans. Far. Soc. 45 : 948. 1949.

132. Orani, R.A. Acta Met. 1 : 448. 1953.

133. Wells, C. and Mehl, R.F. Trans. A.I.M.E. 145 : 329. 1941.

134. Seith, W. and Kottman, A. Ange. Chemic. 64 : 379. 1952.

135. Bardeen, J. and Herring, C. Atom Movements. American Society for Metals, Cleveland, Ohio. 1951.

136. Voight, W. Lehrbuch der Kristallphysik. p. 587. Teubner, Leipzig. 1928.

137. Grüneisen, E. Handbuck der Physik, Vol. X. Springer, Berlin. 1926.

138. Sutton, P.M. Phys. Rev. 91 : 816. 1953.